CONCEPTUAL STUDY TO APPLY ADVANCED FLIGHT CONTROL TECHNOLOGY TO THE COIN OR TRIM AIRCRAFT

Final Report
(1 July 1970 to 3 February 1971)

June 1971

by

G.A. Smith
J.M. Hammer
R.E. Rose

Honeywell Document No. 12225-FR(R)

Prepared Under Contract No. N00019-70-C-0349

for

Naval Air Systems Command
Department of the Navy

by

Honeywell Inc.
Systems and Research Division
Research Department
2345 Walnut Street
St. Paul, Minnesota 55113

DISCLAIMER NOTICE

THIS DOCUMENT IS BEST QUALITY AVAILABLE. THE COPY FURNISHED TO DTIC CONTAINED A SIGNIFICANT NUMBER OF PAGES WHICH DO NOT REPRODUCE LEGIBLY.

DOCUMENT CONTROL DATA - R & D

(Security classification of title, body of abstract and indexing annotation must be entered when the overall report is classified)

1. ORIGINATING ACTIVITY *(Corporate author)*	2a. REPORT SECURITY CLASSIFICATION
Honeywell Inc. Systems and Research Division, Research Department St. Paul, Minnesota 55113	Unclassified 2b. GROUP

3. REPORT TITLE

CONCEPTUAL STUDY TO APPLY ADVANCED FLIGHT CONTROL
TECHNOLOGY TO THE COIN OR TRIM AIRCRAFT

4. DESCRIPTIVE NOTES *(Type of report and inclusive dates)*
Final Technical Report   1 July 1970 - 3 February 1971

5. AUTHOR(S) *(First name, middle initial, last name)*
G. A. Smith
J. M. Hammer
R. E. Rose

6. REPORT DATE	7a. TOTAL NO. OF PAGES	7b. NO. OF REFS
June 1971	153	25

8a. CONTRACT OR GRANT NO. N00019-70-C-0349 b. PROJECT NO. c. d.	9a. ORIGINATOR'S REPORT NUMBER(S) 12225-FR9(R) 9b. OTHER REPORT NO(S) *(Any other numbers that may be assigned this report)*

APPROVED FOR PUBLIC RELEASE;
DISTRIBUTION UNLIMITED

11. SUPPLEMENTARY NOTES	12. SPONSORING MILITARY ACTIVITY Naval Air Systems Command Department of the Navy

13. ABSTRACT

Investigations of the Variable Deflection Thruster (VDT) for a no-external-moving surfaces (NEMS) flight control system have been extended to determine the effects of finite aspect ratio and part-span blowing at subsonic speeds. Wind tunnel tests have revealed that full-span blowing is more effective than part-span blowing for obtaining lift or rolling moments. It was also shown that the "lift effectiveness" decreases when the ratio of blown area to wing area decreases or when a part-span blown area is moved toward the wing tip. The results of the wind tunnel study indicate that available theoretical analyses provide satisfactory predictions of jet-flap lift for full span blowing, but further theoretical work is needed, especially to determine the effects of part-span blowing.

A study to examine the feasibility of using VDT blowing for primary flight control of COIN (counterinsurgency) or TRIM (trails, roads and interdiction missions) aircraft was undertaken. The estimates of the required thrust, mass flow and horsepower seemed reasonable, so duct losses were calculated, and the weight and fuel requirements were estimated. A VDT primary flight control system weighing 480 lb was hypothesized, and the maneuvering capability of an aircraft with this NEMS system was compared to the aircraft with conventional controls. It was found that the aircraft performance was generally improved with the NEMS control system.

KEY WORDS	LINK A		LINK B		LINK C	
	ROLE	WT	ROLE	WT	ROLE	WT
jet-flap						
NEMS						
VTP						
TRIM aircraft						
COIN aircraft						
attack effectiveness						

CONCEPTUAL STUDY TO APPLY ADVANCED
FLIGHT CONTROL TECHNOLOGY TO THE
COIN OR TRIM AIRCRAFT

Final Report
(1 July 1970 to 3 February 1971)

June 1971

by

G.A. Smith
J.M. Hammer
R.E. Rose

Honeywell Document No. 12225-FR(R)

Prepared Under Contract No. N00019-70-C-0349

for

Naval Air Systems Command
Department of the Navy

by

Honeywell Inc.
Systems and Research Division
Research Department
2345 Walnut Street
St. Paul, Minnesota 55113

FOREWORD

This is the final report describing the work performed under Naval Air Systems Command Contract No. N00019-70-C-0349 on investigating the feasibility of a fluid flight control system for low-speed aircraft. The contract technical monitors are Messrs. Jack Crowder and John Schonowski. This report covers progress from 1 July 1970 to 3 February 1971.

The authors wish to express their gratitude to Messrs. Howard Melrose and Del Hogan for their contributions to the experimental program of these investigations and to Messrs. Norman Miller, Stephen Johnson and Shukry Ibrahim for their assistance in analyzing the results of the experimental work.

ABSTRACT

Investigations of the Variable Deflection Thruster (VDT) for a no-external-moving surfaces (NEMS) flight control system have been extended to determine the effects of finite aspect ratio and part-span blowing at subsonic speeds. Wind tunnel tests have revealed that full-span blowing is more effective than part-span blowing for obtaining lift or rolling moments. It was also shown that the "lift effectiveness" decreases when the ratio of blown area to wing area decreases or when a part-span blown area is moved toward the wing tip. The results of the wind tunnel study indicate that available theoretical analyses provide satisfactory predictions of jet-flap lift for full span blowing, but further theoretical work is needed, especially to determine the effects of part-span blowing.

A study to examine the feasibility of using VDT blowing for primary flight control of COIN (counterinsurgency) or TRIM (trails, roads and interdiction missions) aircraft was undertaken. The estimates of the required thrust, mass flow and horsepower seemed reasonable, so duct losses were calculated, and the weight and fuel requirements were estimated. A VDT primary flight control system weighing 480 lb was hypothesized, and the maneuvering capability of an aircraft with this NEMS system was compared to the aircraft with conventional controls. It was found that the aircraft performance was generally improved with the NEMS control system.

CONTENTS

ILLUSTRATIONS

NOTATION

AR   -   wing aspect ratio (b/c)

b   -   wing span length

b_T -   span of tunnel test section

c   -   wing chord length

C   -   wind tunnel test section cross-sectional area (b_T x h)

C_D -   drag coefficient (D/qS_w)

C_{D_i} -   induced drag coefficient

C_{D_o} -   zero-lift drag coefficient

cg   -   center of gravity position

C_L -   lift coefficient ($L/q\,S_w$)

$C_{M_{C/4}}$ -   quarter-chord pitching moment coefficient (M/qS_wc)

C_{M_r} -   rolling moment coefficient

C_P -   pressure coefficient $\left(\dfrac{P_s - P_\infty}{q} \right)$

C_{HP} -   compressor power coefficient

C_μ -   blowing coefficient based on blown wing section, $\dot{m}V_j/qS_B$

C_{μ_T} -   blowing coefficient based on total wing section, $\dot{m}V_j/qS_W$

D   -   drag force

h	-	height of tunnel test section
L	-	lift force
M	-	moment or Mach no.
$\dot{m}$	-	jet-flap mass flow
p	-	roll rate
P_{comp}	-	compressor horsepower
P_p or P_{VDT}	-	plenum pressure in jet-flap or VDT wing
P_s	-	static pressure on airfoil surface
P_1	-	freestream total pressure
P_∞	-	freestream static pressure
q	-	freestream dynamic pressure
S	-	airfoil surface area (b x c)
S_B	-	sectional airfoil surface area where jet-flap blowing exists
t	-	airfoil thickness or time
T	-	thrust ($\dot{m} V_j$)
T_p	-	plenum temperature in jet-flap wing
V	-	freestream velocity
V_j	-	calculated isentropic jet velocity

$$V_j = \left\{ \frac{\gamma}{\gamma - 1} \, RT_p \left[1 - \frac{P_\infty}{P_p}^{\gamma - 1/\gamma} \right] \right\}^{1/2}$$

x	-	chordwise distance from leading edge to points on airfoil
y	-	spanwise distance from root chord to points on airfoil
X_H	-	distance from aircraft horizontal tail aerodynamic center to cg
Z	-	vertical distance from wing aerodynamic center to cg
α	-	airfoil angle of attack
γ	-	ratio of specific heats = 1.4 for air
ρ_1	-	freestream total density
σ	-	density ratio (ρ/ρ sea level)
τ	-	jet angle measured from airfoil centerline

Superscripts

2-D	-	two-dimensional value
3-D	-	three-dimensional value

Subscripts

F	-	undisturbed (free) air measured
H	-	horizontal tail
T	-	tunnel measured
v	-	vertical tail
VDT	-	variable deflection thruster quantity
W	-	wing

SECTION I

INTRODUCTION

This is the final report of Phase IV work in a program directed toward the development of a fluid flight control system with no external moving surfaces (NEMS).

The first phase of investigation (Ref. 1) showed that a jet-flap device called the Variable Deflection Thruster (VDT) can produce high lift with simultaneous drag reduction at low external airspeeds.

Phase II (Ref. 2) of the NEMS work demonstrated the operational usefulness of VDT primary control with low-speed flight tests of a UC-45J aircraft equipped with a vertical tail incorporating VDT control. High-speed wind tunnel tests carried out in this phase of the program showed that jet detachment at transonic and supersonic speeds limits the high lift producing capability of the VDT to subsonic Mach numbers.

Phase III work showed that the useful range of the VDT can be extended by combining the VDT with transverse jet (TJ) blown control to produce lift throughout the speed range of high-performance aircraft (M ≤ 3.0, Ref. 3). Calculations of the maneuvering capability of a Navy F-4 using VDT-TJ control indicated that the VDT-TJ system can meet or exceed the required control capability at subsonic and transonic speeds using bleed air from the engine compressors, but excessive bleed air would be required to execute high-g pull-up maneuvers at supersonic speeds.

One of the objectives of the Phase IV investigation was to examine the effects of finite aspect ratio and partial-span blowing on VDT lift effectiveness at low external airspeeds. To accomplish this task, it was decided to fabricate a jet-flap model to be wind tunnel tested at several aspect ratios. The model was designed to enable a variety of spanwise lengths and positions to be blown.

The second major objective of Phase IV work was to examine the feasibility of using VDT blowing for primary flight control of subsonic TRIM or COIN type aircraft. The experimental wind tunnel results were used to determine the required thrust and power for the low-speed aircraft maneuvers.

Results of the Phase IV work toward achieving these two major objectives are discussed in detail in the following sections of this report.

1

BLANK PAGE

SECTION II
THEORETICAL JET FLAP RESULTS

Many acceptable methods for the theoretical treatment of the jet flap exist, each having some advantage or disadvantage. Reference 4 briefly describes each method and summarizes the major results. Preference is given to Spence's method (Ref. 5) for a variety of reasons. Spence's results are most widely used because his approach incorporates thin airfoil theory and presents practical numerical solutions.

TWO-DIMENSIONAL THEORY

Spence's analysis of the two-dimensional jet-flap wing has been reviewed in numerous jet flap investigations and is not reproduced here. The results of the analysis are summarized as follows: The general expression for the lift coefficient,of symmetrical airfoils, as computed from a numerical solution (see Ref. 5), can be written as

$$C_L^{(2-D)} = \left(\frac{\partial C_L}{\partial \tau}\right)^{(2-D)} \tau + \left(\frac{\partial C_L}{\partial \alpha}\right)^{(2-D)} \alpha \qquad \text{(eqn 1)}$$

where the following interpolation formulae can be used for the partial derivitives

$$\left(\frac{\partial C_L}{\partial \tau}\right)^{(2-D)} = \left[4\pi C_\mu \left(1 + 0.151 C_\mu^{1/2} + 0.139 C_\mu\right)\right]^{1/2} \qquad \text{(eqn 2)}$$

$$\left(\frac{\partial C_L}{\partial \alpha}\right)^{(2-D)} = 2\pi \left(1 + 0.151 C_\mu^{1/2} + 0.219 C_\mu\right)$$

It can be seen that the derivatives are purely functions of the blowing coefficient C_μ.

Two-dimensional experimental data (Ref. 2, 6, and 7, for example) agree well with Spence's thin airfoil treatment of jet-flap wings in two dimensions.

THREE-DIMENSIONAL THEORY

The lift of a jet-flap wing of finite aspect ratio was studied by Maskell and Spence (Ref. 8). The approach extended Spence's two dimensional theory for the simplified case of an elliptically distributed chord and jet momentum flux

3

per unit span. Despite some weaknesses in the theory, previous experimental measurements on wings of rectangular planform (Ref. 9) have shown fair agreement with the theory. Again, the lift coefficient can be expressed in the form

$$C_L^{(3-D)} = \left(\frac{\partial C_L}{\partial \tau}\right)^{(3-D)} \tau + \left(\frac{\partial C_L}{\partial \alpha}\right)^{(3-D)} \alpha \qquad \text{(eqn 3)}$$

The three-dimensional derivatives are obtained by multiplying the two-dimensional values by the factor F, where F can be estimated by

$$F(AR, C_\mu) \approx \frac{AR + \left(\frac{2C_\mu}{\pi}\right)}{AR + 2 + 0.604 \, C_\mu^{1/2} + 0.876 \, C_\mu} \qquad \text{(eqn 4)}$$

In estimating the lift coefficient, many investigators have included a correction for the non-zero thickness of the airfoil section. A crude estimate of $(1 + t/c)$ is often used to correct the slope of the lift curve. However, as pointed out in Reference 10, in practice the increase in the slope of the lift curve is considerably less than that predicted by theory. For four- and five-digit series airfoils, the slope of the lift curve experiences a small decrease with increasing thickness. Thus, the theoretical results used in the remainder of this report neglect thickness corrections to the pressure lift.

Allowance for part span jet flap blowing can be included (Ref. 11) by introducing spanwise extent factors given by

$$\lambda \approx \frac{S_B}{S_w}$$

$$\upsilon \approx \frac{S_B \left(\frac{\partial C_L}{\partial \alpha}\right)^{(2-D)} + (S_w - S_B) \left(\frac{\partial C_L}{\partial \alpha}\right)^{(2-D)} C_\mu = 0}{S_w \left(\frac{\partial C_L}{\partial \alpha}\right)^{(2-D)}} \qquad \text{(eqn 5)}$$

These parameters are tentatively used for part span blowing analysis, as no adequate theoretical approach is available. At small C_μ values or large blowing spans the factor υ can simply be taken as unity. The total expression for the three-dimensional lift can be written as:

$$C_L^{(3-D)} = F \left[\lambda \tau \left(\frac{\partial C_L}{\partial \tau} \right)^{(2-D)} + \upsilon \alpha \left(\frac{\partial C_L}{\partial \alpha} \right)^{(2-D)} \right] \qquad \text{(eqn 6)}$$

It is noted here that the two-dimensional derivatives must be evaluated using the blowing coefficient based on the blown wing area, S_B. In the limit $C_\mu \to 0$ the expression for the lift coefficient becomes the familiar relation

$$C_L^{(3-D)} = C_L^{(2-D)} \left(\frac{AR}{AR + 2} \right) \qquad \text{(eqn 7)}$$

Maskell and Spence also derived a relation for the induced drag due to lift

$$C_{D_i} = \left[C_L^{(3-D)} \right]^2 / \pi \, AR \left(1 + \frac{2C_\mu}{\pi AR} \right) \qquad \text{(eqn 8)}$$

At small C_μ and moderate-to-large aspect ratios the induced drag reduces to the well known formula

$$C_{D_i} = \frac{\left[C_L^{(3-D)} \right]^2}{\pi AR} \qquad \text{(eqn 9)}$$

The C_{D_i} expression is altered by a correction factor for wings of non-elliptic loading.

5

BLANK PAGE

SECTION III
WIND TUNNEL INVESTIGATION

A wird tunnel investigation was conducted at low external airspeeds to
determine jet-flap lift and thrust effectiveness for finite-aspect-ratio wings
with full- and part-span blowing. The experimental results were used to
examine the validity of available theoretical results and determine the feasi-
bility of using the Variable Deflection Thruster (VDT) for primary flight
control of low-speed military aircraft. The tests were conducted in the
12-in. x 17-in. low-speed Honeywell wind tunnel.

WING MODEL

A NACA 0012 airfoil section was chosen for the finite-aspect-ratio tests
based on the following reasons:

- The thickness ratio is common for a low-speed aircraft wing;
  after modifying the trailing edge to incorporate the jet-flap,
  the thickness was 13.5% of the chord.

- It is thick enough to be modified for jet-flap wind tunnel tests.

- Symmetrical airfoils, which have been used for previous VDT
  investigations, facilitate simple evaluation and comparison of
  results.

The model chord length was designed to be as large as possible (consistent
with the wind tunnel test section) to facilitate wing ducting and jet exit slot
fabrication.

The model cross section is shown in Figure 1(a). It was designed as a semi-
span wing model with rectangular planform, a 5.32-in. chord and variable
span length to allow several aspect ratios to be tested. The model was
fabricated from type 355 aluminum (jig plate) by milling the duct area into a
plate of rectangular cross section. A cap [cross-hatched section of model
in Figure 1(a)] was then fastened to the section, and the airfoil profile was
cut out. The plenum chamber was made to be inclined at about 3 deg to the
airfoil chord to provide a contraction ratio (ratio of plenum area to slot area)
of approximately 20.

Jet angles of 26, 40 and 55 deg were available by switching the trailing-edge
inserts shown in Figure 1(b). A semi-circular steel rod was used to con-
struct the inserts. The rod cross-section was cut lengthwise at an angle
equal to 90 deg minus the desired jet angle. A wedge was added to this

PRECEDING PAGE BLANK

355 ALUMINUM

0.30 IN.

3.70 IN.

4.20 IN.

5.20 IN.

3°

0.153 IN.

(a) MODEL CROSS SECTION

0.012 IN. SLOT

INSERT (θ = 30°, 45°, 60°)

0.046 IN.

θ

0.141 IN.

BRASS
SCREEN

(JET ANGLE)

0.12 IN.

FLUID
JET

0-80 SCREW
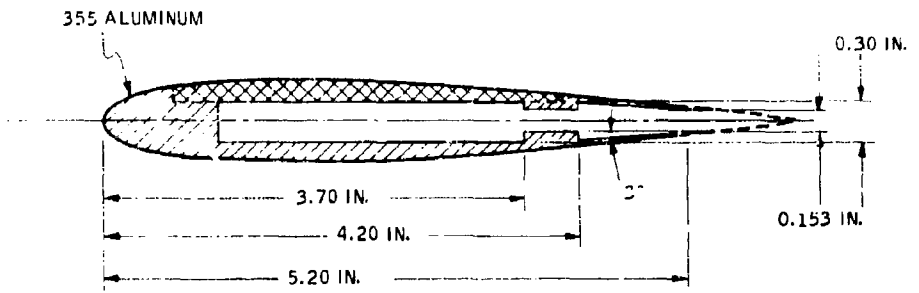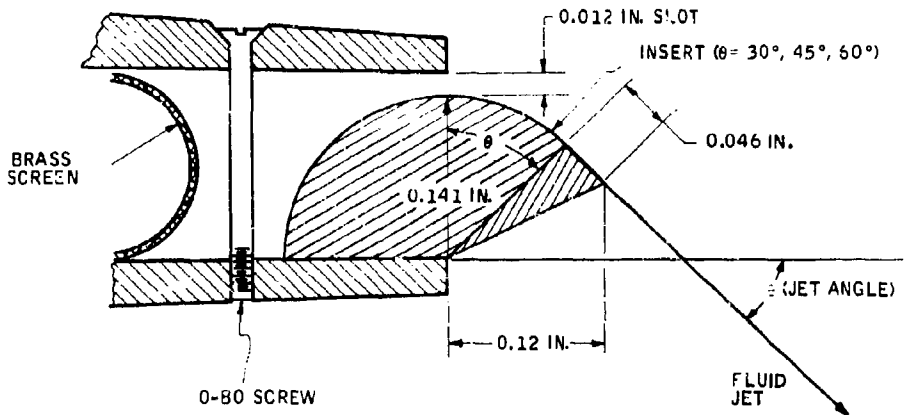
(b) TRAILING EDGE JET-FLAP CONFIGURATION

Figure 1. Jet-Flap Wing Model Configuration

8

section to extend in a straight line along this angle. This ensured that the jet sheet remained attached to the surface to obtain the design jet angle. Minor adjustments of the slot width were made by means of the 0-80 screws located ahead of the inserts [Figure 1(b)]. These screws also strengthen the plenum to sustain the pressures required to attain the desired blowing coefficients. The model tip, trailing edge and an insert are shown in Figure 2. A view of the entire model, as seen looking at the trailing edge, is presented in Figure 3.

Provision for part-span blowing was included in the model by fabricating shims of variable length to be inserted into the trailing-edge slot. The 0-80 screws were used to tighten down these shims and prevent leakage. The span lengths blown were set according to insert lengths, as inserts were fabricated to be 2.6 in. long to minimize bending when machined. Five inserts for each jet angle were made, making it possible to blow a total span of 13 in. The insert positioning on the trailing edge and the numbering system used to identify the blown inserts are shown in Figure 4. This numbering system will be referred to in the test results.

Three sets of inserts were made to create jet angles of 26, 40, and 55 deg as determined from pressure surveys. The pressure rake mounted on the model is shown in Figure 5. Pressures were read from a manometer board, and an example of the resulting jet angle determination is shown in Figure 6. Some variation between inserts is noticeable, but it was assumed to have negligible influence on wind tunnel results.

The uniformity of the jet sheet was found to be very good. The air feed duct was designed to minimize pressure losses and, therefore, maintain constant plenum pressure along the span of the model. Two pressure taps were placed in the plenum, one at the root of the model and one near the tip. The pressure drop was found to be less than 2% for full-span blowing. Thus, the mass flow distribution along the span was nearly constant, any variation occurring mainly because of variations in slot exit width (± 0.0015 in.). A brass mesh screen shown in Figure 1(b) was placed immediately ahead of the converging nozzle formed by the insert and model upper surface to minimize the variation in mass flow.

BALANCE SYSTEM

For horizontal installation of the wing model into the wind tunnel, the maximum finite aspect ratio would be 3.6. Since low-speed aircraft normally have aspect ratios greater than 4, the model was installed vertically in the wind tunnel to give a maximum finite aspect ratio of 5.2.

Mounting the model vertically from the tunnel floor necessitated a balance system capable of measuring the model forces at the floor of the wind tunnel.
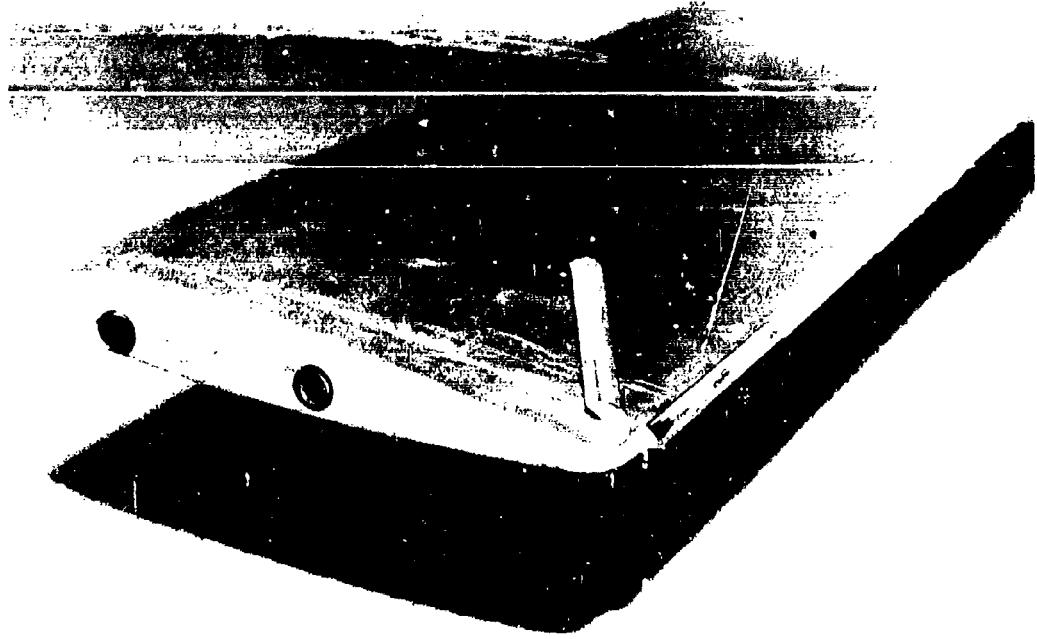
Figure 2. Wing Model Detail
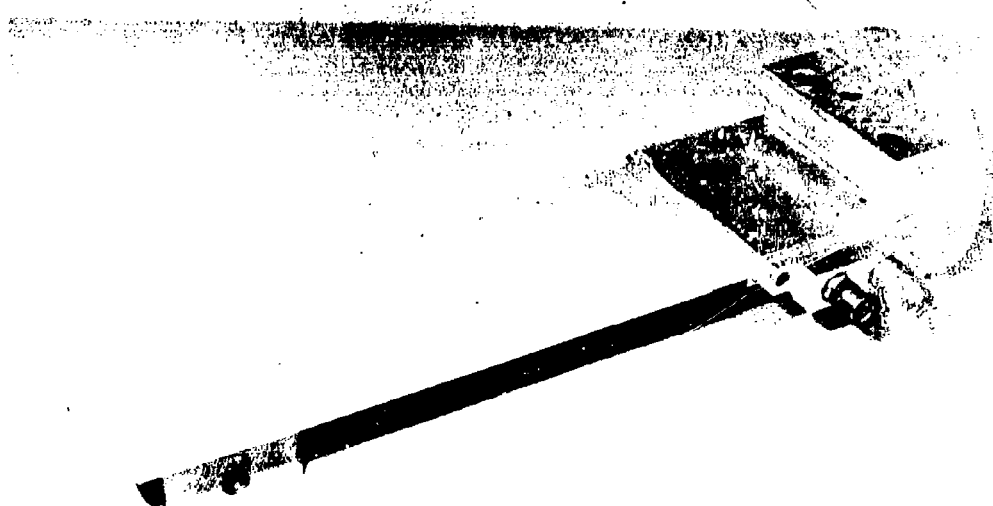
Figure 3. Wing Model Overall View
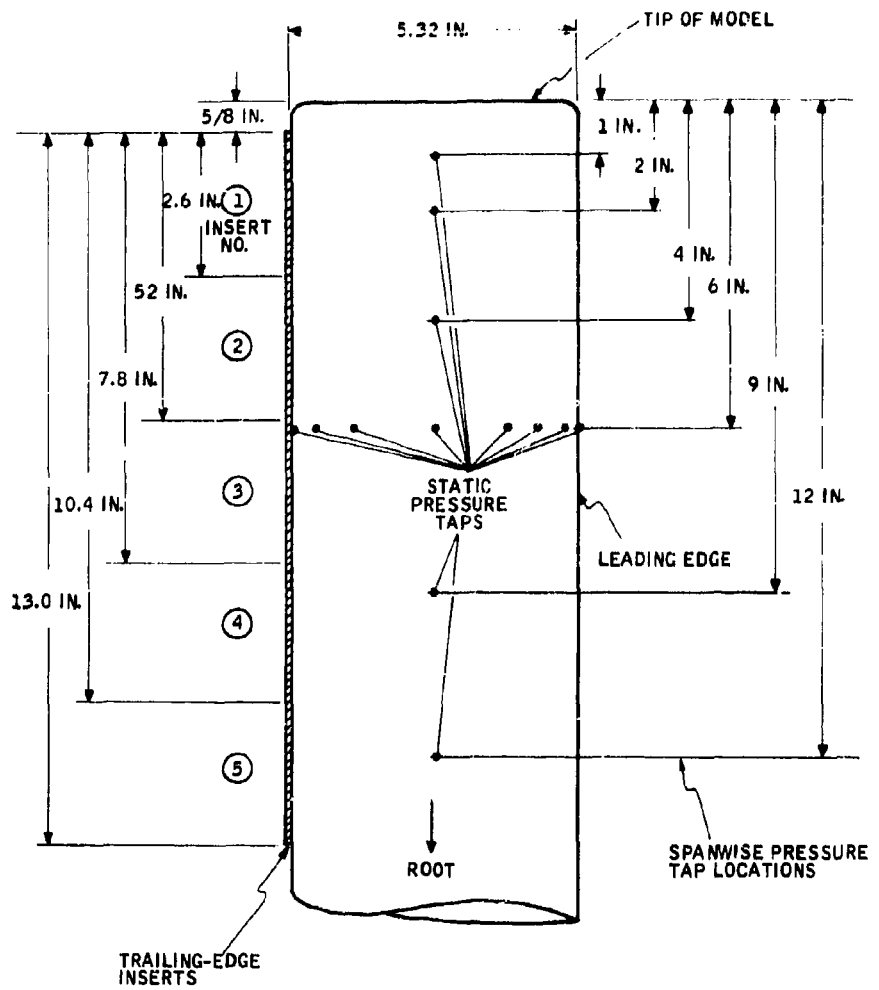
Figure 4.   Location of Pressure Taps and Trailing
Edge Inserts

11
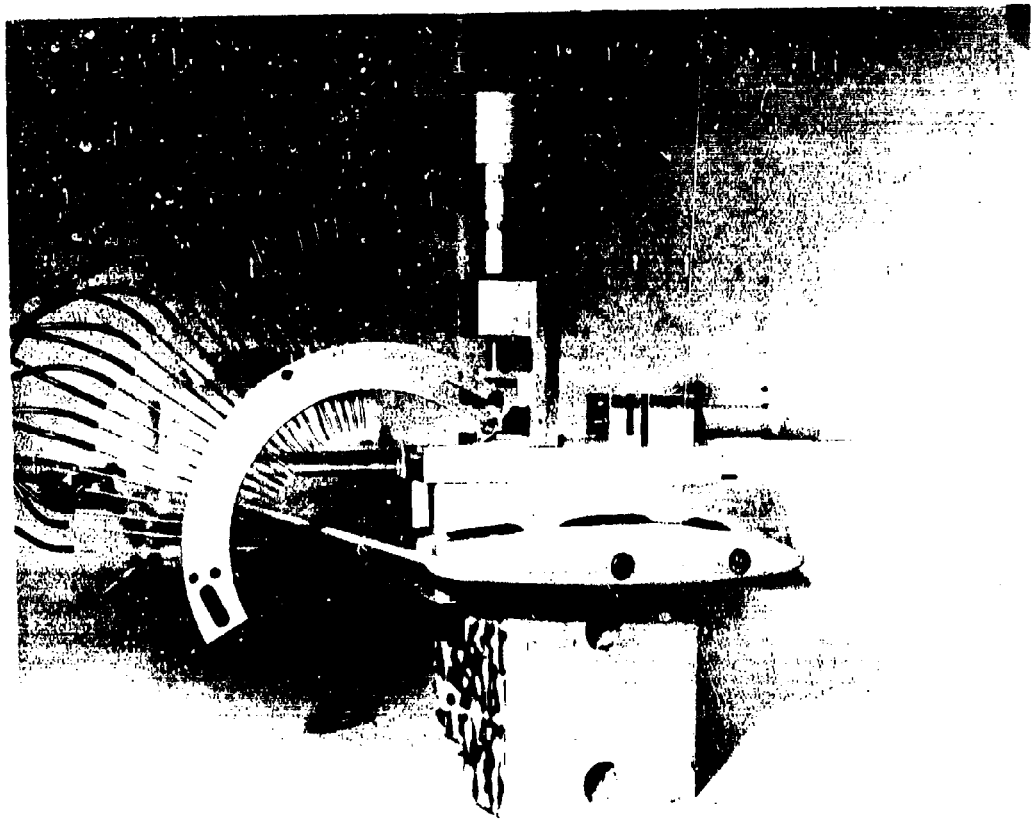
Figure 5. Jet Angle Pressure Rake

Figure 6. Jet Angle Pressure Plots

13
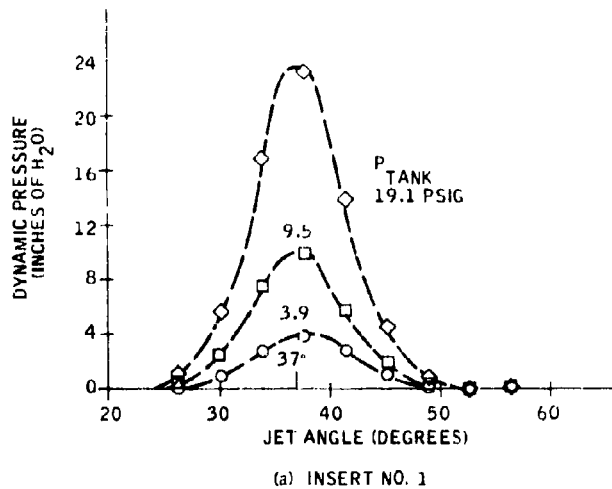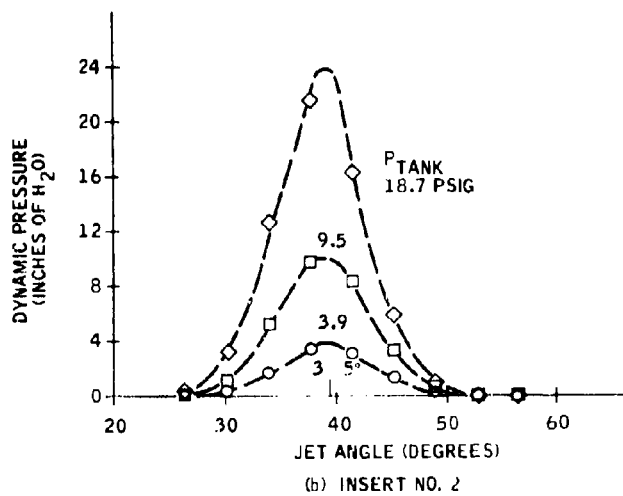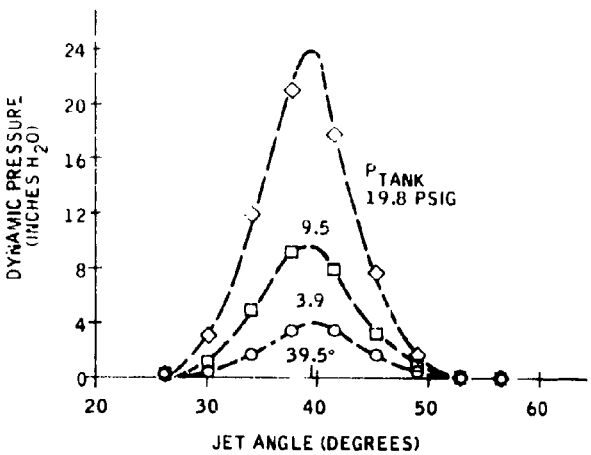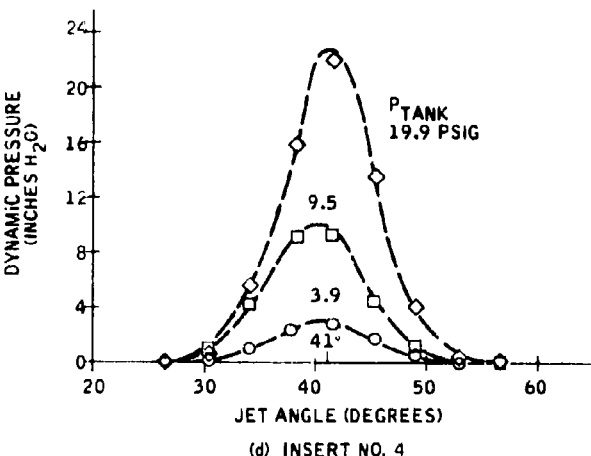
(c) INSERT NO. 3

(d) INSERT NO. 4

Figure 6. Jet Angle Pressure Plots (Continued)
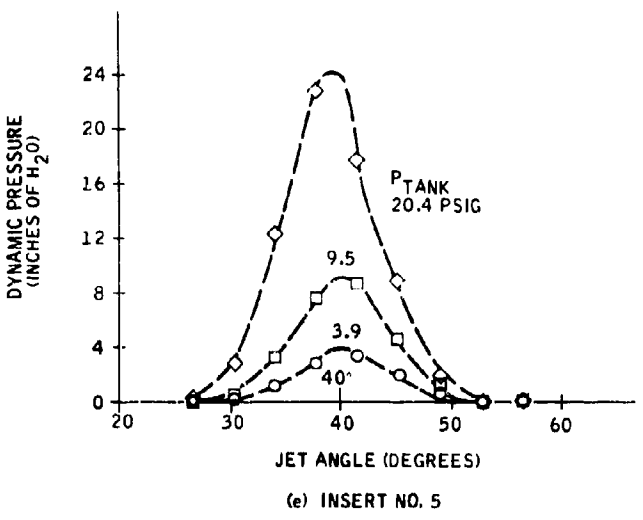
Figure 6. Jet Angle Pressure Plots (Concluded)

15

The wind tunnel strain gage balance designed for the two-dimensional tests of Reference 2 could not be easily converted for this application. Therefore, a three-component force balance table was used that had been recently designed and fabricated by Honeywell for general research laboratory use. The balance table is shown in Figure 7. Lift and drag forces and the pitching moment are measured in the plane of the table top as indicated in Figure 7.

The balance was designed such that each flexure reed (Figure 8) provide the highest possible bending stiffness to oppose loadings not in the direction of loadings measured by the reed. Consequently, the lift reeds are 1000 times stiffer in the drag direction than they are in the lift direction. The bending stiffness of the lift reeds in the lift direction is low enough to permit measurement of the bending strain by the use of strain gages without being affected by any drag loadings. Further information on the balance table design and use is presented in Appendix A.

INSTRUMENTATION

The function of the experimental instrumentation was to provide signals used to measure lift, drag and moment forces acting on the jet-flap wing model. Since the strain gage outputs of the balance table were small, it was necessary to amplify them. The drag and moment signals were amplified by use of BAM-1C amplifier-meters and the lift signals was amplified using a tropel 241 d-c amplifier. Amplified signals were then passed through small rejection filters to filter low-frequency noise picked up during the tests. Decade resistance boxes were used to regulate the amplitude of the signal received by a Honeywell visicorder.

The resistance boxes allowed a wide variety of loadings to be measured on one channel of the visicorder without losing sensitivity. That is, a large range of forces was reduced to a much smaller range of electrical inputs to the visicorder. In this way, it was possible to obtain similar visicorder readings for a 1- or 20-lb force. The magnitude of the force indicated by the visicorder reading was computed by multiplying the reading by the calibration constant appropriate for the resistance box setting used. Figure 9 shows the various components used in the wind tunnel tests.

Pressure tap instrumentation was also used in the wind tunnel tests. Static pressure taps were located on the model surface at both chordwise and spanwise stations, with the objective being to determine the spanwise lift distribution. Some difficulty occurred when attempting to do so; the reason and results are discussed later in this report. The location of the spanwise pressure taps is given in Figure 4, and the location of the chordwise pressure taps is shown in Figure 10.

16
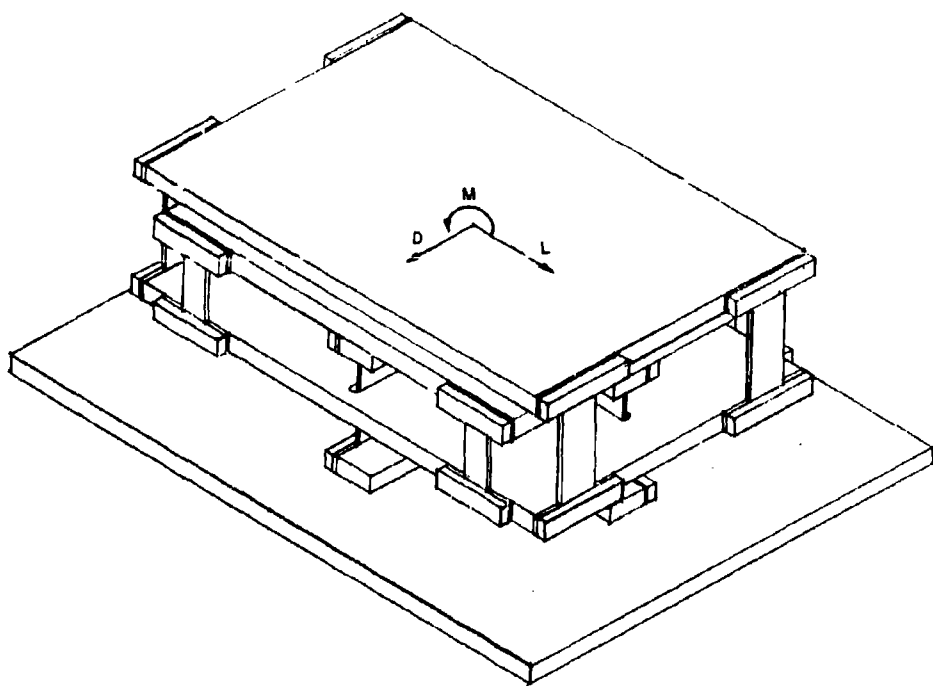
Figure 7.   Force Balance Table
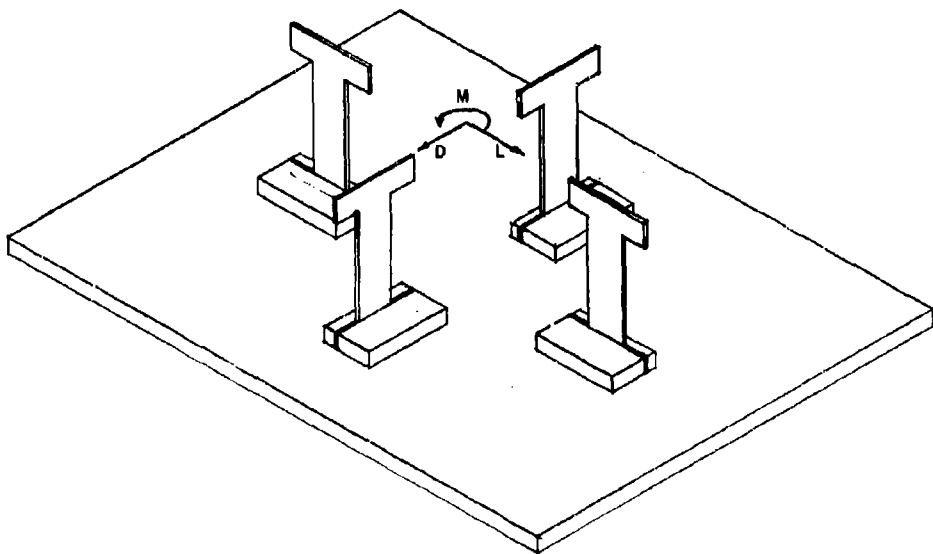
Figure 8.   Force Balance Table Flexure Reed Placement

17

① Visicorder	④ Tropel Amplifier
② Decade Resistance Boxes (3)	⑤ Krone-Hite Rejection Filters (3)
③ BAM I Amplifier-Meters (2)	⑥ Digital Voltmeter
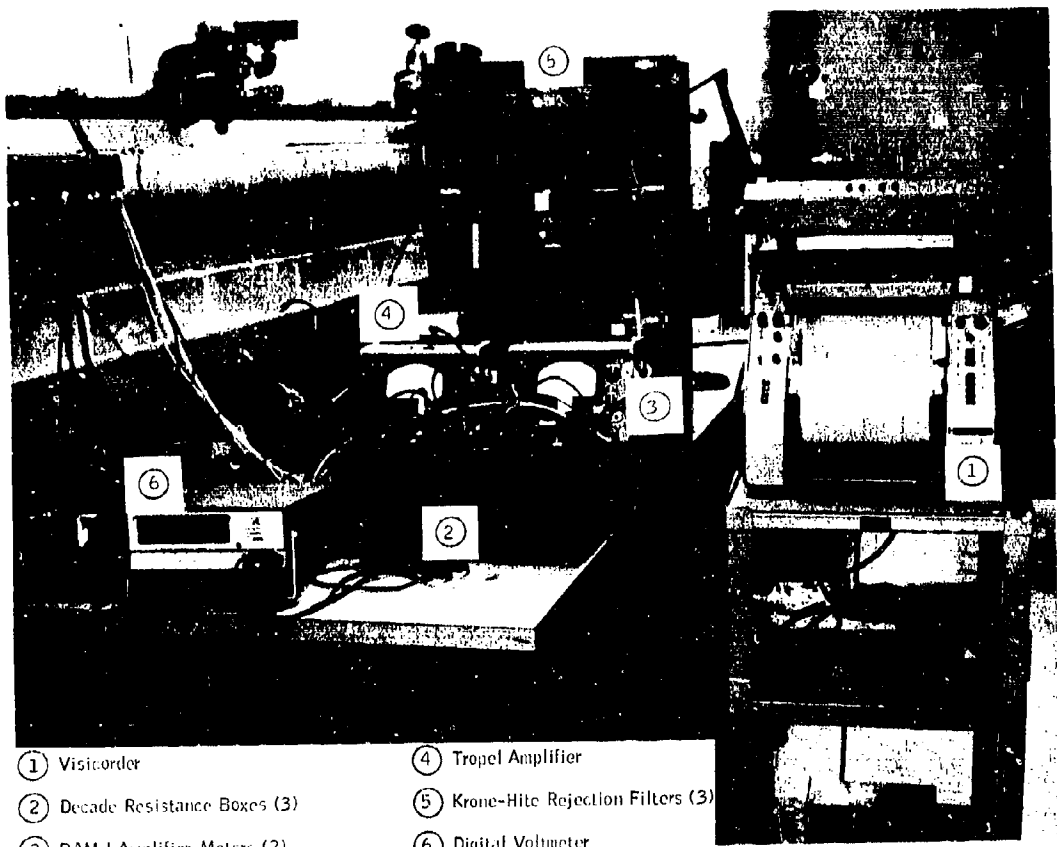
Figure 9.   Wind Tunnel Instruments

CHORD
5.32 IN.

0.25 IN.

0.75 IN.

1.25 IN.

2.60 IN.

4.15 IN.

4.75 IN.

5.15 IN.

• PRESSURE TAPS
(ON TOP AND BOTTOM
AIRFOIL SURFACE)
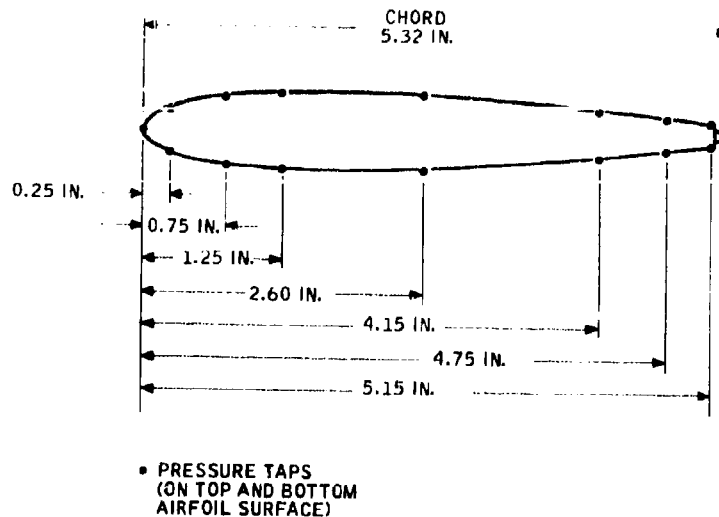
Figure 10. Location of Chordwise Pressure Taps

MEASUREMENT OF JET-BLOWING PARAMETERS

A manifold complex having the required valves, pressure regulators, gages, venturis for flow metering, etc., was used for regulating, controlling and metering the air flow to the jet flap. The manifold complex was also used for the tests of References 2 and 3, but only one arm of the circuitry was used for the present investigation. A diagram of the air supply circuitry is shown in Figure 11. The manifold complex was placed under the wind tunnel, downstream of the test section.

Pressure taps located in the jet flap plenum chamber were used to calculate the jet velocity assuming isentropic expansion from the plenum pressure, P_p, to the free-stream pressure, P_∞. The jet thrust was calculated by multiplying this jet velocity by the venturi-measured mass flow. The blowing coefficient, C_μ, was determined by dividing the calculated thrust by qS_B, where S_B is the wing area over which jet blowing takes place. The blowing coefficient, $C_{\mu T}$, used in the data analysis was defined by the calculated thrust divided by qS_W.

TUNNEL INSTALLATION

The jet-flap wing model, as installed through the tunnel floor, is shown in Figure 12 at an aspect ratio of 5.17. The interface between the test section and the undisturbed air was sealed with latex dental dam. The latex was

19
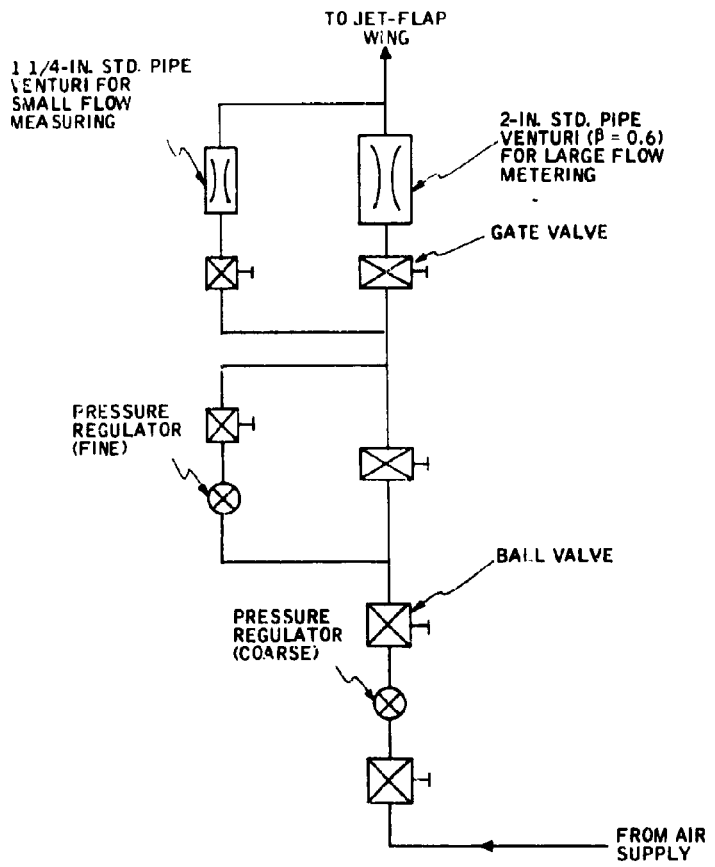
Figure 11. Flow Diagram for Air Supply to Jet-Flap Wing
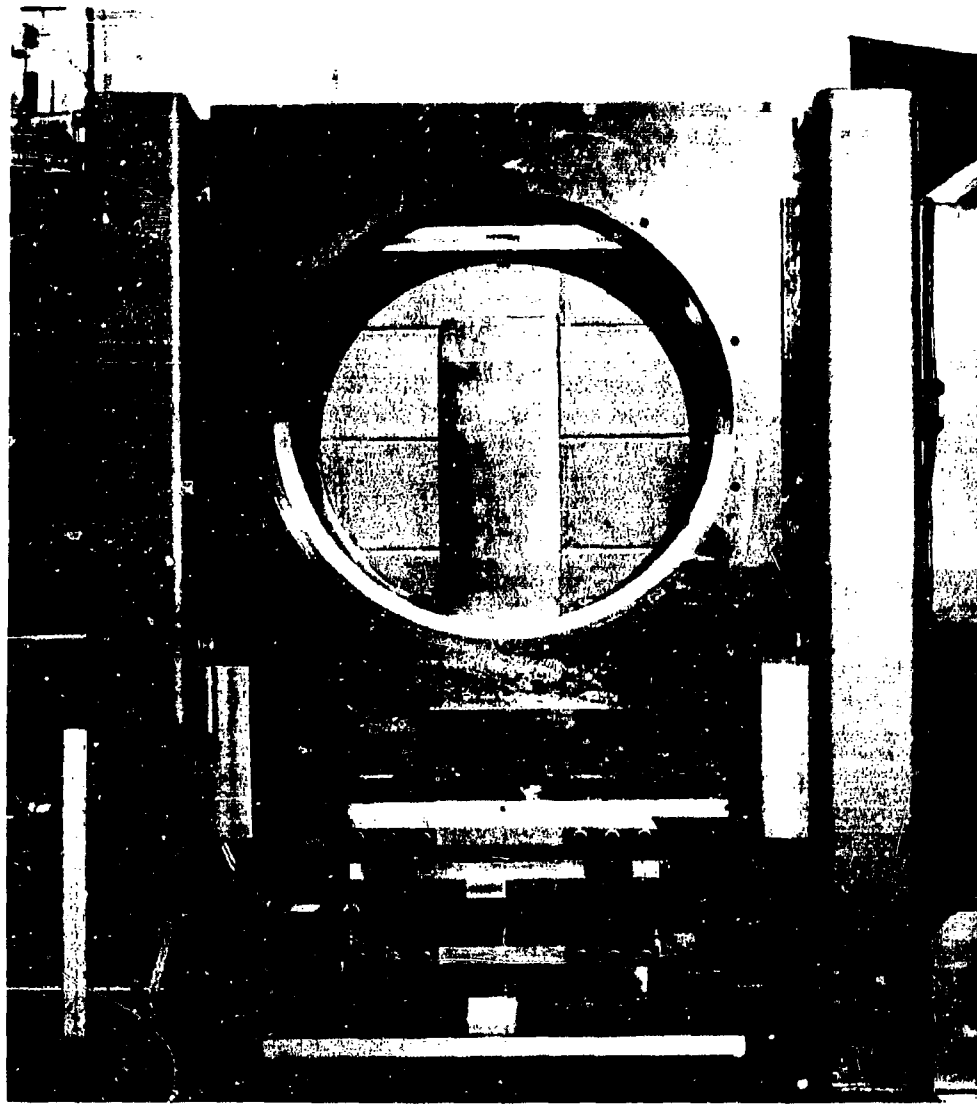
Figure 12. Model Installation in Wind Tunnel Test
Section (aspect ratio = 5.17)

fastened to a circular plate which could rotate through angles of attack from +20 to -20 deg. The latex was stretched from the plate and attached to the model in a way that prevented air from entering the test section from below the tunnel.

In choosing the material for a seal, it was necessary to minimize the possibility of force transmittal through the seal. The latex sheet chosen was thin and flexible enough to move with the model without affecting the force transmitted from the model to the balance system. This was ascertained by applying a known force to the tip of the model and obtaining the strain gage reading from the balance system. Using the same force applied directly to the balance system yielded the same strain gage reading, thus showing that the latex was not transmitting a force to or from the wing model.

The balance system was mounted below the test section as shown in Figure 12 at a height corresponding to a model aspect ratio of 5.17. The balance system was clamped to a table which stood on the floor of the wind tunnel room, forming a solid base. Several aspect ratios were attained by raising or lowering the support table. This arrangement avoided any possibility of the balance system reacting to vibrations in the wind tunnel support beams. Careful examination of the balance system preparation was undertaken to ensure that the interpretation of measured forces was accurate.

The direction of measured forces is determined by the alignment of the balance system, as can be seen from the balance table configuration (Figure 7). While misalignment of the balance table cannot create significant error in lift readings, the relatively small drag readings can be influenced by a small position error. If the balance table was aligned such that some small component of lift was read by the drag reeds, it could be a significant portion of the drag force read. Thus, great care was taken to arrange the force balance table to read only forces perpendicular and parallel to the free-stream direction. The alignment could be accurately completed to within approximately 1/2 deg, or a possible error of less than 0.9% of the lift being read by the drag strain gages. At L/D ≈ 10, for example, the drag error could be 9% and result in some uncertainty. However, the error introduced by this type of experimental difficulty remains constant and should not influence the qualitative interpretation of the drag results.

The drag readings should be carefully interpreted, since other sources of error are possible. The pressure lines used to supply high-pressure air to the wing model were stiff to avoid movement when pressurized and could transmit tunnel vibrations to the balance system. Since the drag forces are small in magnitude, the forces transmitted by the supply lines, although small themselves, could be noticed on the visicorder output. Zero shifts were noted in the drag bridge that were larger than those encountered in lift or moments readings and could have been caused by the supply line. Therefore, the validity of the drag readings were sometimes questionable.

22

The drag results used in the remainder of this report have been selected by eliminating those data points where visicorder readings were very small or zero shifts very large.

DATA REDUCTION

The primary force data was recorded on the Honeywell visicorder and reduced to lift, drag and moment using balance system calibration constants. These calibration constants were found by applying known loads and moments for four resistance settings on each of the decade resistance boxes.

The corresponding forces and moments were calculated by multiplying the calibration constants by the visicorder readings.

- Hose tare corrections were found to be negligible for the lift and moment readings, but a correction to the drag force was required.

- Wind tunnel corrections were made to the aerodynamic coefficients as outlined in References 12 and 13. No theoretical corrections have been derived for part span blown jet flap wind tunnel work. For short blown spans, where loading is not elliptic, the corrections are only a small percentage of the measured forces, and therefore, have a negligible effect.

TEST PROCEDURE

The experimental tests conducted in Honeywell's low-speed wind tunnel were designed to determine the lift effectiveness of a jet blowing at the trailing edge of a finite-aspect-ratio wing model. Aspect ratios of 3.85, 5.17 and infinity were tested. An infinite aspect ratio was obtained by adding a wooden NACA 0012 airfoil section onto the finite model tip so that it would span the tunnel test section. Part-span blowing was available over the middle part of this model.

Wind tunnel tests were generally conducted in the following order:

1. The jet-flap wing model jet angle was fixed by installing one of the available sets of inserts.

2. The blown span length and position were selected, and any shims which were to be used were inserted into the appropriate slot position.

23

3. The model was set at the desired angle of attack, and balance force readings were zeroed.

4. The tunnel was run at a selected speed, and data was recorded for a series of jet blowing thrusts; some thrusts were repeated to establish the validity of the data.

5. All pertinent temperature and pressure data were recorded, and the model static pressures were photographed from the manometer board during tunnel operation.

Both before and after the tests the calibration, hose tares, and possible interference effects were checked. All these factors were found to remain constant during the wind tunnel experiments. A total of approximately 320 test runs were completed.

RANGE OF TESTS

Tests were conducted in the following ranges:

- Wind tunnel velocity

    $70 \leq V \leq 170$ mph

- Jet flap angles

    $26 \leq \tau \leq 55$ deg

- Angle of attack

    $-8 \leq \alpha \leq 8$ deg

- Blowing coefficient

    $0 \leq C_{\mu_T} \leq 0.4$

24

SECTION IV
TEST RESULTS AND DISCUSSION

INFINITE ASPECT RATIO

Initially, infinite-aspect-ratio tests had not been scheduled for this investigation. However, for completeness, it was decided to determine the model characteristics at infinite aspect ratio to see if lift, moment and drag values differed from those of earlier infinite-aspect-ratio tests. The model geometry was somewhat different from previous VDT models (Ref. 1 and 2) because of the shape of the model trailing edge [Figure 1(a)]. Due to the insert shape the wing model of this investigation was not perfectly symmetrical but should have been adequate for differences to be evaluated. Therefore, a brief investigation of the wing model's two-dimensional characteristics was conducted.

The unblown ($C_\mu = 0$) lift, moment and drag results are shown in Figures 13, 14 and 15. Referring to Figure 13, it is seen that the lift coefficient agrees well with theoretical results, as was the case for the wing models in References 1 and 2. For a symmetrical airfoil section the quarter-chord moment coefficients should be approximately zero for angles of attack below stall. Figure 16 shows the wing model moment coefficients closely resemble those of a symmetrical airfoil. The drag results presented in Figure 15 are compared with the results for a truncated VDT airfoil (Ref. 6) and the standard NACA 0012 airfoil (Ref. 14). It is seen that both jet flap models exhibit a higher drag coefficient than the sharp trailing edge NACA 0012.

Figure 15 also shows that some difference exists between the present drag results and those of Reference 6. The jet-flap model constructed for the finite-aspect-ratio tests displays some asymmetry about the C_D axis, exhibiting more drag at the positive angles of attack. This asymmetry is probably a result of the trailing edge configuration. It appears that the insert trailing edge acts as a flap deflected positively at some small angle and produces more drag at positive α's than at negative α's. This effect is due to small deviation in trailing edge symmetry and has no noticeable effect on the lift measurements. The influence of this trailing edge configuration is retained in all test results.

The two-dimensional tests were conducted at two wind tunnel velocities, 120 mph and 130 mph, corresponding to a Reynolds number of approximately 4.5×10^5. It is expected that large variations in the Reynolds number will influence the drag results, and this was investigated briefly at a finite aspect ratio.

Some photographs of the manometer board were taken to check the pressure instrumentation. A typical chordwise pressure distribution is shown in

25
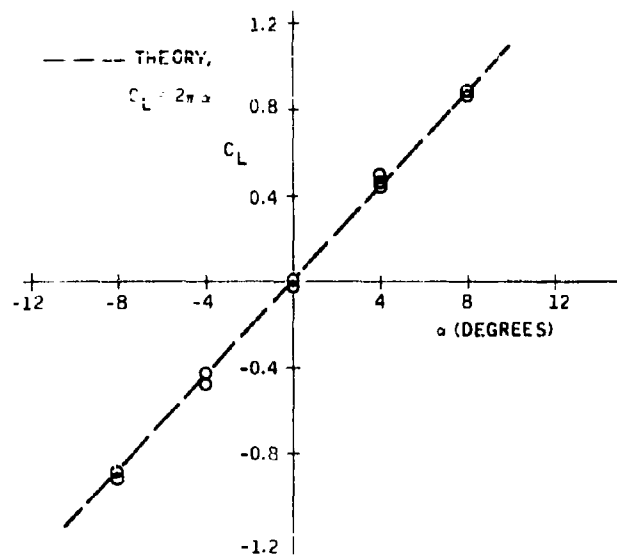
Figure 13.   Infinite-Aspect-Ratio, No-Blowing
Lift Characteristics
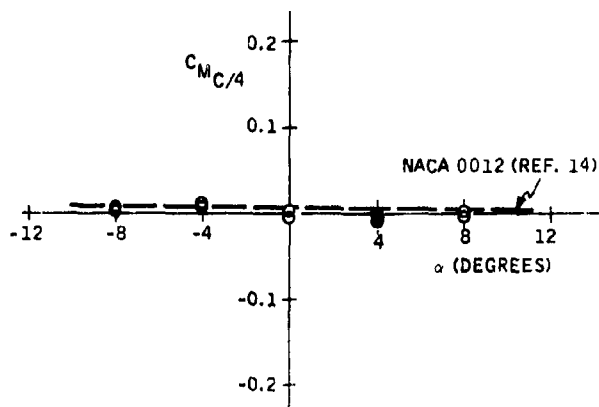
Figure 14.   Infinite-Aspect-Ratio, No-Blowing
Moment Characteristics

26
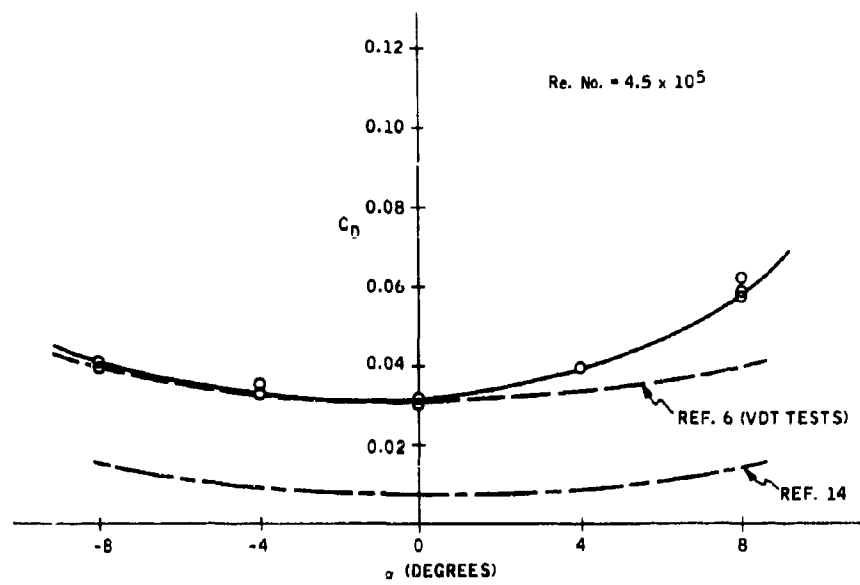
Figure 15. Infinite-Aspect-Ratio, No-Blowing Drag Characteristics
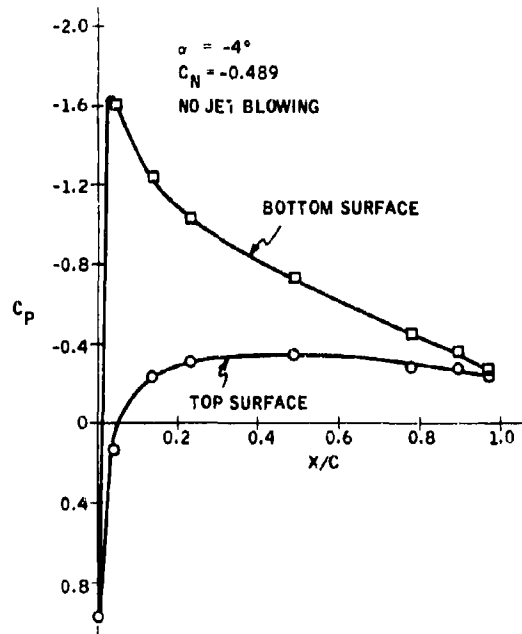
Figure 16. Chordwise Pressure Distribution for Jet-Flap Modified 0012 Airfoil

Figure 16 for the model at $\alpha = -4$ deg and $C_\mu = 0$. This distribution was integrated to obtain the normal force coefficient at a spanwise station 46% of the tunnel span measured from the tunnel floor.

As mentioned earlier, the wing model was instrumented with pressure taps at several spanwise stations (see Figure 4) on both the top and bottom airfoil surface. In an attempt to determine the spanwise lift distribution, these taps were located at approximately the midchord position. The midchord pressure difference between the top and bottom airfoil surface is directly proportional to the lift for two-dimensional jet-flap airfoils. This has been verified both experimentally (Ref. 6) and theoretically, using Kuchemann's method as described in Reference 15. The experimental results presented in Figure 17 show that the relationship holds true for this jet-flap model.
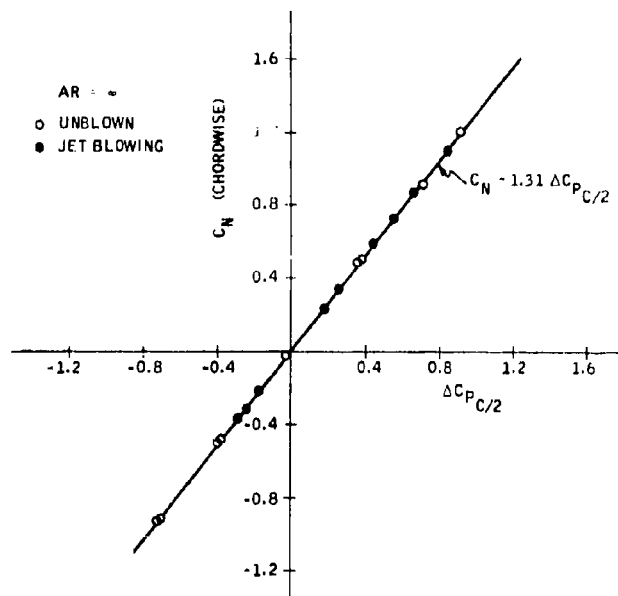
Figure 17. Correlation of Midchord Pressure Difference to Normal Wing Force

The spanwise pressure tap readings were reduced and plotted versus their spanwise position as shown in Figure 18. As expected, the spanwise distribution of the midchord pressure difference is constant; implying that a constant lift distribution prevails. Since the lift measured at the 0.46 span station represents the C_L of the entire wing, it can be compared to the balance system lift coefficient. The two measurements are compared in Figure 19. It is noted here that the force coefficients given in Figures 16 through 19 are uncorrected for tunnel interference effects.

23
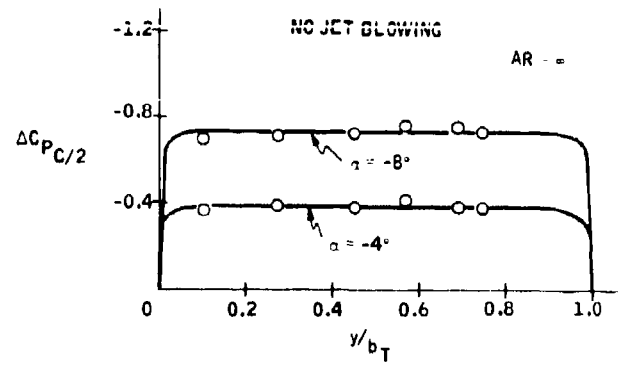
Figure 18. Spanwise Distribution of Midchord
Pressure Difference
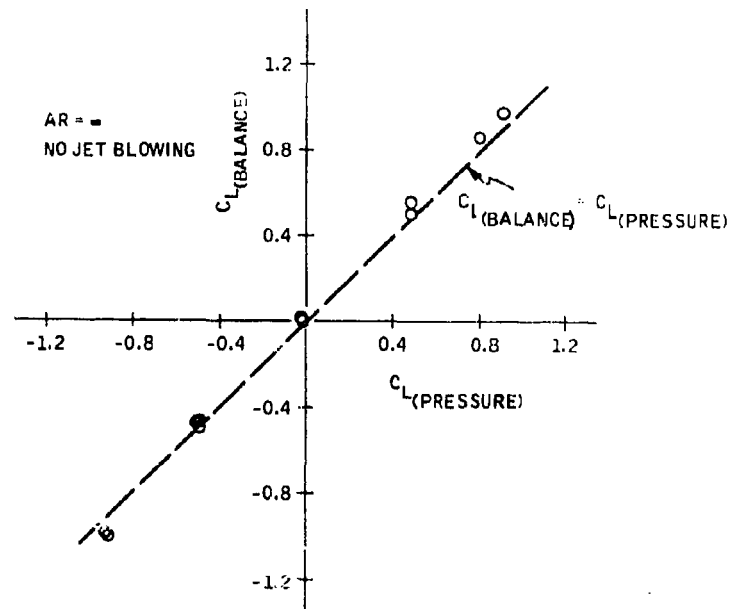
Figure 19. Comparison of Pressure Lift to Balance Lift

Since the model was initially designed for finite-aspect-ratio tests only, provision for two dimensional full-span blowing was not included. However, a series of tests were made at a jet angle of 40 deg for insert numbers 1, 2 and 3 (see Figure 4) blowing. The blown span extended from 0.31 y/b_T to 0.77 y/b_T, a total of 46% of the tunnel span.

The chordwise pressure taps lie in the blown span at 0.46 y/b_T, and a typical pressure distribution at this station is shown in Figure 20. Due to the restricted size of the model, the last 3% of the chord could not be instrumented with surface pressure taps. Accordingly, the lift on the last 3% of the chord was approximated by 0.75 C_μ sin $(\alpha + \tau)$. Since the blowing coefficients obtained in these tests were small, the added term had little effect on the total lift coefficient. As was seen in Figure 17, normal force coefficients at the chordwise pressure tap location can be estimated using $C_N = 1.31 \Delta C_{p_c/2}$

for the blown runs as well as the unblown runs. For the range of the current tests, $C_L \approx C_N$.

It is assumed that the normal force can be obtained from the midchord pressure difference independently of the span station. Figure 21 is included to show the result of this assumption. Although the spanwise taps are insufficient to determine the full-span distribution, the figure indicates the change in lift over the span. One curve in Figure 21(b) has been extrapolated over the entire span in a manner such that the integrated distribution results in a normal force coefficient approximately equal to that obtained from the balance system. This distribution indicates that the entire span is influenced by the blown section. The data is not complete enough to adequately analyze this result. The effect of part-span blown sections on neighboring unblown sections is further discussed in the subsections on the finite-aspect-ratio results.

It can be concluded that the three-dimensional effects decrease the peak of the lift distribution over the blown section of the wing. This result is similar to that reported in Reference 6 where, at $C_\mu = 0.3$, the lift produced when blowing one-third span was found to be 34% lower than full-span two-dimensional blowing. The two-dimensional theoretical lift distribution peak is shown for one test case in Figure 21(b).

The part-span blowing lift results are shown in Figure 22. The lift coefficient is that obtained from the balance system for the entire wing.

ASPECT RATIO 5.17

Unblown Results

The basic non-blowing airfoil characteristics are given in Figures 23 through 25. The results are from balance measurements as are all experimental results unless specifically designated to be pressure data.

30
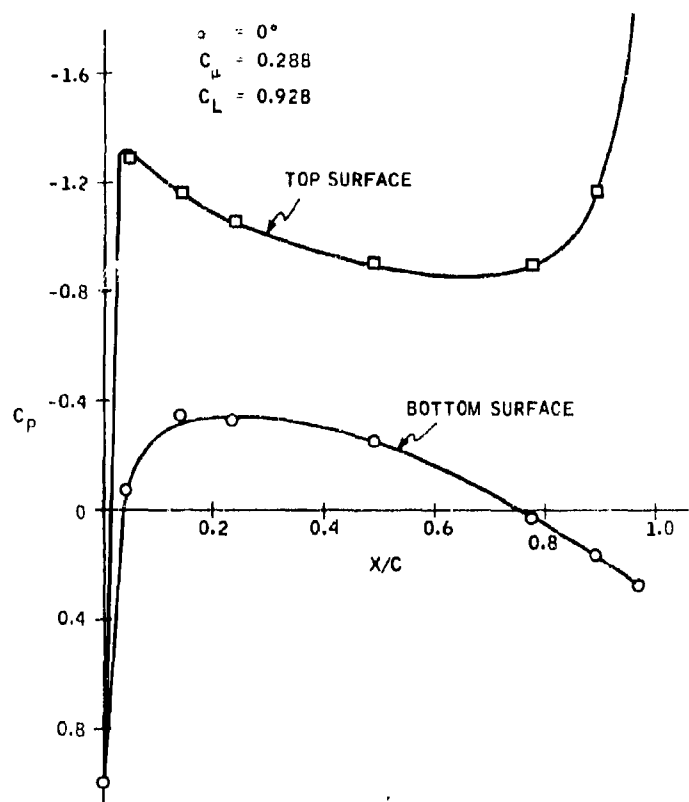
Figure 20. Chordwise Pressure Distribution, Infinite-Aspect-Ratio Wing with Blowing
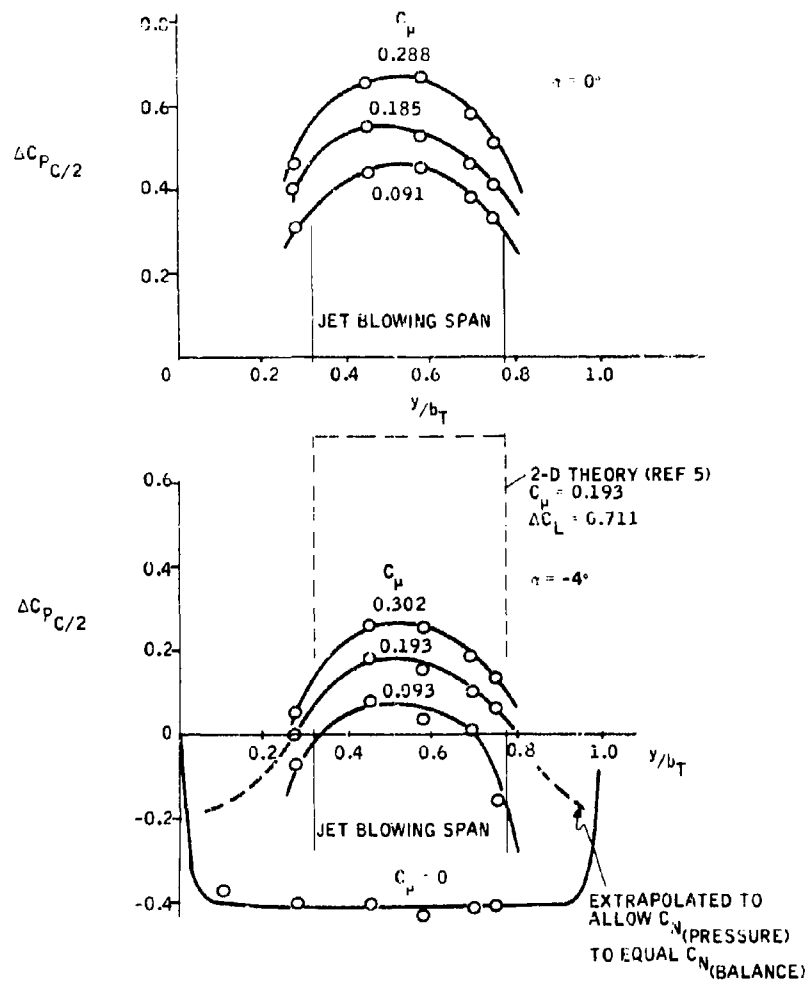
Figure 21.   Spanwise Midchord Pressure Distribution,
             46% Blown Span, Infinite-Aspect-Ratio Wing
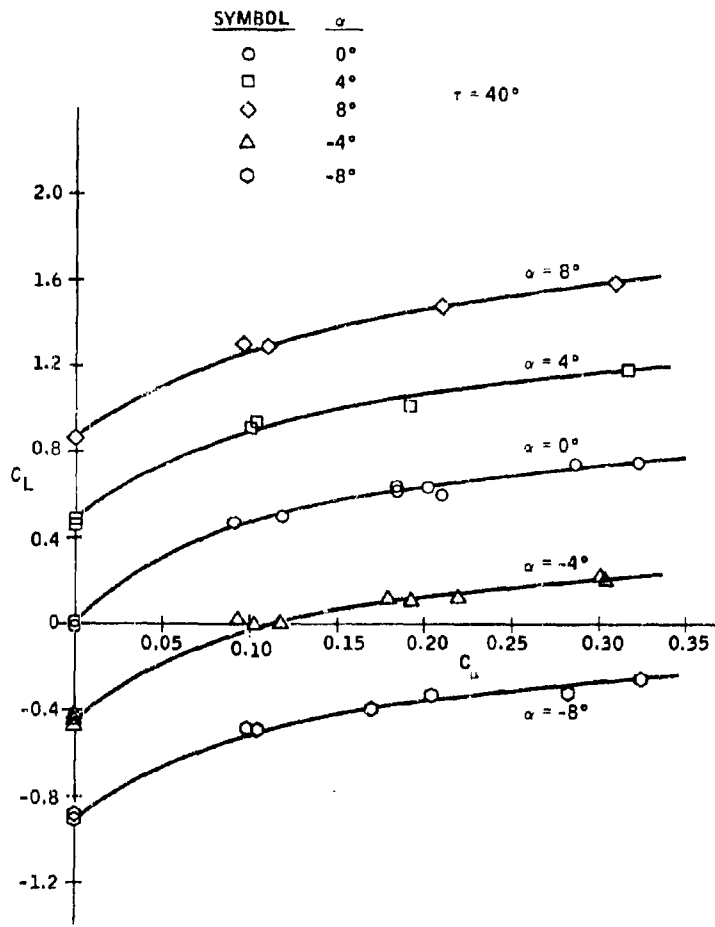
Figure 22. Lift of a Part-Span-Blown Infinite
Wing Model

33

Figure 24. Aspect Ratio 5.17, No Blowing Moment Characteristics

Figure 23. Aspect Ratio 5.17, No Blowing Lift Characteristics

34

Figure 23 compares the truncated jet-flap model lift to that predicted from three-dimensional theory. For the angle-of-attack range tested, the experimental unblown lift coefficients agree with the theoretical lift coefficients.

The jet-flap drag is presented in Figure 25 where changes in the Reynolds number are shown to affect the unblown drag curves. The model chord length and low wind tunnel speeds restricted the Reynolds number to values far below full-scale Reynolds numbers. Figure 26 shows that the zero-lift drag (C_{D_o}) is close to the NACA 23012 minimum drag at the very lowest Reynolds number tested and that, beyond a Reynolds number of 4×10^5, the model drag characteristics indicate that transition Reynolds numbers were tested. The NACA 23012 characteristics were obtained from Reference 16, where it is pointed out that below Reynolds numbers of approximately 1.5×10^6 the drag values are too irregular for extrapolation to full-scale. Thus, the current drag values should not be applied to full-scale wings.

No measurable Reynolds number effect on the lift coefficient can be determined for the angles of attack tested.

Pressure Data

For the model at aspect ratio 5.17, the chordwise pressure taps were located at a station 56% of the span from the root chord. At this location the pressure distribution was integrated to obtain the local normal force on the model. Figures 27 and 28 present typical pressure distributions for the unblown wing and for the full-span blown wing. The pressure difference at midchord was again plotted versus the normal force coefficient. Figure 29 indicated that the normal force coefficient is given by $C_N \approx 1.38 \, \Delta C_{pc/2}$.

Using the relation $C_N = 1.38 \, \Delta C_{pc/2}$ over the entire span of the wing, a pressure-calculated normal force was obtained at each of the midchord pressure tap locations. The resulting normal forces were resolved to lift forces which were integrated over the wing span to obtain the total lift coefficient. A typical unblown distribution obtained from the pressure data is compared to the theoretical lift distribution (Ref. 17) in Figure 30. The theoretical unblown lift distribution was integrated, and it was found that the balance-measured lift agrees with the theoretical lift. (This was shown in Figure 23.) Figure 30 shows the pressure data lift distribution falls below that predicted from theory. This was found to hold true for the blown test cases as well as the unblown tests. The balance lift data is compared to the pressure lift data in Figure 31 where it is seen that balance lift is always about 20% higher than the pressure-calculated lift.

From a few chordwise pressure distributions at various span locations on a wing of AR = 2.75, (Ref. 9) it was found that $C_N / \Delta C_{pc/2} \approx 1.39$ at $y/b = 0.20$
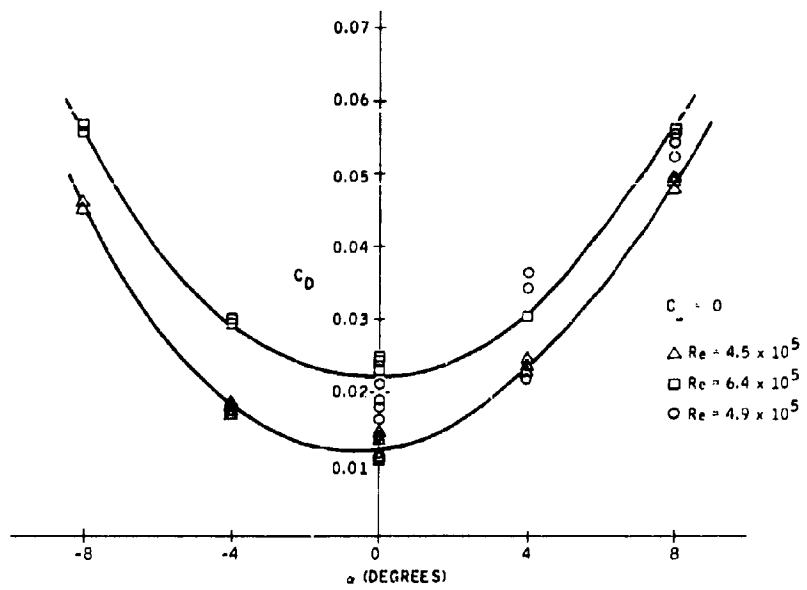
Figure 25. Aspect Ratio 5.17, No Blowing Drag Characteristics
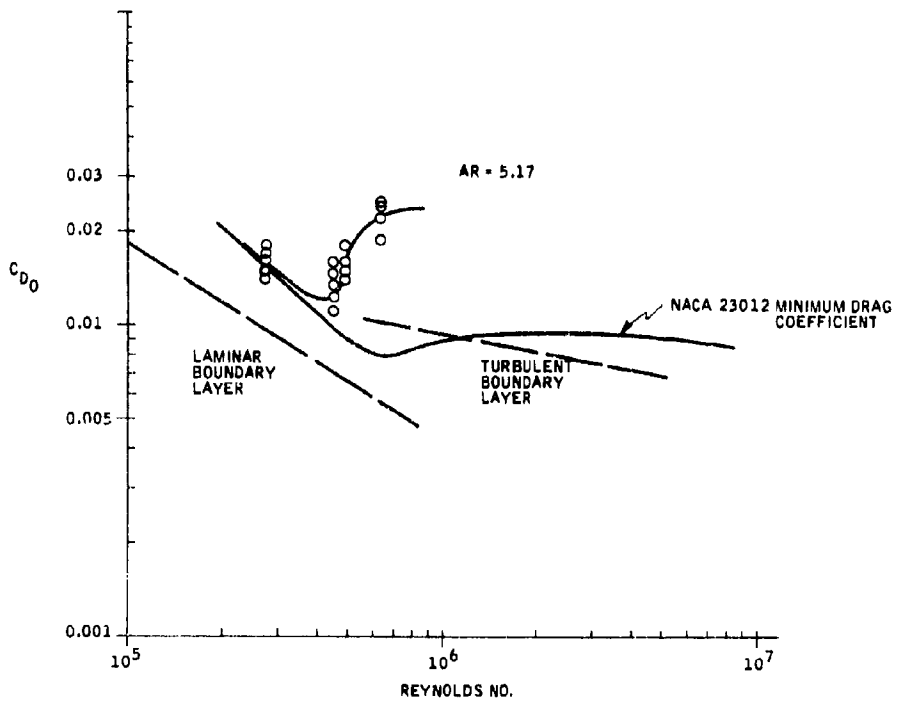
Figure 26. Reynolds Number Effect on Zero-Lift Drag
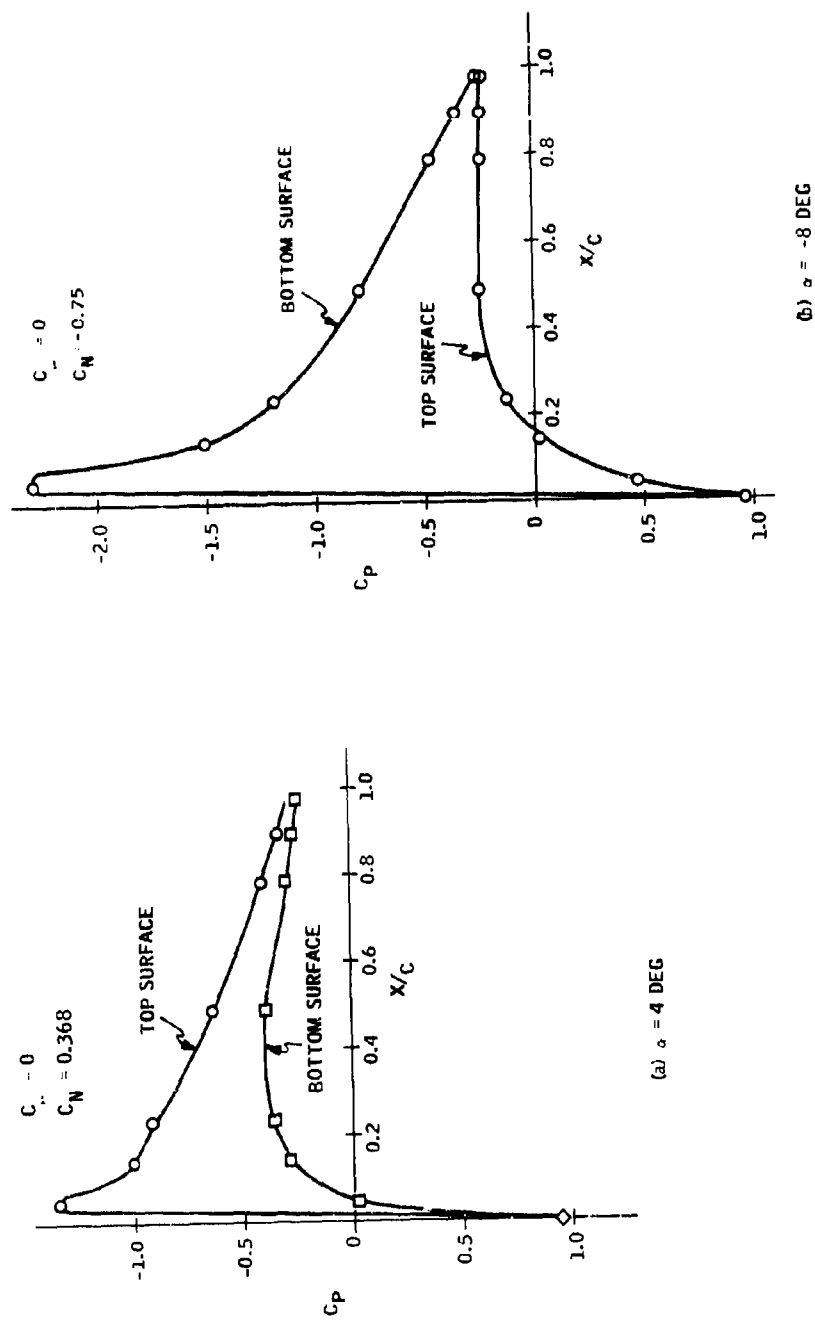
Figure 27. Chordwise Pressure Distribution of Unblown Aspect
Ratio 5.17 Wing
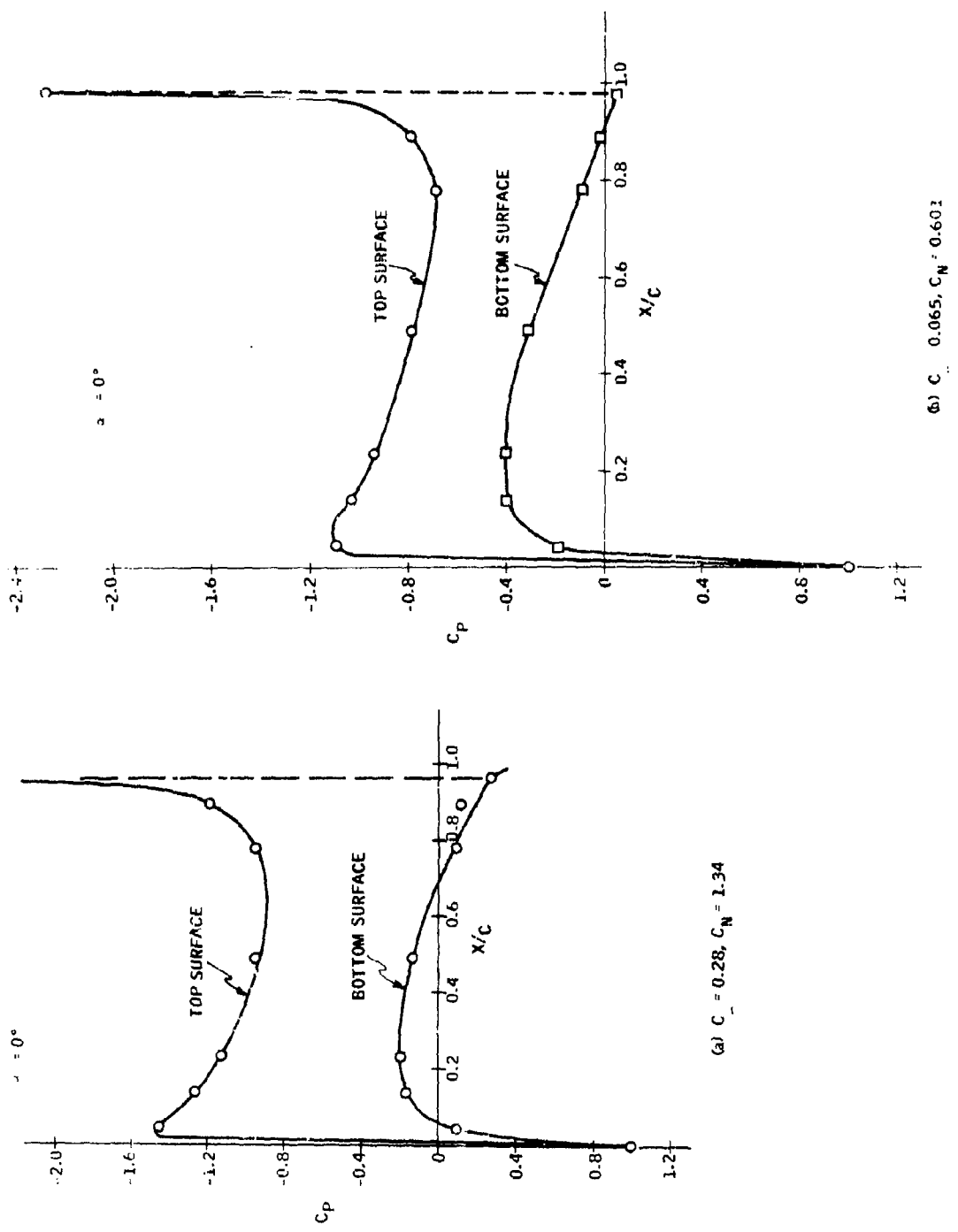
37

$\alpha = 0°$

TOP SURFACE

BOTTOM SURFACE

C_P

$X/_C$

(b) C_μ 0.065, C_N = 0.602

$\alpha = 0°$

TOP SURFACE

BOTTOM SURFACE

C_P

$X/_C$

(a) C_μ = 0.28, C_N = 1.34

Figure 27.   Chordwise Pressure Distribution of Blown Aspect
Ratio 5.17 Wing

38
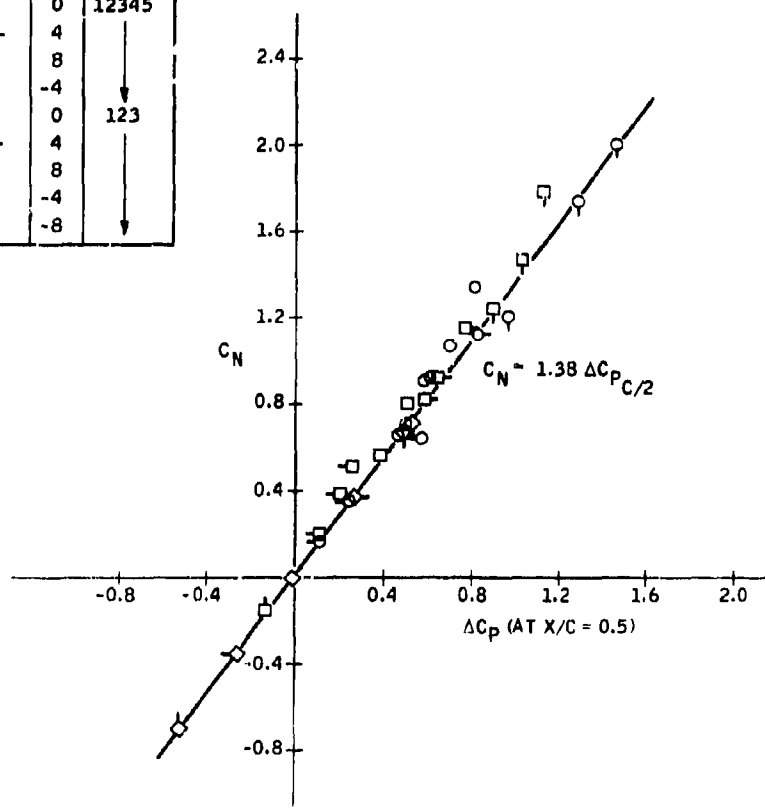
Figure 29. Midchord Pressure Difference versus Normal
Force of Aspect Ratio 5.17 Wing
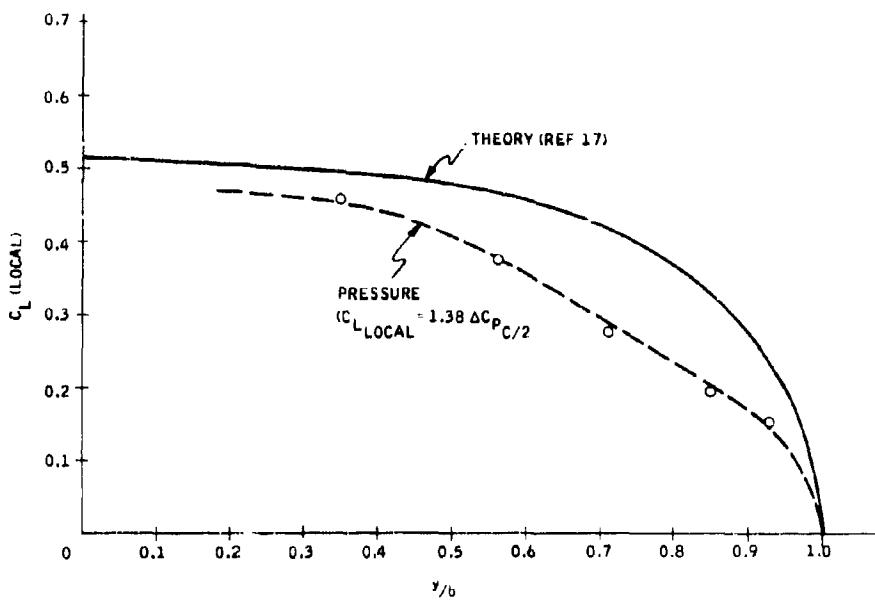
Figure 30. Spanwise Lift-Force Distribution of Unblown Aspect Ratio 5.17 Wing
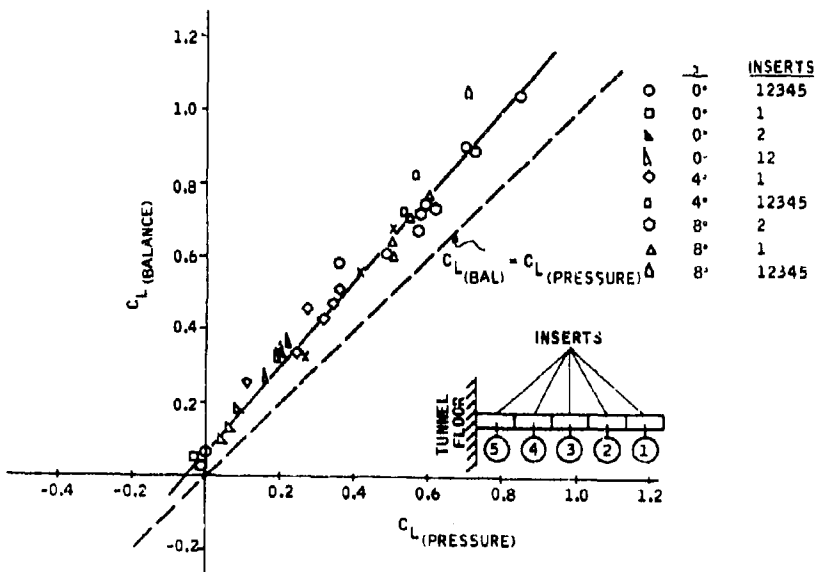
Figure 31. Comparison of Balance and Pressure Lift of Aspect Ratio 5.17 Wing

40

and $C_N/\Delta C_{p_{c/2}} \approx 1.70$ at $y/b = 0.95$, implying that the slope $C_N/\Delta C_{p_{c/2}}$ varies along the span.

In previous VDT studies (Ref. 6), a control system was designed to operate by sensing lift at the half-chord position of a two-dimensional airfoil. From the current experimental results and those of Reference 9, lift sensing on three-dimensional airfoils can not be done as simply as this. In order to study these three-dimensional effects, a large model incorporating chordwise pressure taps at several spanwise stations should be wind tunnel tested at finite aspect ratios.

The pressure data from the wind tunnel tests of this phase of the NEMS development must be interpreted with the above results in mind. Although there is some disagreement between the pressure and balance data, the mid-chord distribution is indicative of the lift distribution. The shape of the lift distribution can be identified and the midchord pressure difference is valuable in evaluating the effect of blown sections on neighboring unblown sections.

Full Span Blowing

The spanwise distribution of lift indicated by the pressure distribution (see Figure 32) is nearly elliptic in shape. Thus, the distribution is similar to that obtained for an unblown wing at angle of attack. This elliptic loading is consistent with the theoretical analysis for full span jet flaps (Ref. 8). The experimental jet blowing actually extends over 93% of the span, but will be referred to as full-span blowing throughout this report.

The total lift coefficient at $\alpha = 0$ deg is plotted against C_μ in Figure 33 for jet angles of 40 and 55 deg. The theoretical values (Ref. 8) are also plotted. Throughout the range of blowing coefficients tested, the experimental results at AR = 5.17 are higher than the theoretical results. This finding was true for previous finite-aspect-ratio investigations also. Reference 9 reported that the experimental lift for a jet angle of 30 deg at $\alpha = 0$ deg was reasonably close to $C_L / 1.4\, C_\mu^{1/2}$ at AR = 2.75 for blowing coefficients, $C_\mu < 1.0$. Theoretical calculations (Ref. 8) indicate that $C_L \approx 1.15\, C_\mu^{1/2}$ for the conditions stated in Reference 9. Therefore, these experimental results give higher lift values than theory would indicate. Curves of C_L versus C_μ for other angles of attack and a jet angle of 40 deg are grouped in Figure 34.

Effect of Part Span Blowing

The total lift coefficient is plotted against the blowing coefficient C_μ in Figures 35 through 38. The theoretical curves use the tentative method of analysis presented in Reference 11 to account for the part-span effects.

41
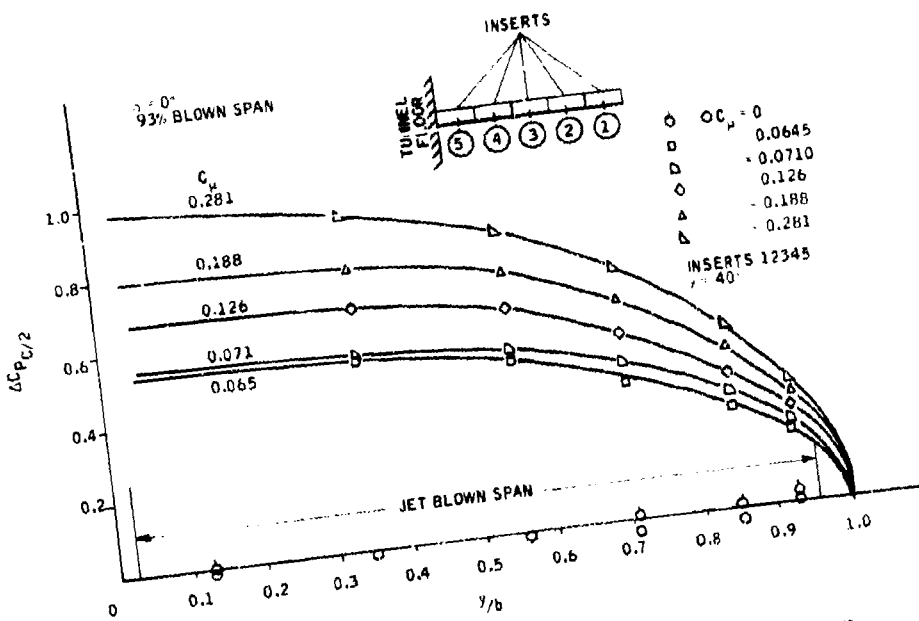
Figure 32. Spanwise Pressure Distribution of Blown Aspect Ratio 5.17 Wing
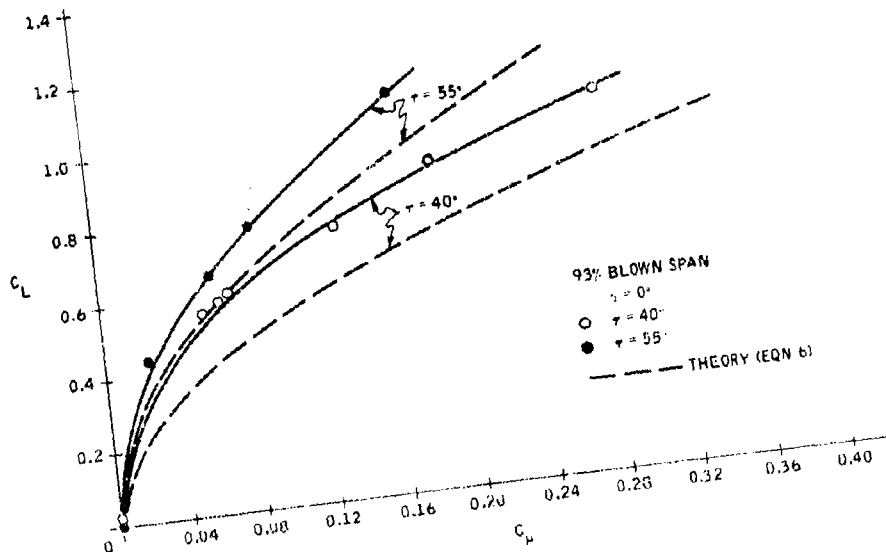
Figure 33. Lift Force of Blown Aspect Ratio 5.17 Wing for Two Jet Angles

42
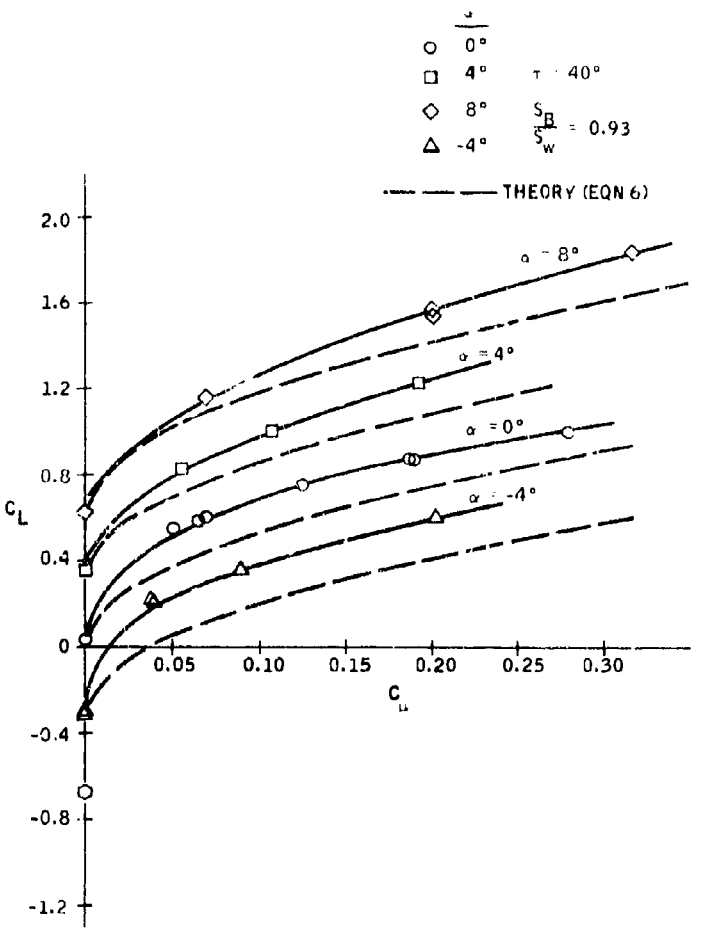
Figure 34. Angle-of-Attack Lift Variation of a
Blown Aspect Ratio 5.17 Wing
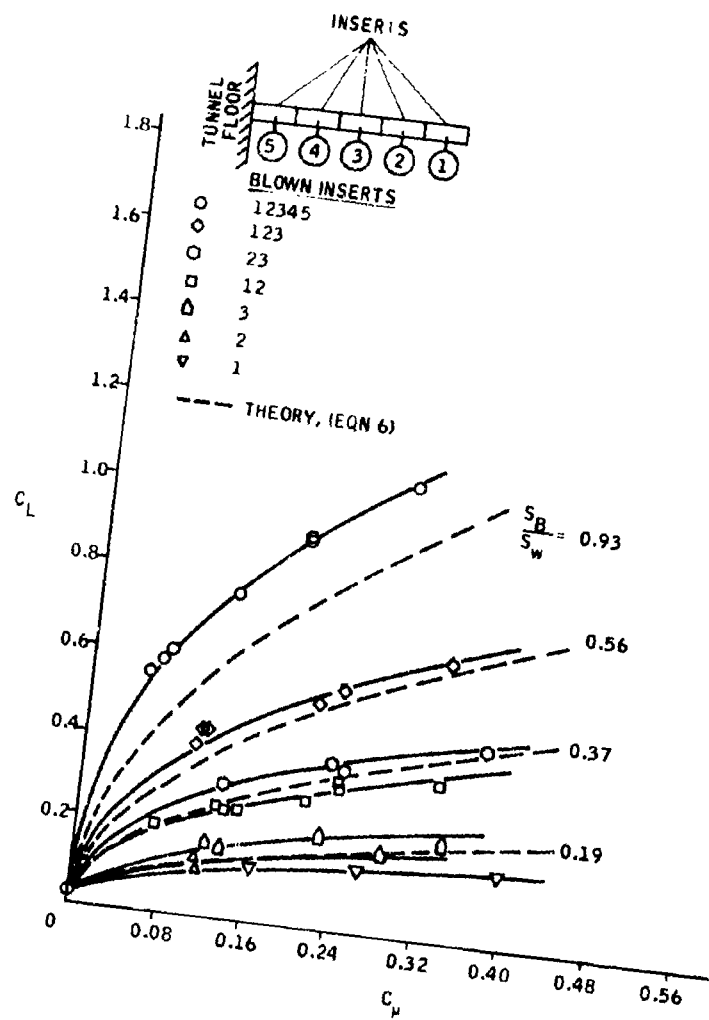
Figure 35.   Effect of Part-Span Blowing on an Aspect Ratio 5.17
Wing at α = 0 deg, τ = 40 deg

44
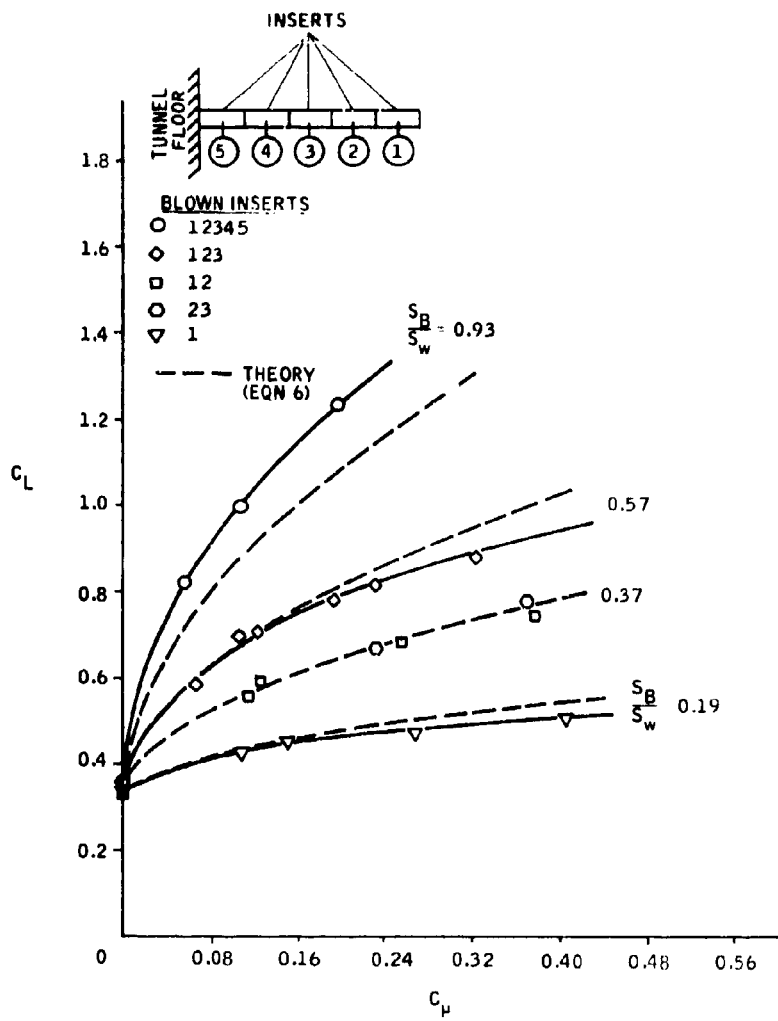
Figure 36.   Effect of Part-Span Blowing on an Aspect Ratio 5. 17
Wing at α = 4 deg, τ = 40 deg

45
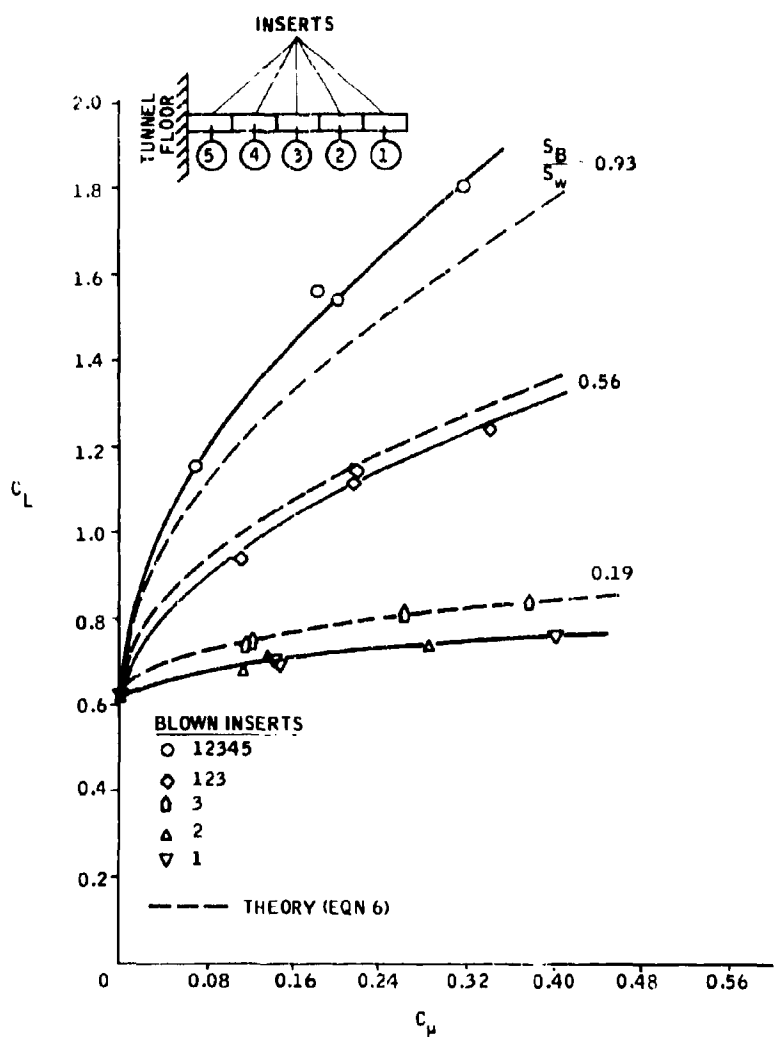
Figure 37.   Effect of Part-Span Blowing on an Aspect Ratio 5.17
Wing at α = 8 deg, τ = 40 deg

46
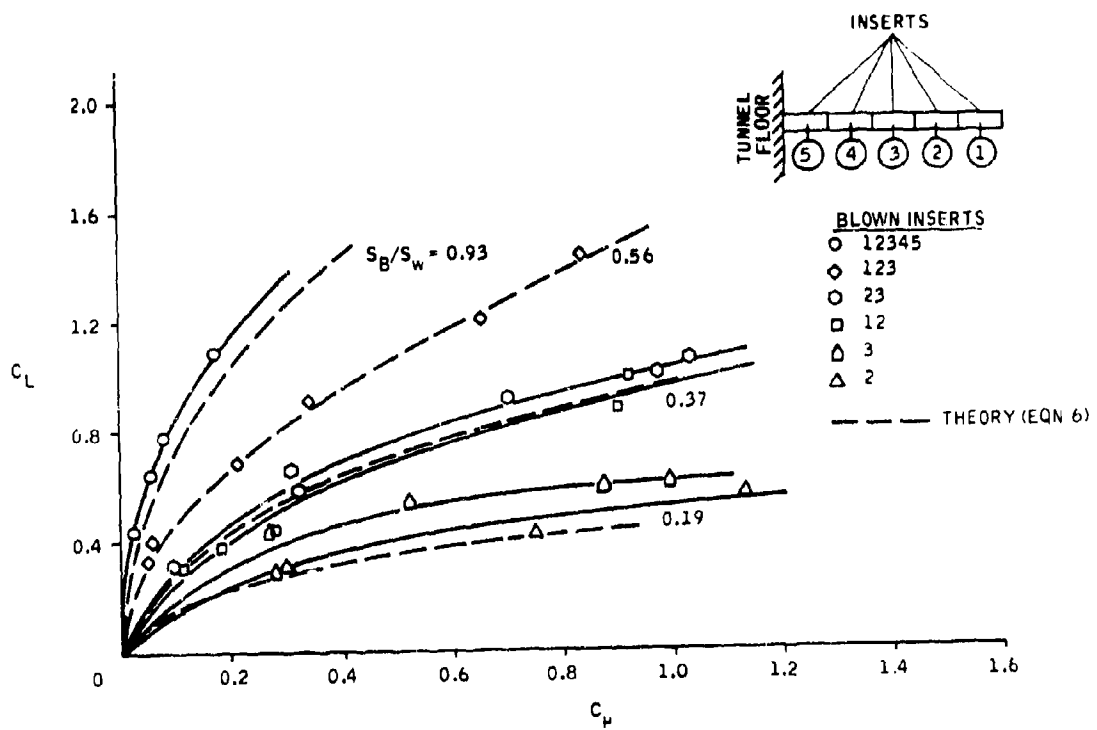
Figure 38. Effect of Part-Span Blowing on an Aspect Ratio 5. 17
Wing at α = 0 deg, τ = 55 deg

47

These curves seem to give a reasonable estimate of the lift obtained from the various part span blowings.

Where the data is sufficient to allow a comparison, it appears that the position of the jet blowing influences the lift results. Referring to Figure 35, for example, at $S_B/S_W = 0.37$, inserts 2 and 3 create more lift than inserts 1 and 2 at the same C_μ. A similar comparison made at $S_B/S_W = 0.19$ indicates that insert 3 creates more lift than insert 2 and insert 2 results in slightly higher lift than insert 1. Thus, the experimental results indicate that the further inboard a blown area is located, the higher the lift is which can be attained for a given C_μ. Part-span blowing results given in Reference 18 reinforce this conclusion. Figure 39 from Reference 18 shows the configurations tested and the test results. The results cannot be directly compared to the results of this investigation because the model of Reference 18 used a small trailing-edge flap (0.10 c) to direct the jet sheet. The blowing configurations of Reference 18 all had the same blown area, and it is again indicated that the lift is increased for inward shifts of the blown section.

When jet flaps are to be used in place of aircraft ailerons, the rolling moment produced by a given thrust is a more valuable measure of jet-flap capabilities than the lift produced. For a full-span jet-flap the rolling moment may be theoretically derived assuming an elliptic lift distribution. The semi-span rolling moment due to full span jet blowing can be estimated from

$$C_{M_r} = C_L \frac{(3-D)}{3\pi} \frac{4}{3\pi} \qquad \text{(eqn 10)}$$

Part-span rolling moments cannot be predicted, since no theory exists which considers the modified shape of the lift distribution.

The balance table could not measure experimental rolling moments, but, with some limitations, pressure data can be used for this purpose. Although the pressure data did not give acceptable lift results, it was found that the loading indicated by the pressure readings could be used to identify the shape of the spanwise lift distribution. These pressure distributions can then be used to find an approximate rolling moment about the root chord location. The rolling moment will not be numerically accurate, but can be used to establish the trends in rolling moment with varying blown spans. When blowing part span, it was found that the span position and blown area influenced the lift distribution as shown in Figure 40.

The blown sections seem to have a substantial effect on the adjacent unblown sections. Tuft studies conducted in Reference 18 allowed the investigators to observe strong trailing vortices at the edges of the jet sheet. These vortices exert their influence on the wing by altering the entire spanwise loading.

48
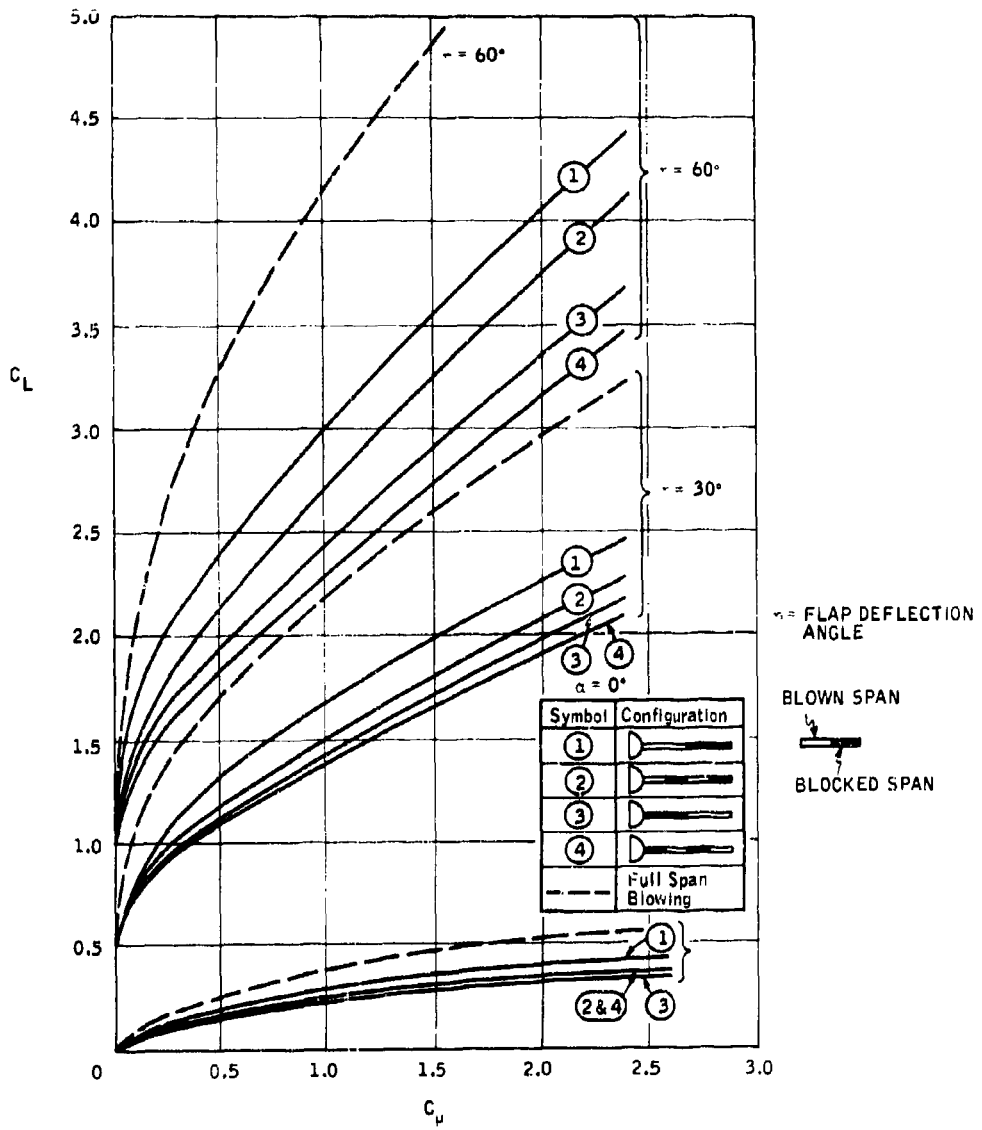
Figure 39. Lift for Part-Span Blowing with Full-Span
Flap, α = 0 deg (Ref. 18)

49

(a) INSERT NO. 1 BLOWING

(b) INSERT NO. 2 BLOWING

Figure 40. Spanwise Midchord Pressure Distribution

50
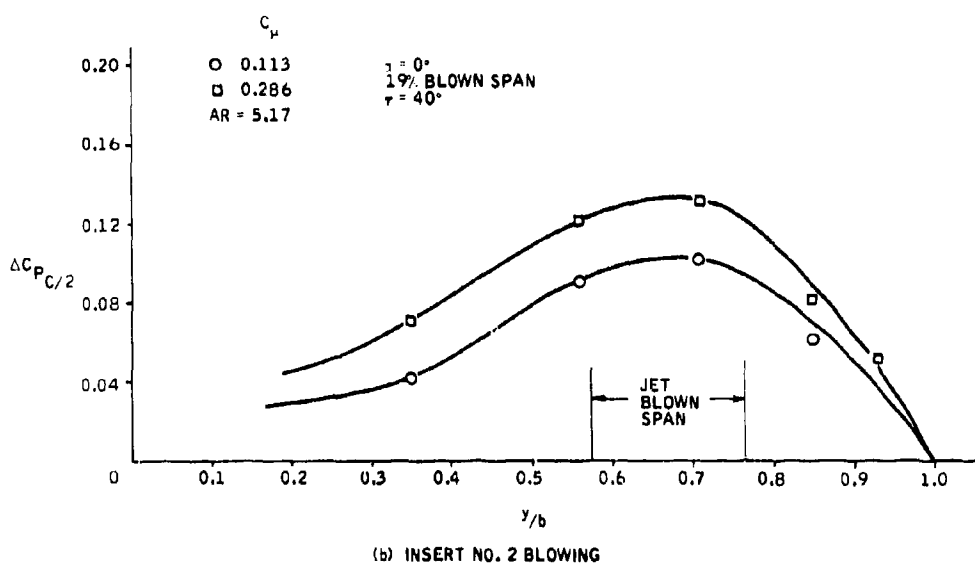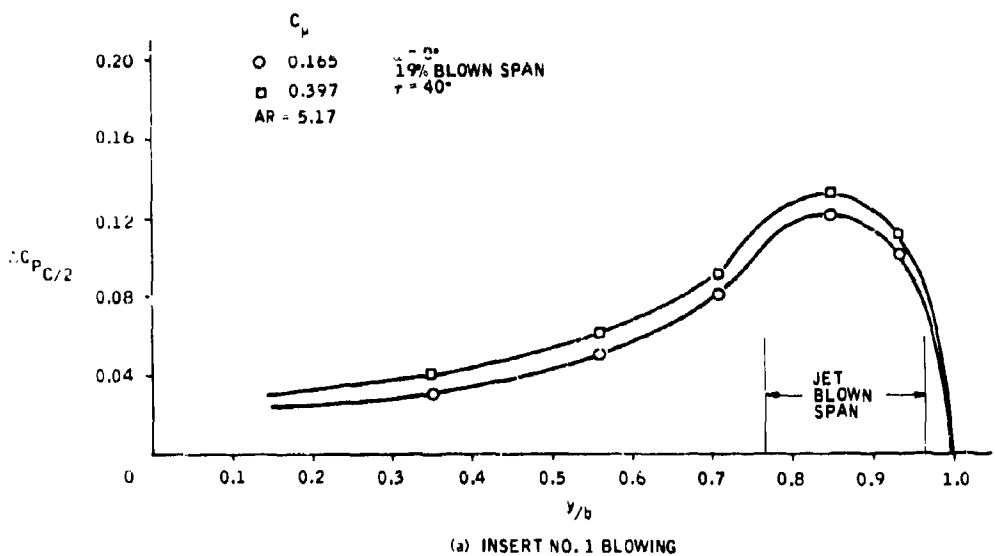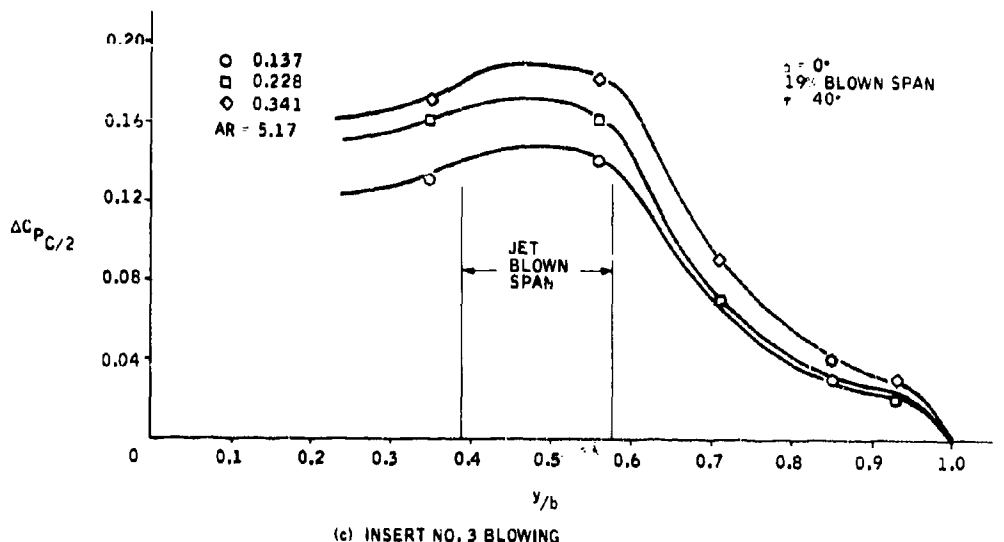
(c) INSERT NO. 3 BLOWING
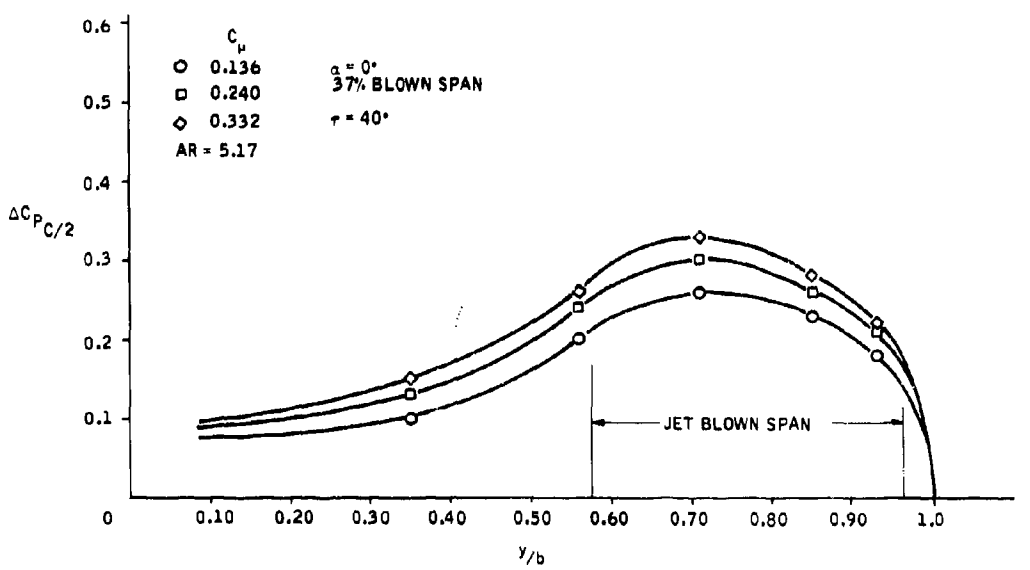
(d) INSERTS 1 AND 2 BLOWING

Figure 40. Spanwise Midchord Pressure Distribution (Continued)

51
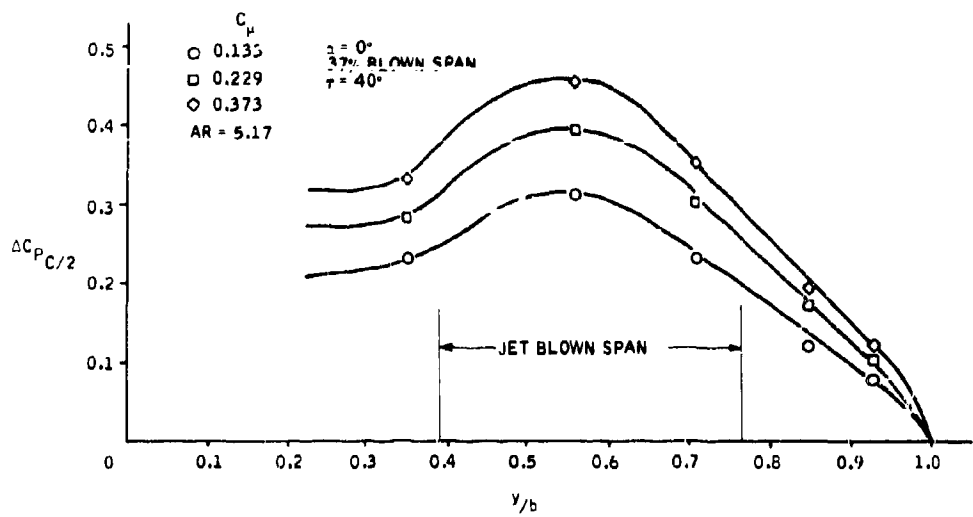
(e) INSERTS 2 AND 3 BLOWING
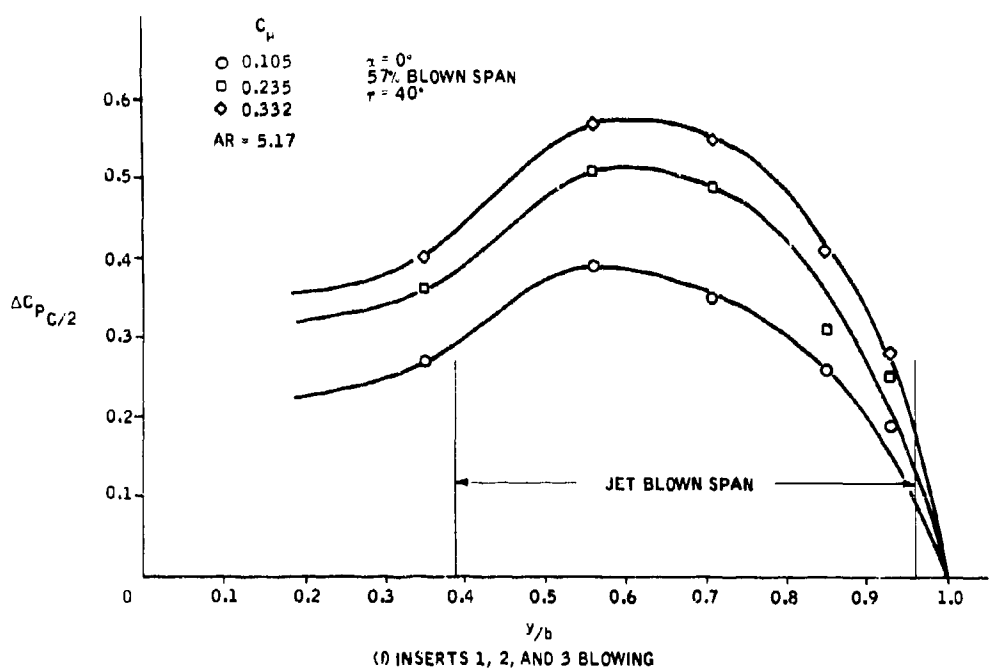
(f) INSERTS 1, 2, AND 3 BLOWING

Figure 40. Spanwise Midchord Pressure Distribution (Concluded)

The semi-span rolling moment was found by integrating the curves in Figure 40 according to the relation

$$C_{M_r} = \int_0^1 1.38 \, \Delta C_{p_{c/2}} \, (y/b) \, d(y/b)$$

The results for $\tau = 40$ and 55 deg are plotted in Figure 41 versus the blowing coefficient based on the total wing area (C_{μ_T}). C_{μ_T} is used instead of C_μ as it better facilitates comparison between the different blown spans. For a given thrust, the full-span blowing provided the highest rolling moment, and the rolling moment decreased as the area of the blown span decreased.

As was the case for the lift results, inserts 2 and 3 provide higher rolling moments than do inserts 1 and 2. However, at $S_B/S_W = 0.19$, no differences in rolling moment were noted between insert 1, 2 or 3.

The lift producing capability of jet-flap devices can be evaluated by the ratio of the lift due to blowing, ΔC_L, to the jet reaction lift, $C_{\mu_T} \sin (\tau + \alpha)$. This ratio is often called the "lift effectiveness" and indicates how much the lift component of jet thrust can be amplified. The experimental results are presented in Figures 42 and 43, for jet angles of 40 and 55 deg, respectively. The full-span blowing configuration is most "effective" at producing lift with a given thrust, and the "lift effectiveness" of jet blowing is diminished when the ratio of the blown area to the wing area is decreased.

The data presented in Figures 42 and 43 shows that the "lift effectiveness" becomes smaller as the blowing coefficient becomes larger. This means that the ratio of the circulation lift to the lift component of jet thrust is decreased for increasing jet thrust. If the thrust were increased to very large values, relatively little circulation lift would be produced. The value of $\Delta C_L/C_{\mu_T} \sin (\tau + \alpha) \leq 1.0$ when the thrust component of lift is the only lift produced. It is evident that the effectiveness of jet-flaps is limited when high blowing coefficients are required.

Pitching Moment

A curve of the quarter-chord pitching moment versus the lift at constant values of α is shown in Figure 44. The curves include all blowing positions and blown spans such that the variation in $C_{M_{c/4}}$ with with C_L is independent of the amount or position of jet blowing.

It is seen that the slope, $dC_{M_{c/4}}/dC_L$, of the curves at constant C_μ is approximately zero or slightly negative. The aerodynamic center is then
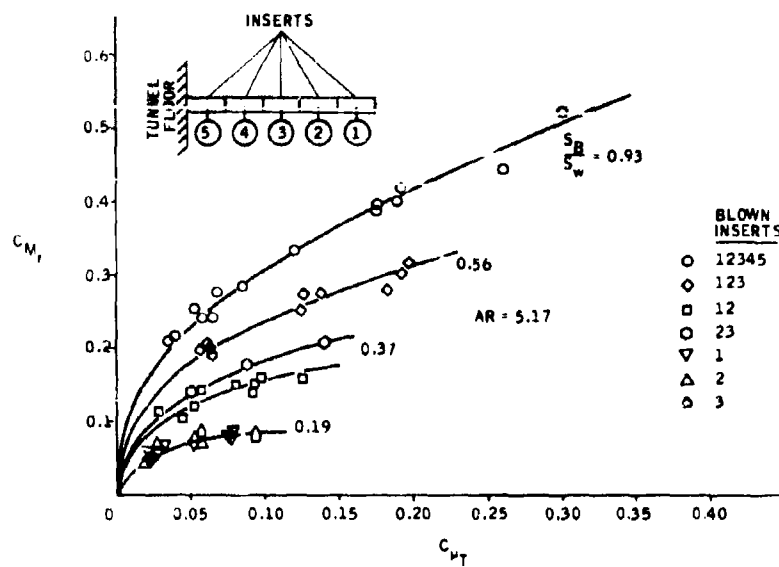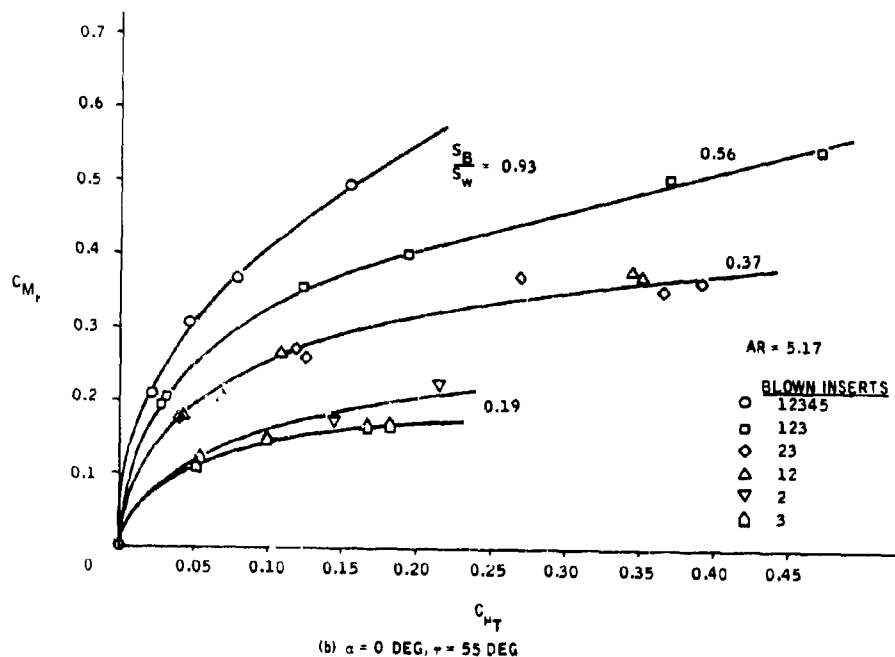
Figure 41.   Effect of Part-Span Blowing on
Rolling Moment

54
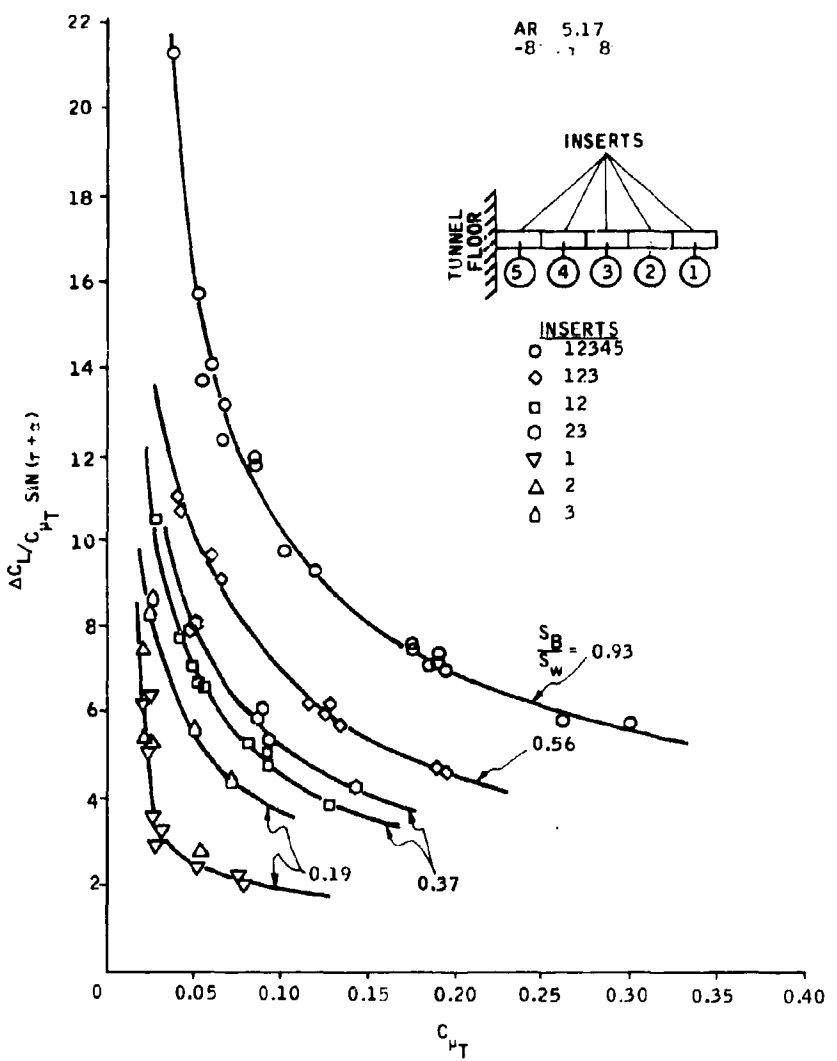
Figure 42. Effect of Part-Span Blowing on "Lift
Effectiveness" for $\tau = 40$ deg
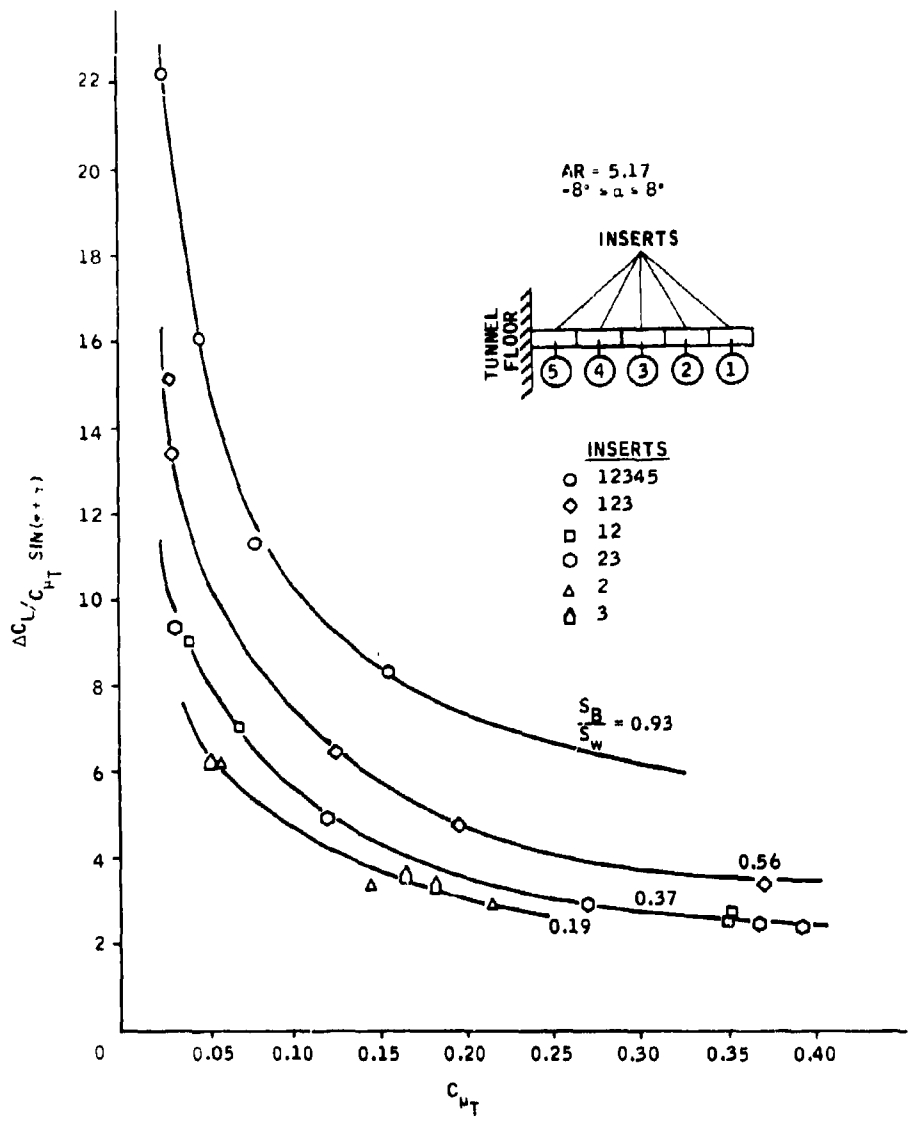
Figure 43. Effect of Part-Span Blowing on "Lift Effectiveness" for τ = 55 deg
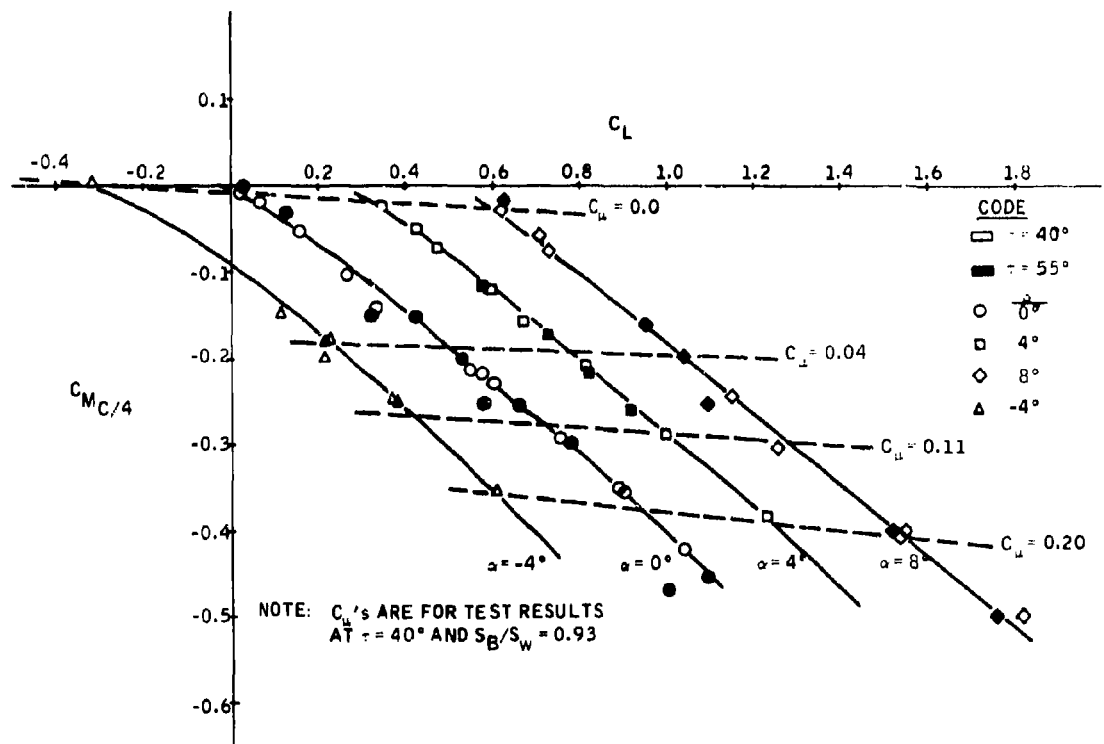
Figure 44. Quarter-Chord Pitching Moment and Lift Results
for Blown Aspect Ratio 5.17 Wing

located close to or slightly behind the quarter-chord position. $dC_{Mc/4}/dC_L$ may decrease somewhat as C_μ is increased, implying that the aerodynamic center moves aft as C_μ increases beyond the data of these tests.

As C_μ increases at constant α, the quarter-chord moment becomes increasingly negative because the induced lift is concentrated closer to the trailing-edge than the leading edge. Thus, the center of lift is moved rearward causing nose-down pitching moments. This is particularly important to the aircraft designer who must size the tail control to trim the plane when jet flaps augment the wing lift.

Drag

The drag coefficient of a jet-flap wing can be expressed as

$$C_D = C_{D_0} + K C_L^2 + \Delta C_D \qquad \text{(eqn 11)}$$

where C_{D_0} is the zero lift drag coefficient, K is the slope of the curve of C_D versus C_L^2 for the unblown wing and ΔC_D represents the recovered thrust.

Theoretical and experimental plots of C_D versus C_L^2 are shown in Figure 45. The slopes of the experimental curves are greater than those of the theoretical because of the efficiency factor, e. The efficiency factor, inherent in the experimental results, includes the effects of increased drag due to parasite drag variation with lift and non-elliptic loading. The difference between the slopes of the experimental curves at positive and negative angles of attack is apparently the result of trailing-edge asymmetry.

The ΔC_D term of the total drag coefficient was found by rearranging the above equation to

$$\Delta C_D = C_D - (C_{D_0} + K C_L^2)$$

where C_D is the measured wind tunnel value. The recovered thrust is 68 percent of the calculated thrust as shown in Figure 46.

Blowing Power

The power requirements of blown control devices can be used to evaluate the efficiency of blown control. In general terms, a control is most efficient when it produces a control force (lift or moment) with a minimum expenditure

58

Figure 46. Thrust Recovery for the Blown Aspect Ratio 5.17 Wing Model

Figure 45. Induced Drag Results for Aspect Ratio 5.17 Wing

of power. The power to compress the freestream air to the jet total pressure is the jet kinetic energy used per unit time. A nondimensionalized compressor power coefficient is defined as

$$C_{HP} = \frac{P_{comp}}{q\, S_W\, V} \qquad \text{(eqn 12)}$$

The power required to compress freestream air to the jet total pressure is

$$P_{comp} = \frac{\dot{m}}{2\eta} (V_j^2 - V^2)/550 \qquad \text{(eqn 13)}$$

where η is the compression efficiency (assumed $\eta = 1$).

Curves of the rolling moment and lift due to blowing versus the power used are presented in Figures 47 and 48. The results are as expected; full-span blowing makes the most effective use of the compressor power.

To examine the efficiency of the jet blowing, a parameter containing the lift and drag produced for various power inputs was used. For steady flight, L/D is normally used to evaluate the lift per pound of aircraft thrust. When jet flaps are incorporated into the aircraft system, the compressor power used to produce the lift must be added. Thus, a lift to "equivalent" drag parameter is defined as

$$L/D_e = \frac{C_L}{C_D + C_{HP} \cdot 550} \qquad \text{(eqn 14)}$$

This parameter can be used as a measure of jet flap efficiency (see Figure 49). Figure 49 shows that the full blown span is the most efficient lift producer.

When compared to L/D_e for the unblown wing, the jet-flap efficiency is relatively low. For primary flight control (replacing movable surfaces) the comparison of angle of attack efficiency to jet-flap efficiency is not valid. The value of the efficiency parameter is apparent when jet flaps are intended for direct lift control. In this case, the power added to compress freestream air is used to increase lift without changes in α or to increase the maximum lift beyond the stall-angle value. Figure 50 presents the possible increases in lift due to blown control as compared to the angle-of-attack lift.

60
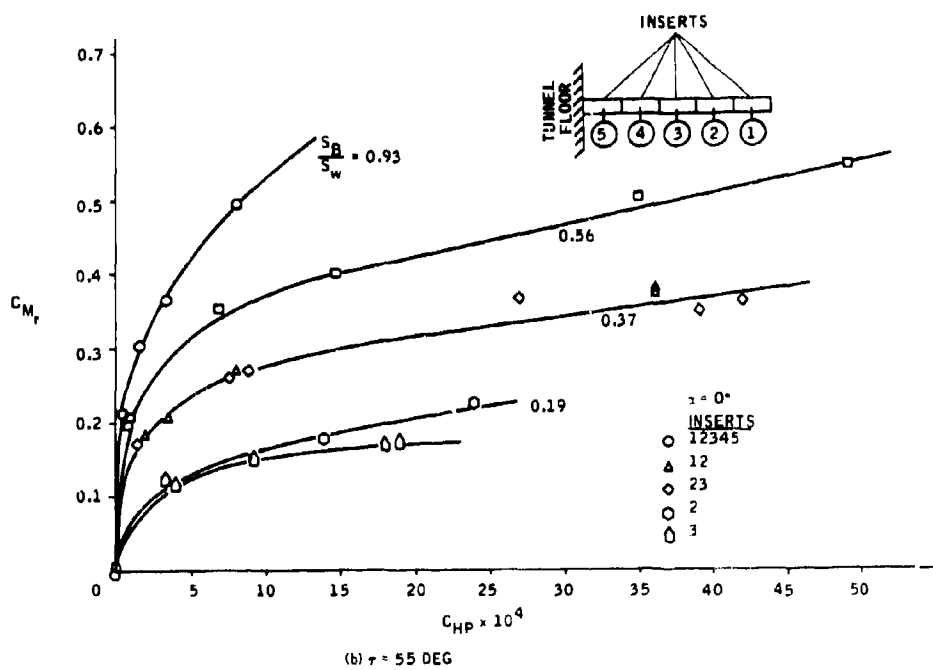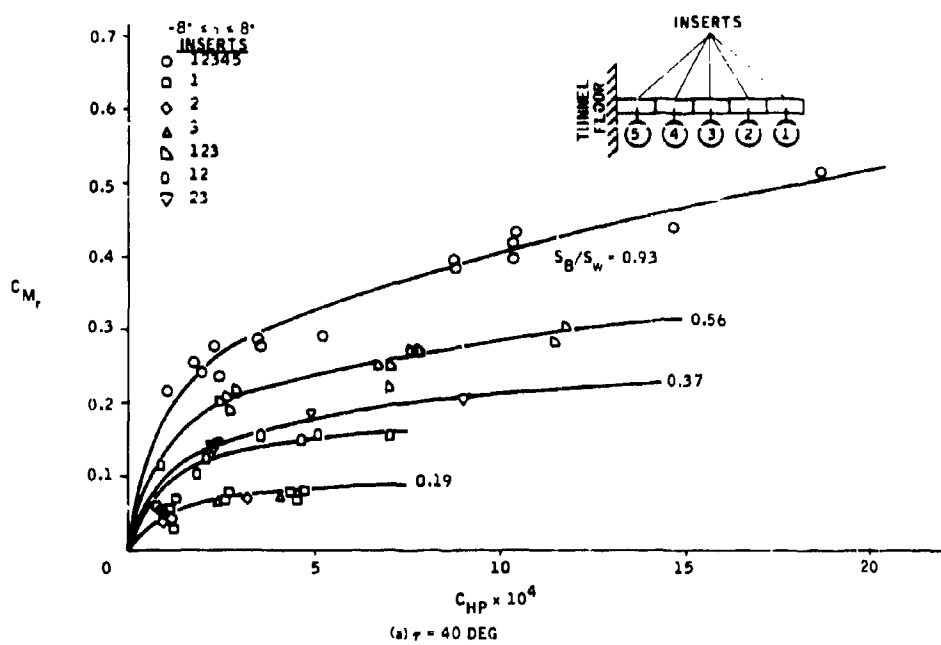
Figure 47. Rolling Moments for Different Blown-Span
Configurations, Aspect Ratio 5.17 Wing
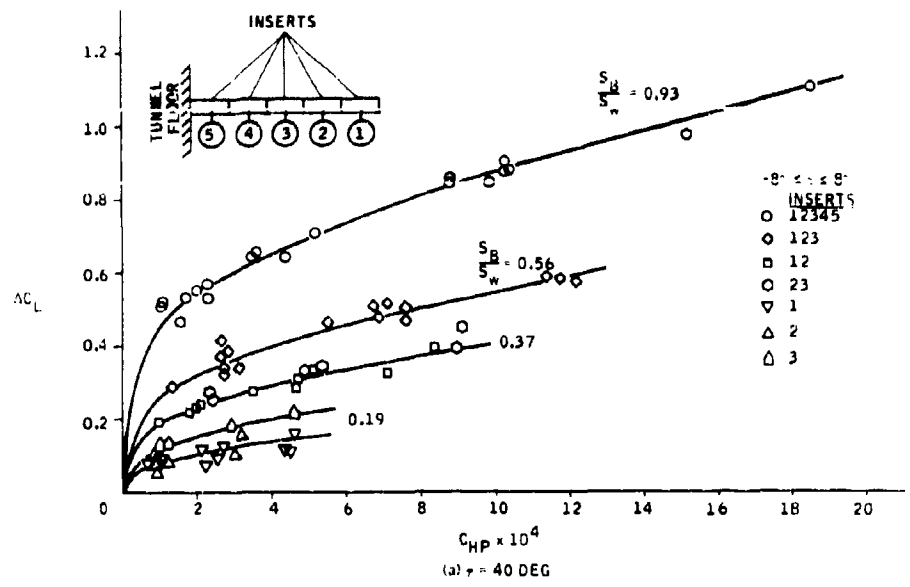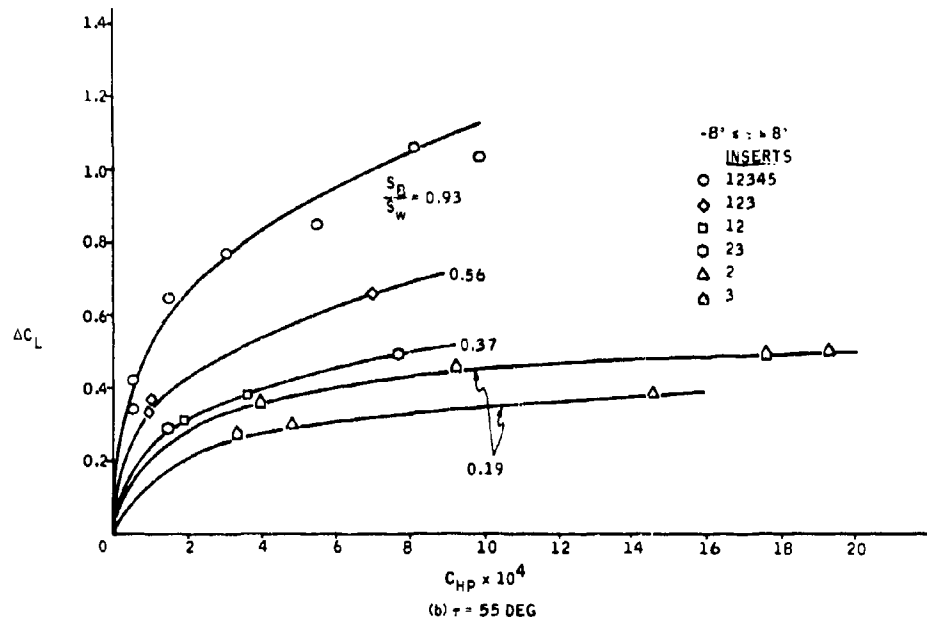
Figure 48.   Lift Due to Blowing for Different Part-Span
Configurations, Aspect Ratio 5.17 Wing

62

(a) $\tau = 40$ DEG

(b) $\tau = 55$ DEG
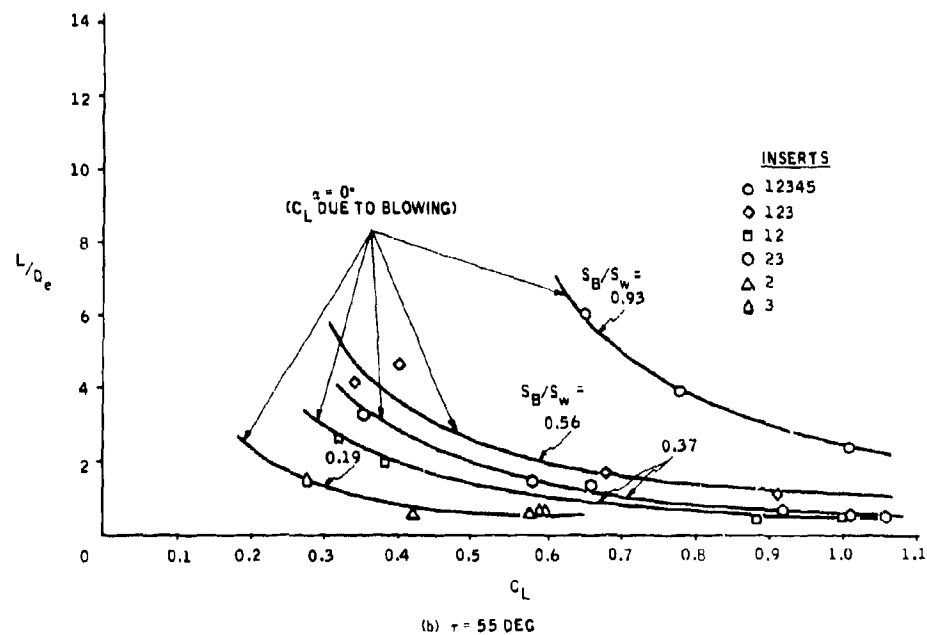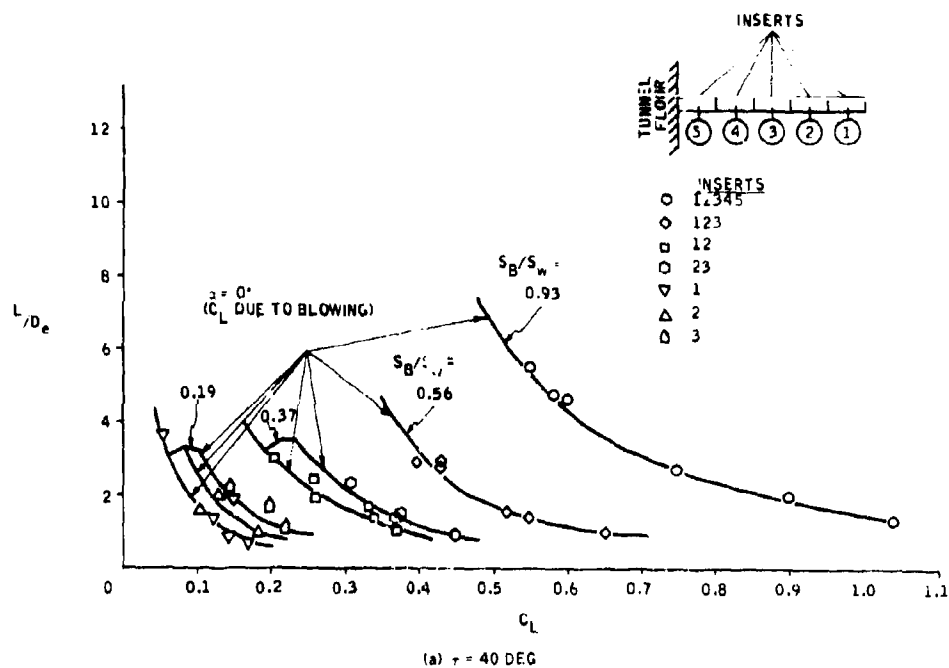
Figure 49.   Jet-Flap Efficiency, Aspect Ratio 5.17 Wing

63
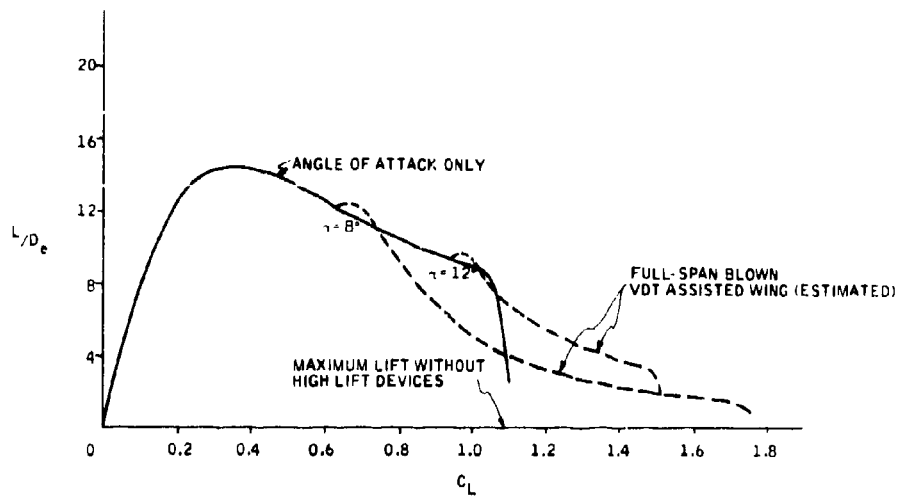
Figure 50.   High-Lift Jet-Flap Efficiency

ASPECT RATIO 3.85

The jet-flap wing model was tested at AR = 3.85 with no jet blowing and full-span blowing.   Part-span blowing configurations were not tested at this aspect ratio.   The following discussion is abbreviated, since many of the results of this section are little different from those at AR = 5.17.

Unblown Results

The non-blowing characteristics are shown in Figures 51 through 53.   The drag coefficients are again effected by variations in the Reynolds number.   Drag results are widely scattered at the lowest Reynolds number tested where the wind tunnel dynamic pressure was small.   It was reasoned that small experimental errors, for example, could become a significant portion of the drag reading at low wind tunnel velocities.

Pressure Data

The chordwise pressure taps for the AR = 3.85 tests were located a distance 0.46b from the root chord.   Typical chordwise pressure distributions are shown in Figure 54.   Normal force coefficients at y/b = 0.46 were found to be related to the midchord pressure difference by

64
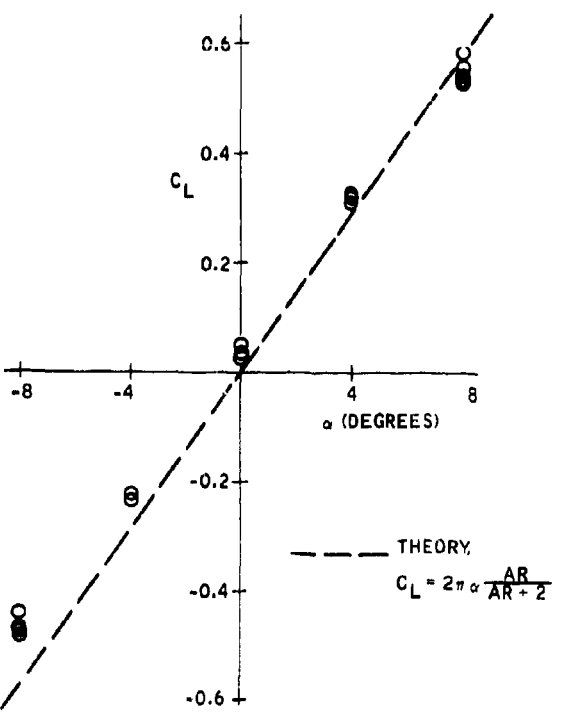
Figure 51. Aspect Ratio 3.85 No-Blowing Lift
Characteristics
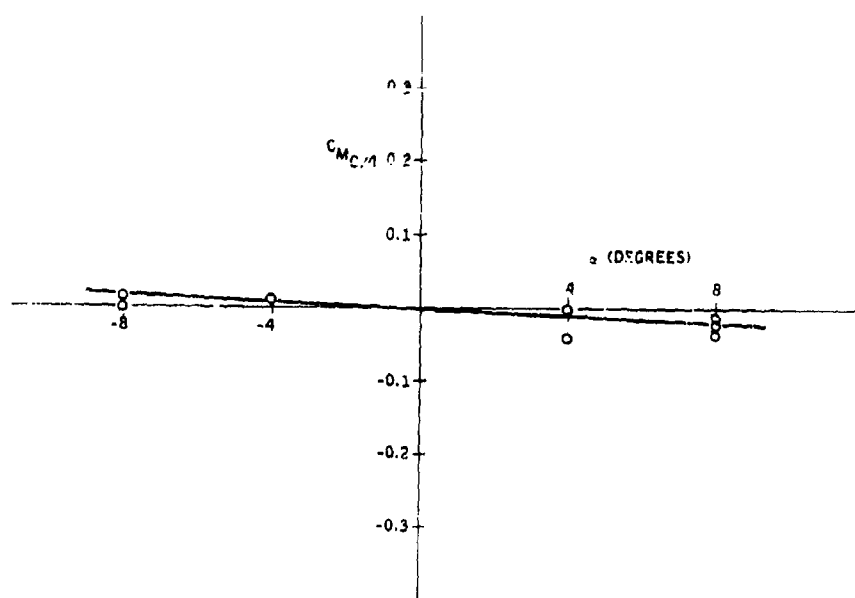
Figure 52. Aspect Ratio 3. 85 No-Blowing
Moment Characteristics
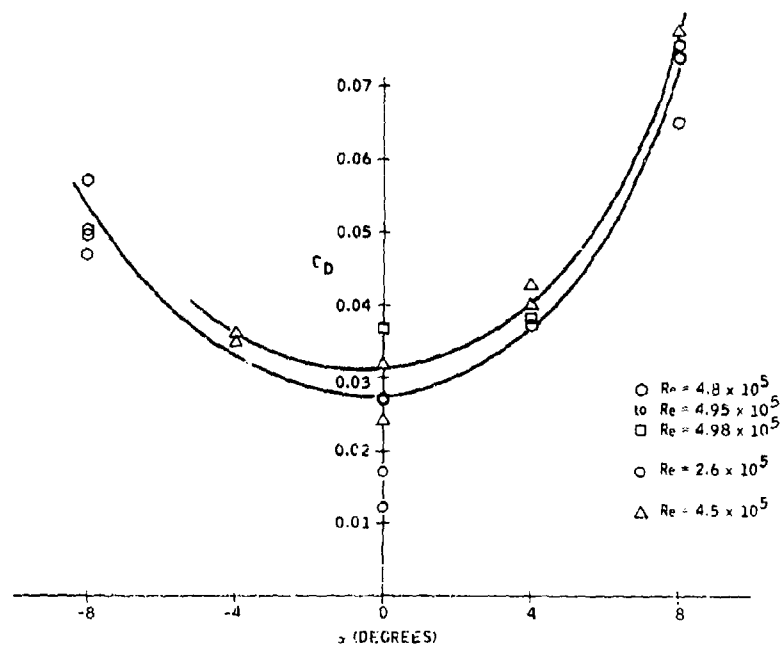
Figure 53. Aspect Ratio 3. 85 No-Blowing Drag
Characteristics

66
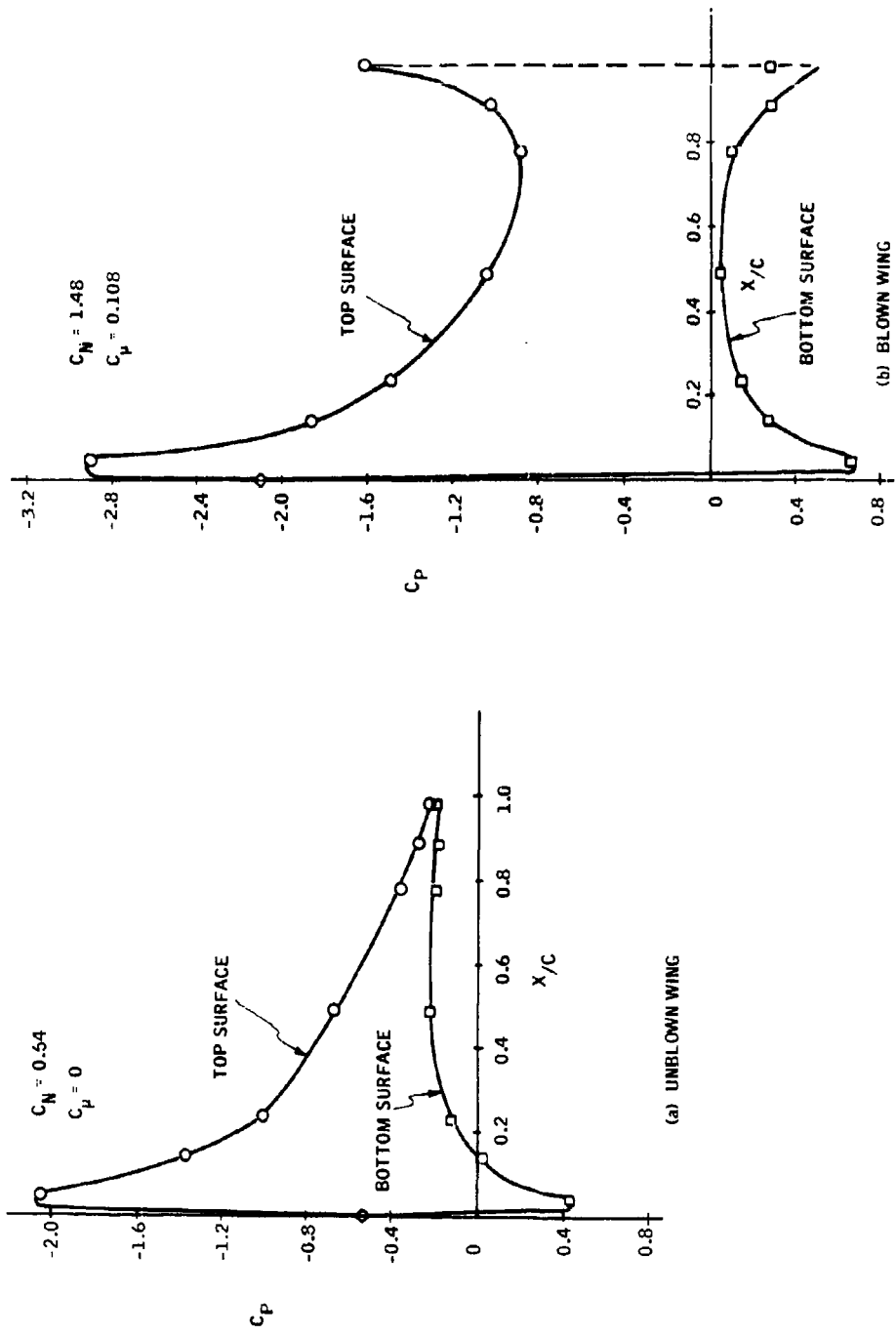
Figure 54. Chordwise Pressure Distribution of an Aspect Ratio 3.85 Wing at α = 8 deg

$$C_N = 1.30 \, \Delta C_{p_{c/2}} \quad \text{(Figure 55)}$$

A typical plot of the pressure-indicated lift distribution is compared to the theoretical lift distribution (Ref. 17) in Figure 56. The pressure-calculated curve is lower than the theoretical curve such that the pressure integrated lift coefficient is roughly 20% lower than the theoretical lift coefficient.

Figure 57 compares the balance-measured lift with the pressure-measured lift. At negative angles of attack, where C_L is negative, the balance and pressure lift show fair agreement. The balance-measured lift is about 20% higher than the pressure-measured lift for the remainder of the data, including blown and unblown test configurations. Thus, the spanwise distribution of the midchord pressure difference is used only to identify the form of the lift distribution.

Full-Span Blowing

Several midchord pressure distributions are shown in Figure 58. The spanwise distribution identified is elliptic independent of the angle of attack, jet angle or blowing coefficient.

Theoretical and experimental curves of the lift coefficient versus the blowing coefficient are shown in Figures 59 through 61 for jet angles of 26, 40 and 55 deg and angles of attack throughout the test range. Figure 62 shows the variation of the lift with jet angle.

The "lift effectiveness" of the jet blowing is shown in Figure 63. It is seen that the 55 deg jet angle is superior for amplifying the lift component of thrust. This is expected from theory since Spence's equation (eqn 3) at $\alpha = 0$ deg can be written as

$$\frac{C_L^{(3-D)}}{C_\mu \sin (\tau)} = \left[\left(\frac{\partial C_L}{\partial \tau} \right)^{(3-D)} \Bigg/ C_\mu \right] \frac{\tau}{\sin (\tau)} \; .$$

At a given C_μ, the only variable term of the expression is τ. For increasing jet angle, $1/\sin (\tau)$ decreases faster than $\tau/\sin (\tau)$. Thus, the lefthand side of the expression ("lift effectiveness") decreases with increasing jet angle.

Pitching Moment

The quarter-chord pitching moment is plotted against the lift coefficient in Figure 64. At constant α, the moment decreases with increasing lift,

Symbol	a	Blowing
◇—	4	Unblown
◇	8	
—◇	-8	↓
○	0	1234
○—	4	
○	8	
○	-4	
—○	-8	↓

C_N

$C_N = 1.39 \, \Delta C_{P_{C/2}}$

ΔC_P (AT X/C = 0.5)
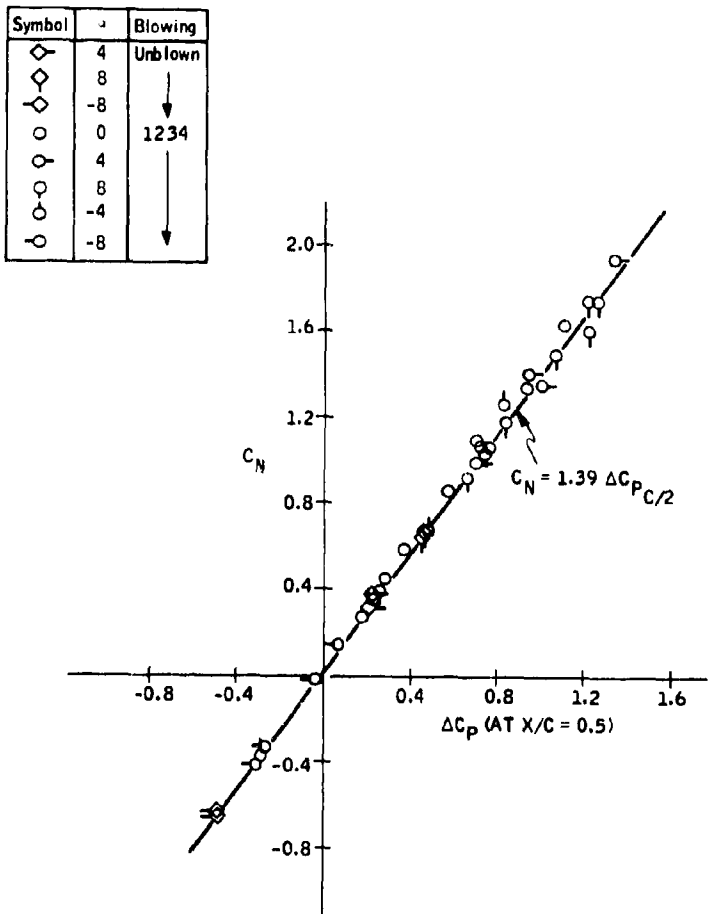
Figure 55. Relationship Between the Midchord Pressure
Difference and the Normal Force on an
Aspect Ratio 3.85 Wing

69
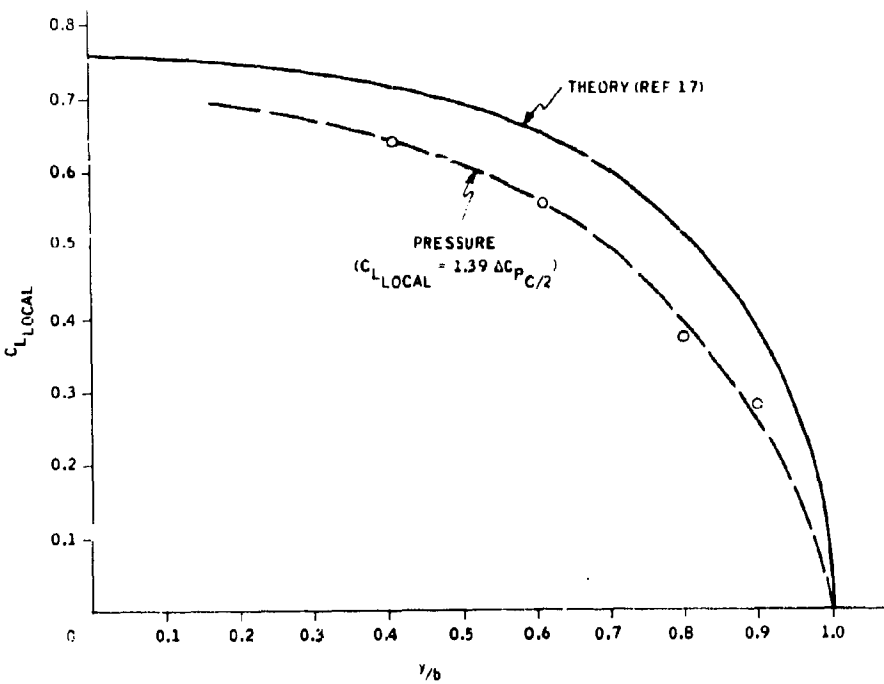
Figure 56. Spanwise Lift Distribution of an Unblown Aspect Ratio 3.85 Wing
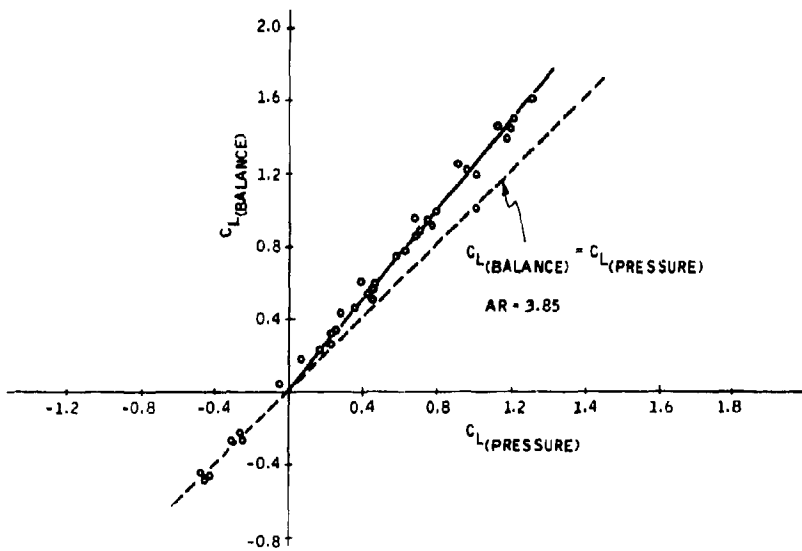
Figure 57. Comparison of Pressure-Integrated Lift to Balance System Lift
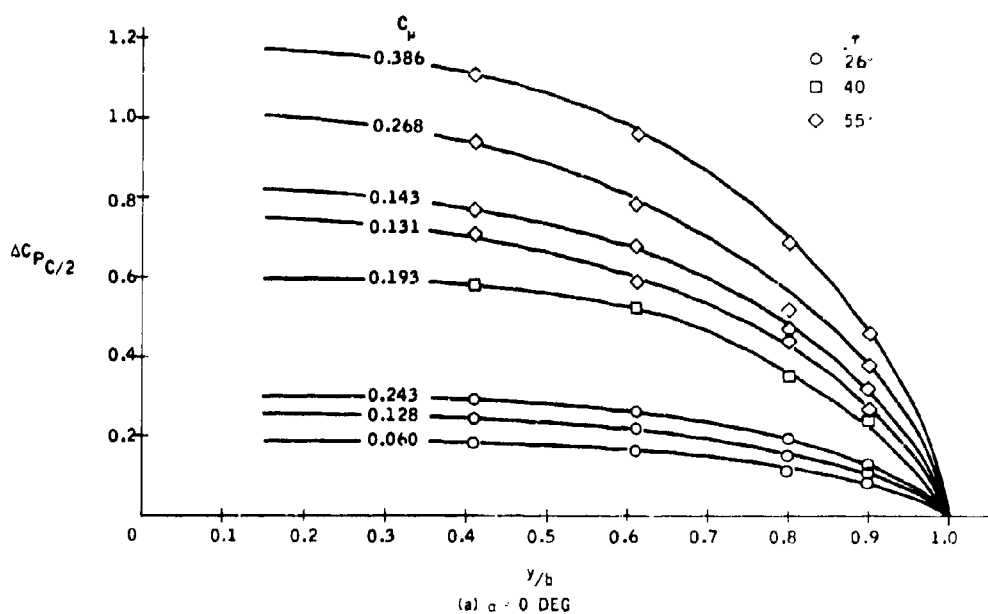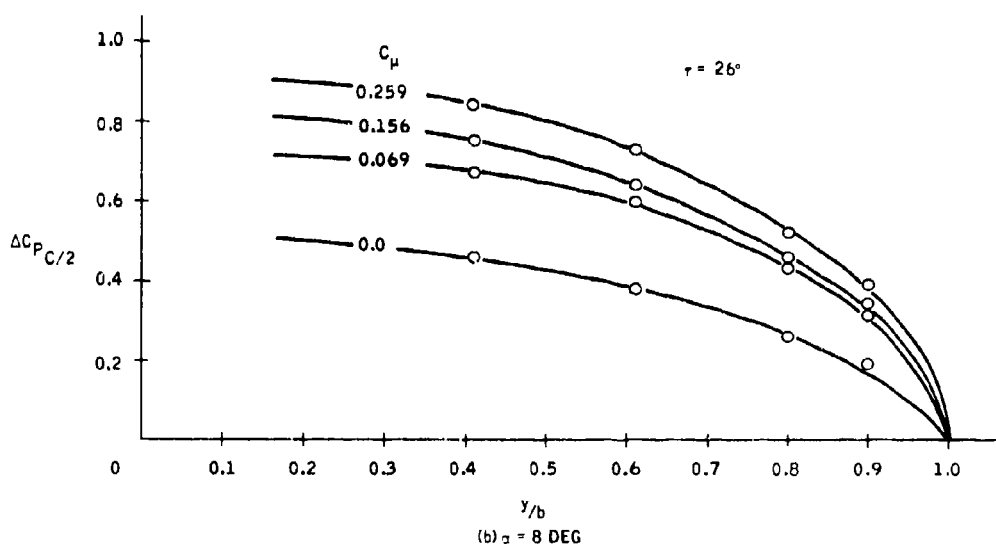
Figure 58. Spanwise Midchord Pressure Distribution of an Aspect Ratio 3. 85 Wing

71
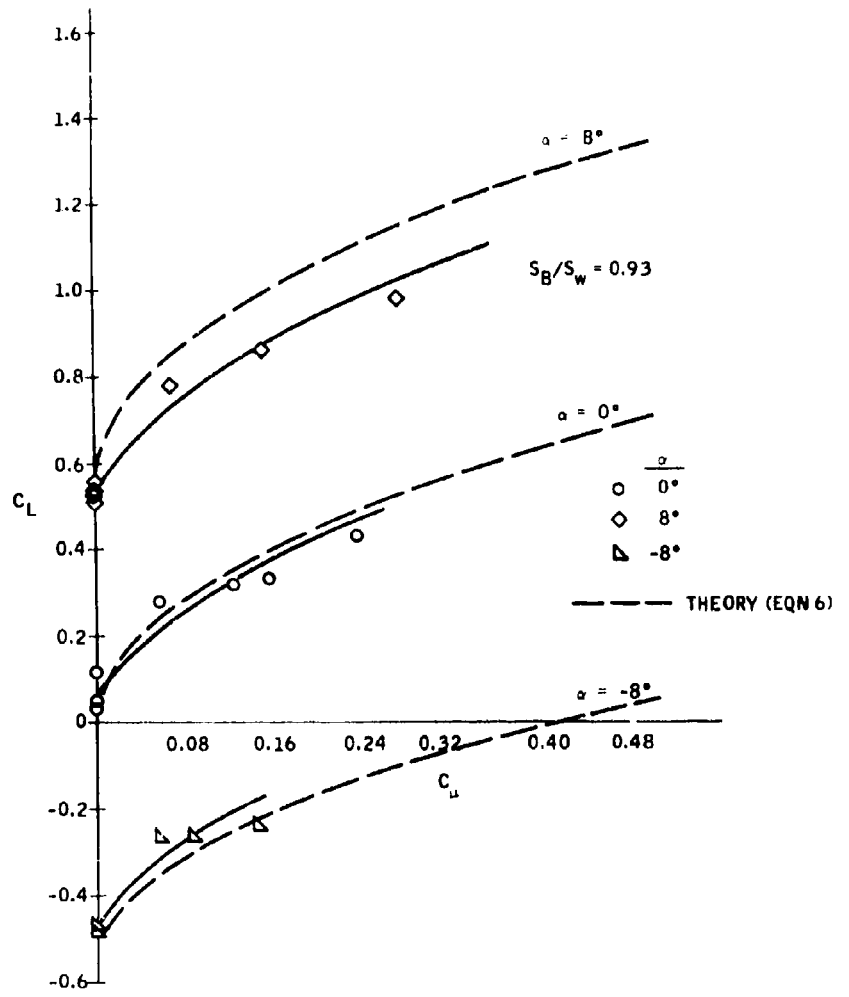
Figure 59. Angle-of-Attack Variation in Lift of a Blown
Aspect Ratio 3. 85 Wing with τ = 26 deg
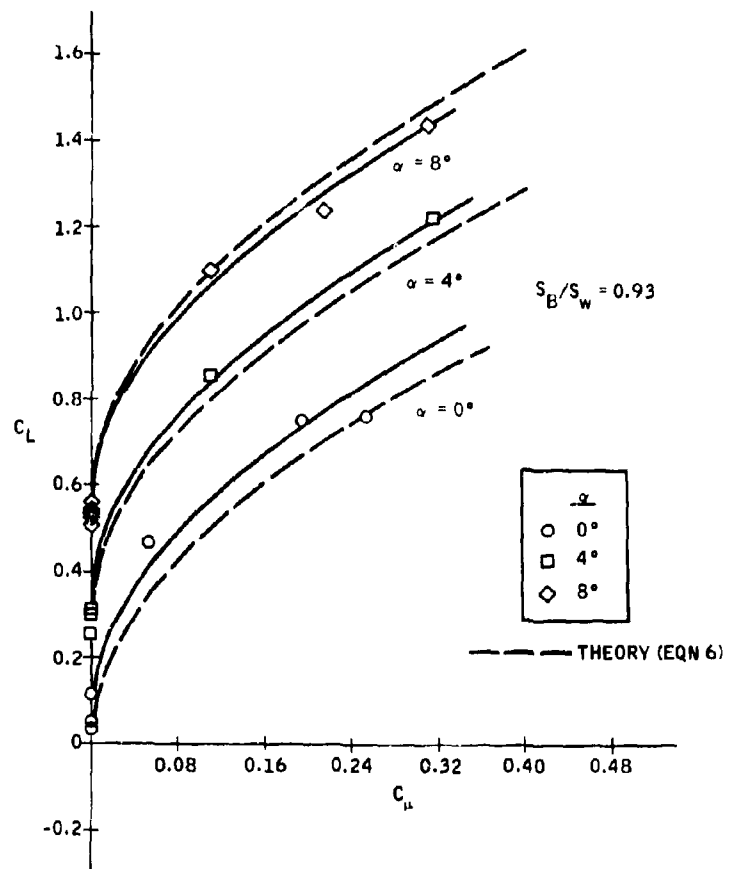
Figure 60.   Angle-of-Attack Variation in Lift of a Blown
Aspect Ratio 3. 85 Wing with τ = 40 deg
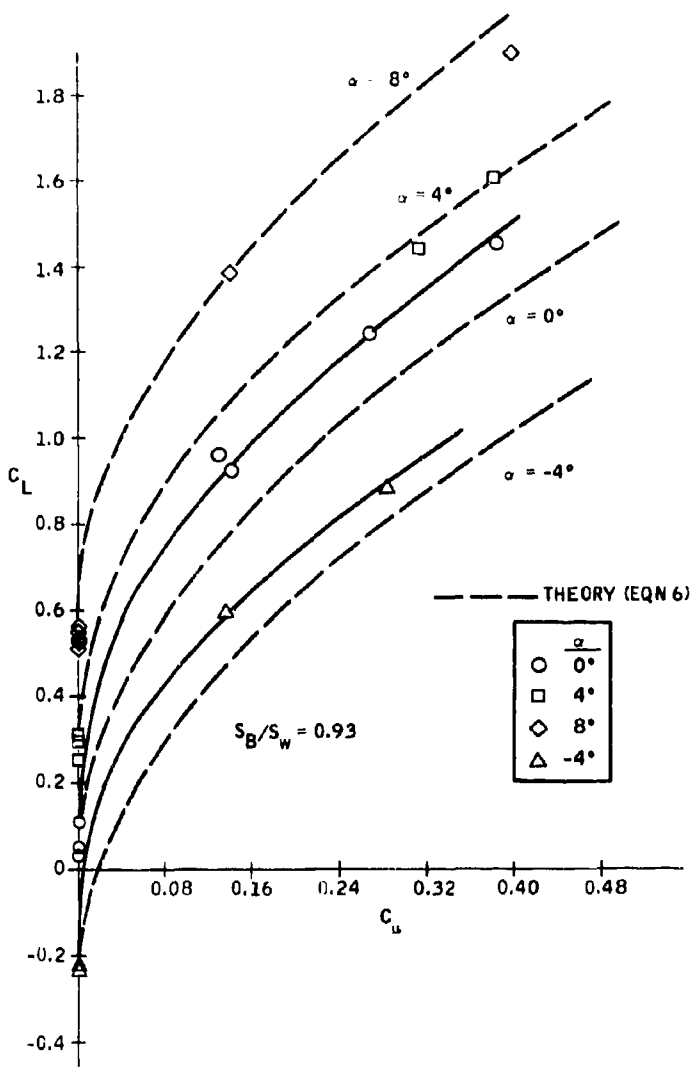
Figure 61. Angle-of-Attack Variation in Lift of a Blown
Aspect Ratio 3. 85 Wing with τ = 55 deg

74
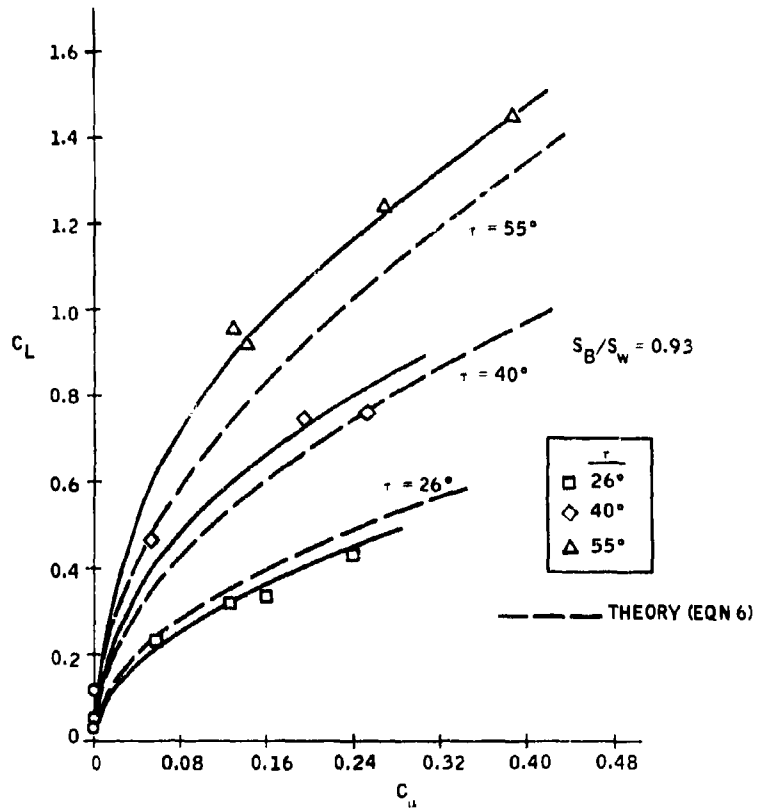
Figure 62. Jet Angle Variation in Lift of a Blown Aspect
Ratio 3. 85 Wing at α = 0 deg
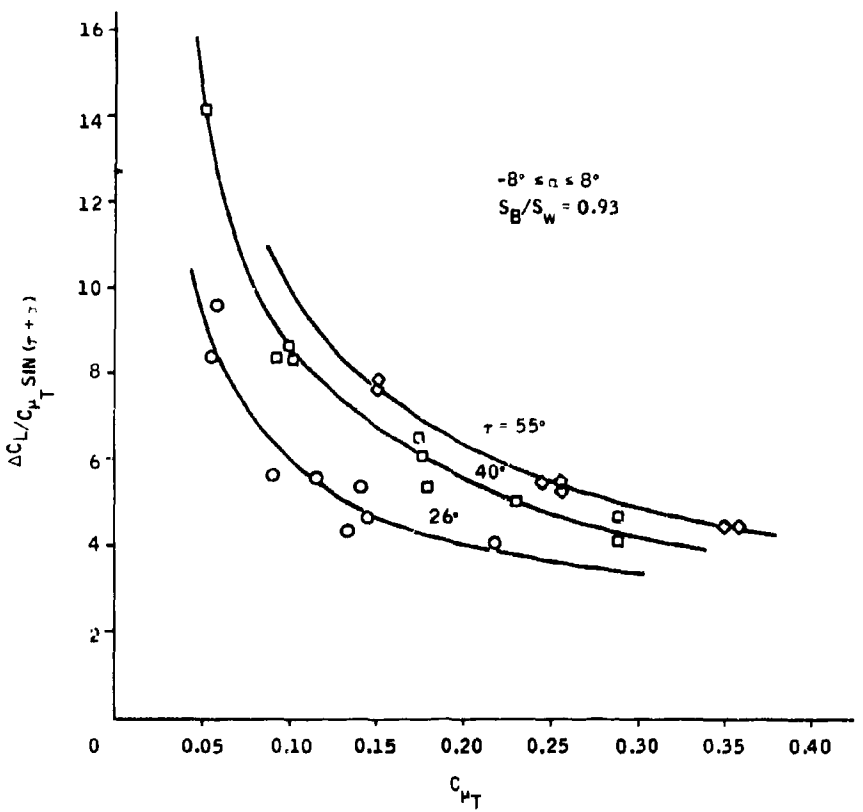
Figure 63. Wing Model "Lift Effectiveness" Variation with
Jet Angle at Aspect Ratio 3. 85
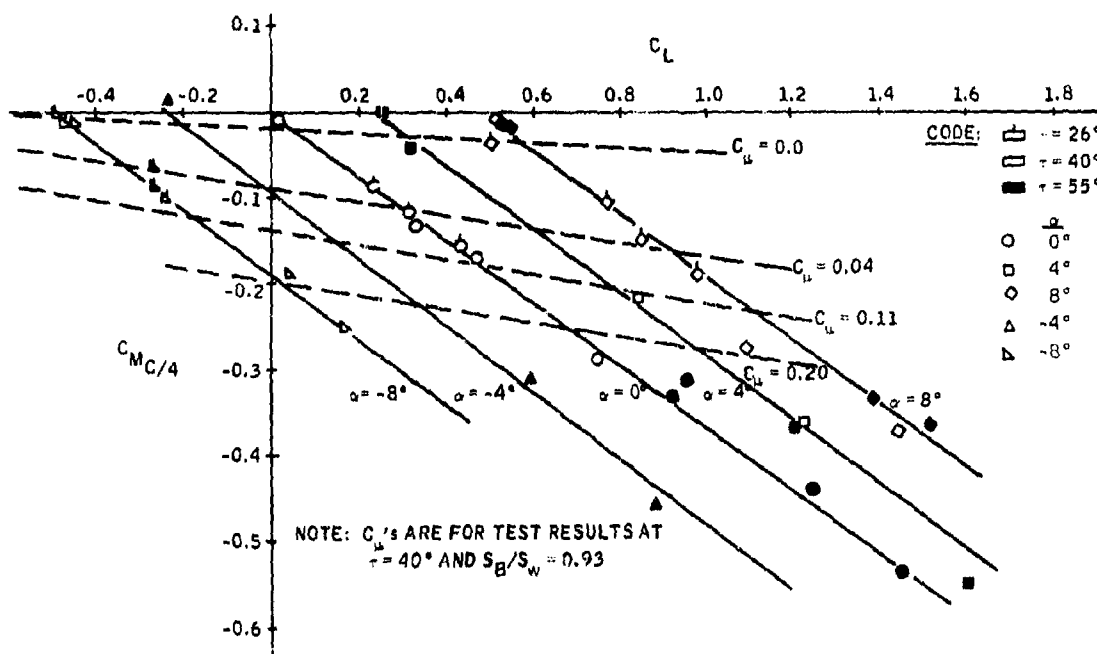
Figure 64. Quarter-Chord Pitching Moment and Lift
Results for a Blown Aspect Ratio 3. 85 Wing

suggesting a rearward movement of the center of lift. The experimental results at constant C_μ show that $dC_{Mc/4}/dC_L$ is more negative for the blown than unblown wing.

Drag

Figure 65 shows the variation of drag with lift squared for the unblown wing. The results are similar to those shown in Figure 45 for the AR = 5.17 wing. Figure 66 shows that approximately 74% of the ideal thrust is recovered irregardless of the jet angle.

Blowing Power Efficiency

The lift coefficient is plotted against the compressor power needed to produce this lift in Figure 67. It is seen that the 55 deg jet angle creates the most lift for a given power input. Assuming that a 100% efficient air supply system is available, the power coefficients can be translated to compressor horse-powers. For an example, an aircraft with an aspect ratio 3.85 wing is considered. At a velocity of 200 mph, sea level altitude, a wing of 300 sq ft, equipped with a 26 deg jet blowing full span, would require 1,260 compressor horsepower to develop 6,125 lbs of lift.

The efficiency parameter, L/D_e, is shown in Figure 68. The efficiency of jet flaps decreases as the lift due to jet blowing increases and increases as the jet angle increases.

EXPERIMENTAL RESULTS, $3.85 \leq AR \leq \infty$

A brief summary of the experimental results throughout the aspect ratio range of the tests is presented in Figures 69 through 72.

Figure 69 presents the experimental and theoretical lift characteristics of the unblown jet-flap wing. Good agreement was found throughout the aspect ratio range.

The variation in lift coefficient for several aspect ratios with the blowing coefficient is shown in Figure 70. The curves show that at τ = 40 and 55 deg the experimental lift is greater than the theoretical values for full span blowing.

Figure 71 shows the variation in the lift effectiveness $\left[\Delta C_L / C_{\mu_T} \sin (\tau + \alpha) \right]$ with jet angle, and Figure 72 shows the variation in lifting efficiency (L/D_e) with jet angle for the aspect ratios 3.85 and 5.17. Adding these Figures to those for the part-span blowing results, it is concluded that jet flaps can

78
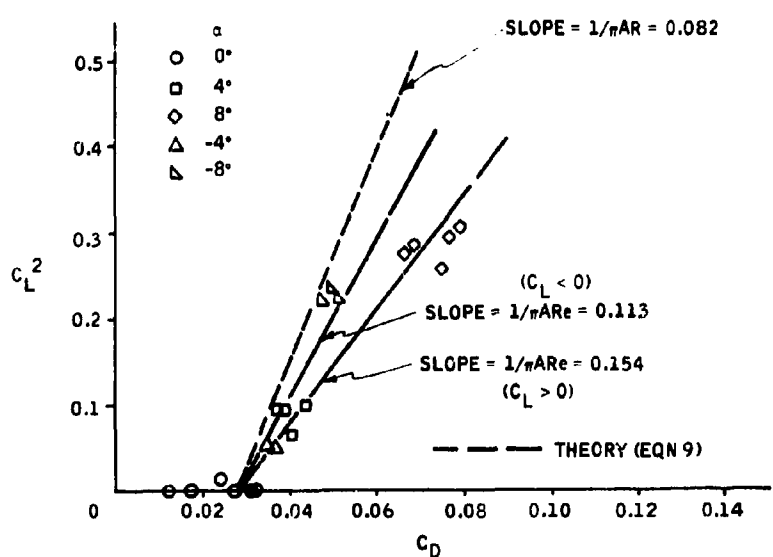
Figure 65. Induced Drag Results for an Unblown Aspect Ratio 3. 85 Wing
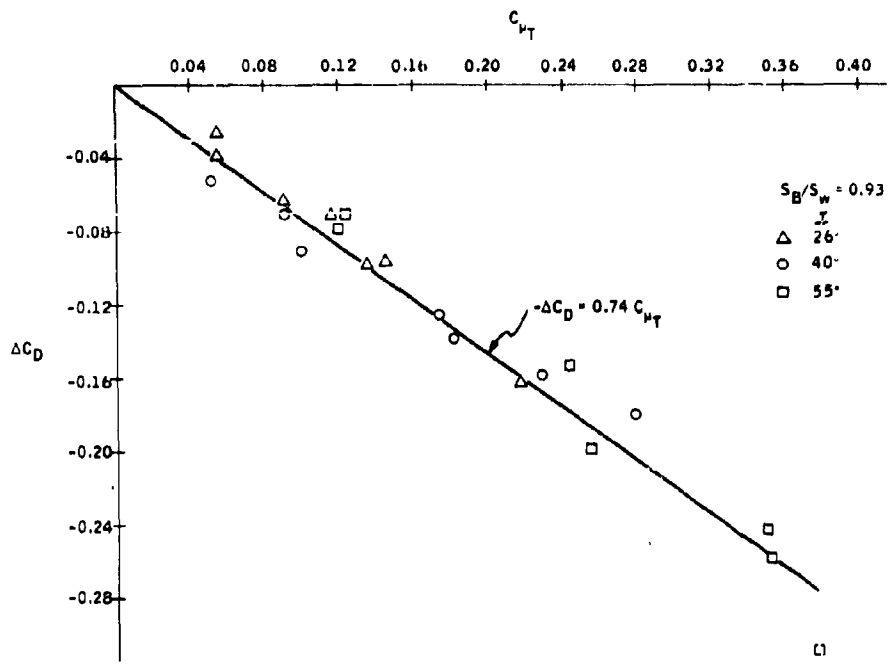
Figure 66. Thrust Recovery for a Blown Aspect Ratio 3.85 Wing
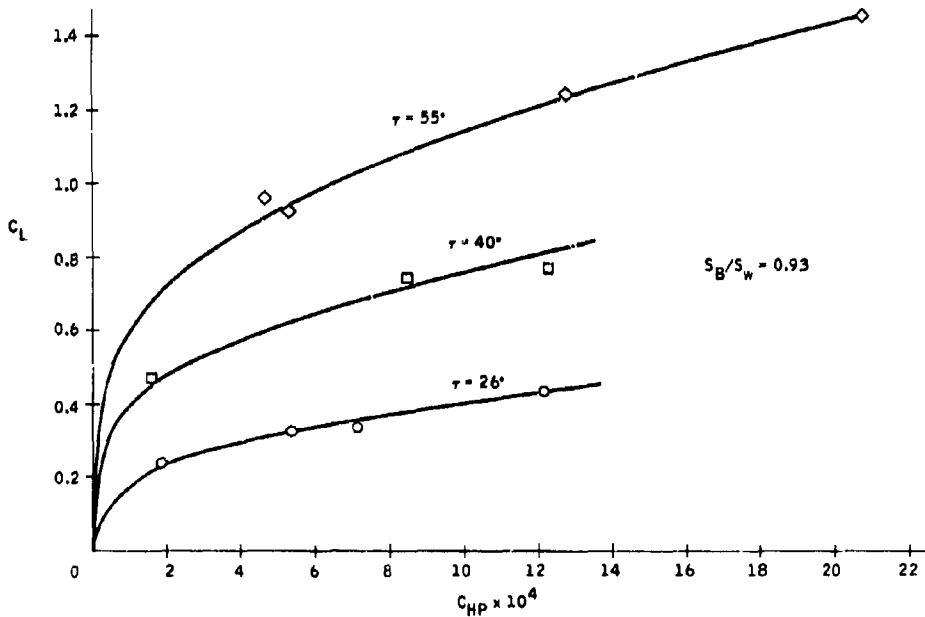
Figure 67. Power Required for Lift at $\alpha = 0$, Aspect Ratio 3.85 Wing
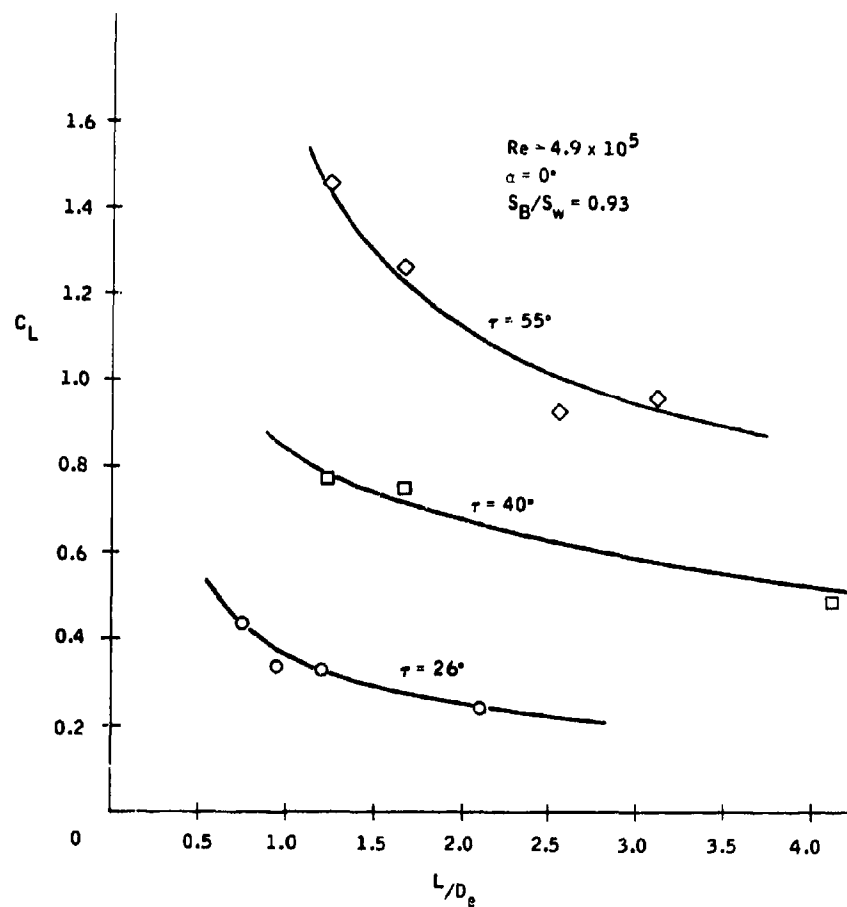
Figure 68.   Efficiency of Jet-Flap Blowing at Aspect
Ratio 3. 85
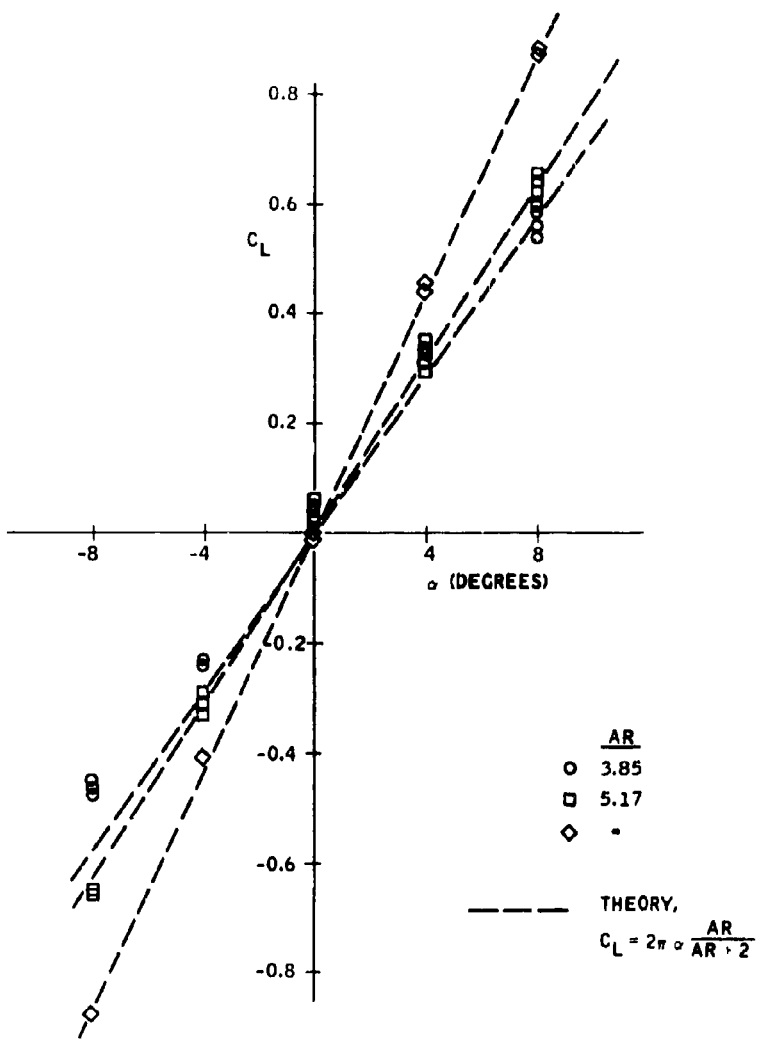
Figure 69.   Coefficient of Lift of an Unblown Wing at Aspect
Ratios 3. 85, 5. 17 and Infinity
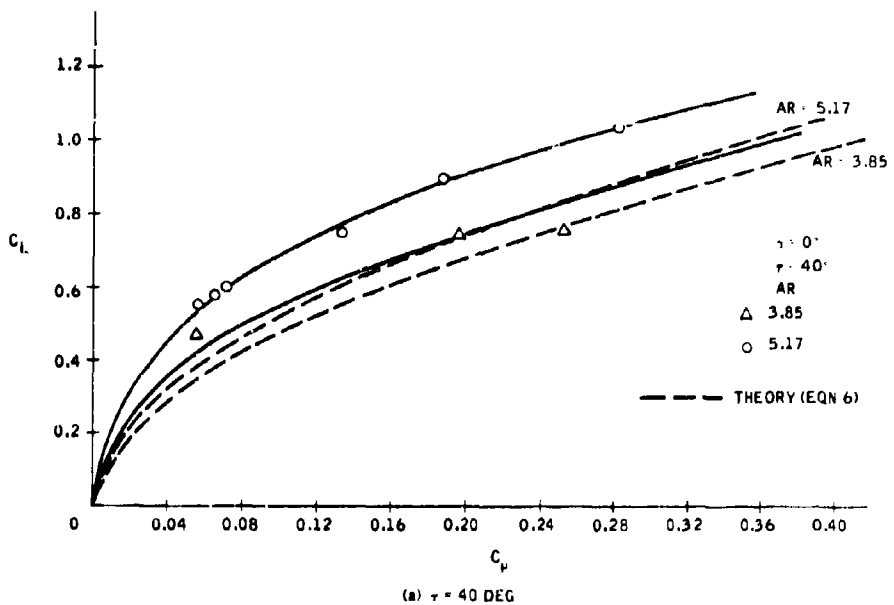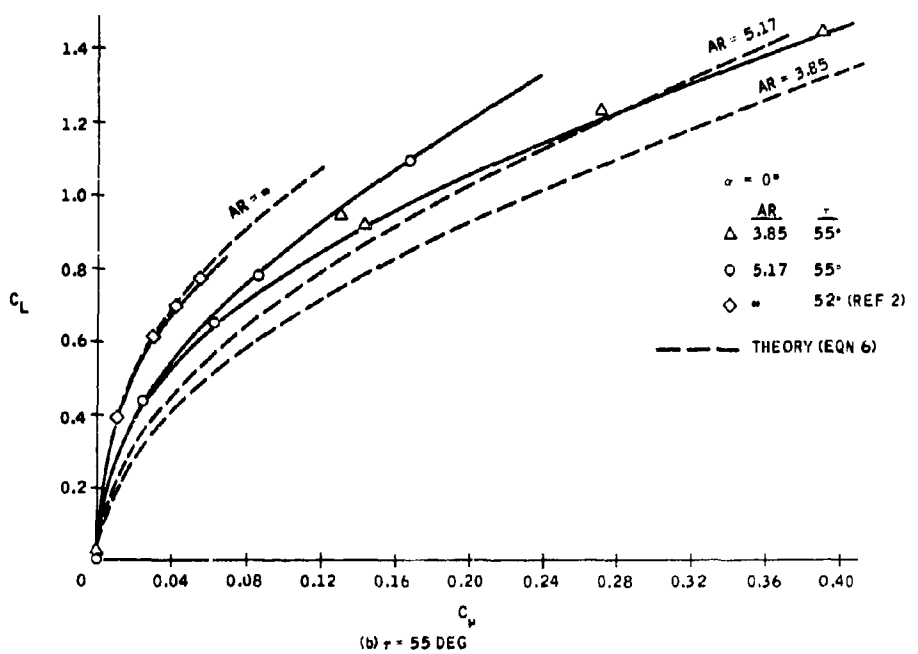
Figure 70. Effect of Aspect Ratio on the Lift of a
Blown Wing

83
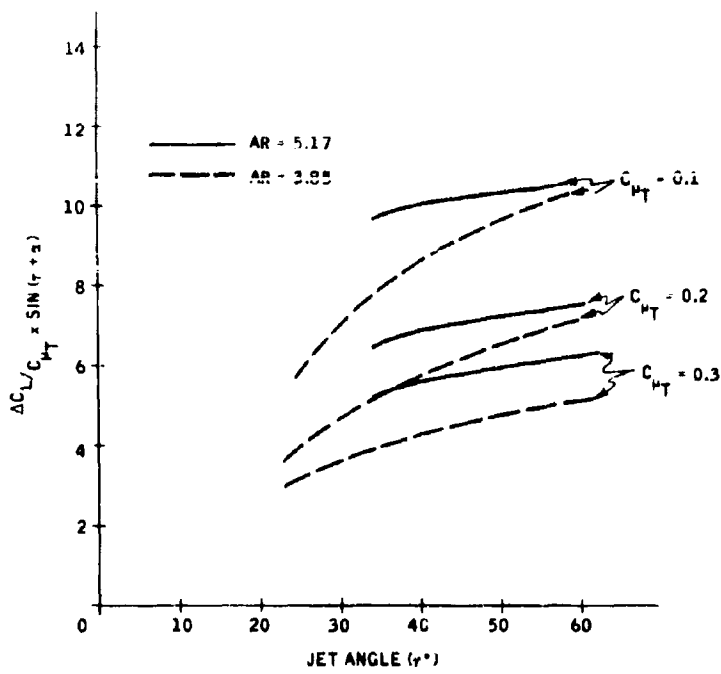
Figure 71. Variation in Lift Effectiveness with Jet Angle
for Aspect Ratios 3. 85 and 5. 17
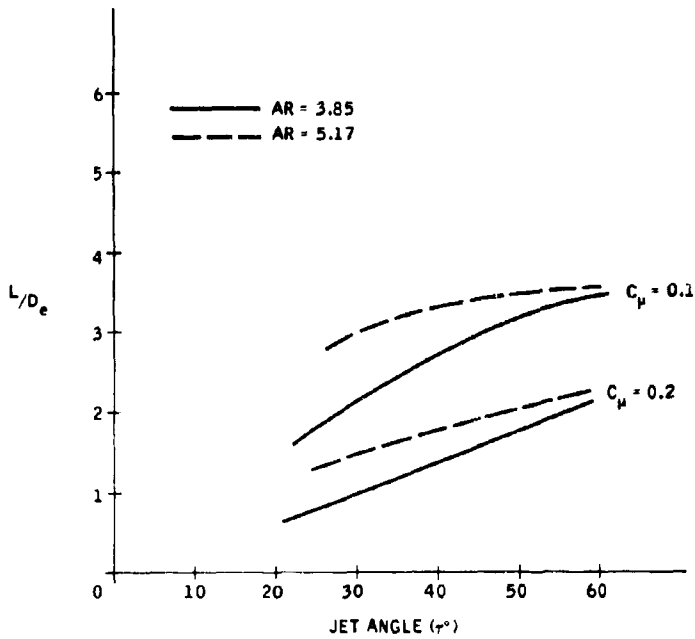
Figure 72. Variation in Lifting Efficiency with Jet Angle
for Aspect Ratios 3. 85 and 5. 17

84

produce the greatest lift with the least thrust, power and drag penalties when blowing the largest wing area available at jet angles of 55 deg or higher. Two-dimensional investigations of Reference 3 indicated that a jet angle as high as 120 deg may be most efficient at subsonic speeds.

BLANK PAGE

SECTION V

VDT PRIMARY FLIGHT CONTROL
FOR OV-10A AIRCRAFT

The main purpose of studying the VDT system in this report is to develop a
primary flight control system for military aircraft which has no external
moving surfaces. The experimental results contained in this report, along
with the results of References 1, 2, and 3, were used to examine the feasi-
bility of NEMS primary flight control for low-speed, highly maneuverable
military aircraft, such as those used for TRIM and COIN missions. The
study was made to determine the NEMS system characteristics required to
meet severe military control specifications which ensure high mission suc-
cess probability. An OV-10A aircraft selected for the study is a likely candi-
date for VDT control. The OV-10A has a high degree of survivability, good
STOL performance, is faster and more tactically versatile than helicopters,
and is slower but more maneuverable than jets. It can withstand high struc-
tural loads and is adapted for modern limited war and counterinsurgency.
TRIM and COIN operations require a simple, rugged, reliable aircraft capable
of easy, simple maintenance. The VDT control concept matches these aircraft
requirements.

The OV-10A aircraft's pertinent dimensions are shown in Figure 73. VDT
blown control was assumed to replace the present aileron-spoiler, elevator,
and rudder control surfaces. Aerodynamic characteristics of the OV-10A
were obtained from Reference 19.

DESIGN ANALYSIS PROCEDURE

To examine the feasibility of using VDT blowing for primary flight control of
TRIM (trails, roads, and interdiction mission) or COIN (counterinsurgency)
type aircraft, the OV-10A (a COIN aircraft) maneuvering characteristics were
specified and the VDT system requirements established. VDT system require-
ments for the OV-10A aircraft can be assumed to be representative of the
requirements needed for other aircraft with similar weight and mission char-
acteristics. The steps taken in determining the system requirements were:

1. Calculate VDT thrust required for specified maneuvers to
   find maximum VDT thrust.

2. Define several pressure ratios for VDT blowing and calculate
   the required horsepower and mass flow for maximum VDT
   thrust requirements.

3. Using the results of 2., approximate duct losses for duct areas
   suitable to OV-10A aircraft VDT primary flight control system.

PRECEDING PAGE BLANK

RUDDER

15 FT 1 IN.

4 FT 4 IN.

39 FT 10 IN.

14 FT 7 IN.

14 FT 10 IN.

40 FT

AILERON

ELEVATOR
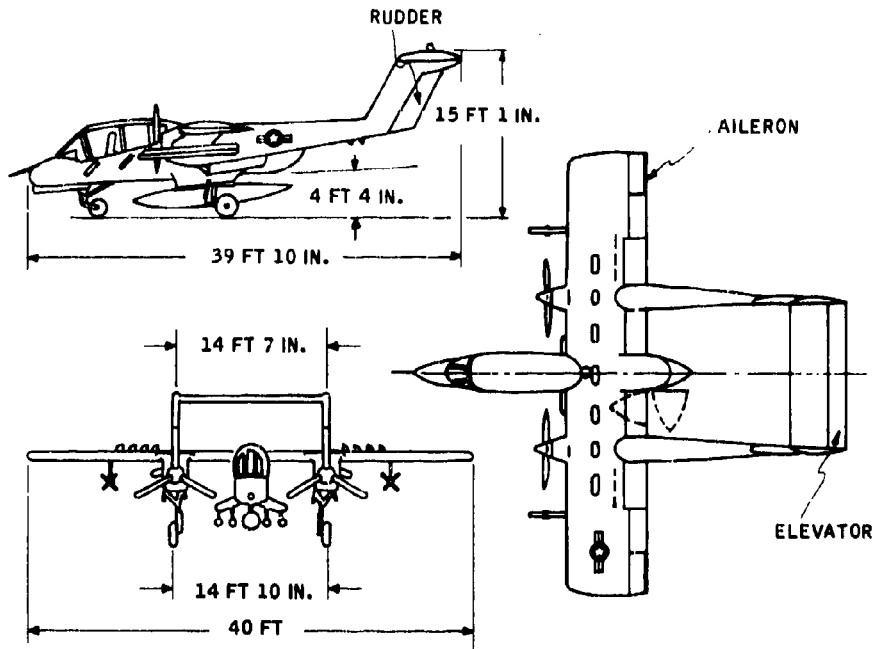
WEIGHTS

EMPTY WEIGHT	6,969 LBS
MAXIMUM TAKE-OFF GROSS WEIGHT	13,800 LBS
FUEL (SELF-SEALED)	1,638 LBS
OIL AND TRAPPED FUEL	57 LBS
WING LOADING	37 LBS/SQ FT
TWO CREW AND PROVISIONS	587 LBS
ARMOR	328 LBS
SPONSONS RACKS AND	
FOUR MACHINE GUNS WITH 500 RPG	569 LBS
FIVE STORE STATIONS	3,600 LBS
	TOTAL CAPACITY
TWO WING STATIONS (AS REQUIRED)	300 LBS
	CAPACITY EACH

PERFORMANCE

V_{MAX} AT SEA LEVEL, STANDARD DAY   244 KTS
RATE OF CLIMB AT TOGW LEVEL,
  STANDARD DAY   2,600 FT/MIN
SERVICE CEILING .... TWO ENGINES 26,000 FT
                ONE ENGINE   13,000 FT
SINGLE ENGINE FLYAWAY AT 11,300 LBS
  GEAR AND FLAPS UP   95 KTS (1.05 V_s)
STRUCTURAL LOAD FACTOR AT 9,690
                LBS 8 g's
FERRY RANGE WITH 150-GAL
  FUEL TANK   1200 NMi

POWER PLANT

TWO T-76 ENGINES	TWO THREE-BLADED
MIL RATED AT	PROPELLERS
715 SHP	(8 FT 6 IN. DIA)

Figure 73. OV-10A Aircraft Configuration and Design Data

88

4. Estimate energy required tor VDT primary control when aircraft executes specified maneuvers.

5. Size weight and fuel requirements for candidate VDT air supply systems.

These steps are accomplished in the following analysis.

THRUST REQUIREMENTS

Roll Control

Roll performance of military aircraft is specified in MIL-F-008785A (USAF) (Ref. 20) in terms of the bank angle change in a given time, ϕ_t. For the following analysis, these roll rates were nondimensionalized by multiplying them by the ratio of wing span over twice the forward velocity. By doing this, the roll rates specified can be expressed in terms of the helix angle made by the wing tip during a rolling maneuver.

The OV-10A was classified a "highly maneuverable" class IV aircraft, and roll requirements were obtained from Reference 20. This class of aircraft requires the greatest roll capability for its activities. Some additional specifications are usually made for class IV aircraft, but for the present study only the general roll performance requirements specified will be used. These are:

Table 1. MIL-F-008785 (USAF) Roll Specification for Class IV Aircraft (Ref. 20)

Flight Phase Category	Required Maximum Roll Performance
A	ϕ_t = 90 deg in 1.3 sec
B	ϕ_t = 90 deg in 1.7 sec
C	ϕ_t = 30 deg in 1.0 sec

The categories A, B and C correspond to different flight phases for normal military airplane missions. Category A requires "rapid maneuvering, precision tracking, or precise flight-path control" as in air-to-air combat, ground attack or weapons delivery. Category B refers to cruise, loiter, climb or descent activity which can be accomplished with "gradual maneuvers and without precision tracking, although accurate flight-path control may be required." Terminal flight phases such as takeoff, approach and landing are listed in Category C. Category C phases require "accurate flight-path control." The roll rates specified are shown in Figure 74 as required wing tip helix angles, based on the 40 ft OV-10A wing span.

89
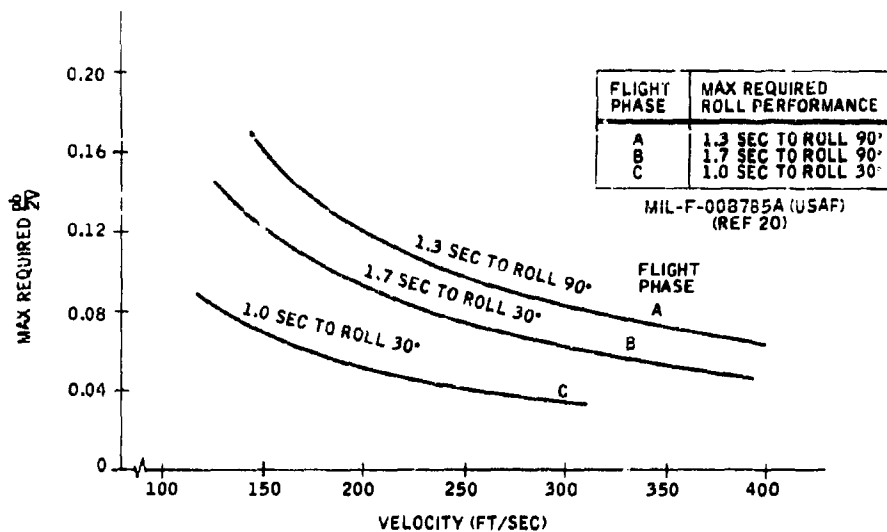
Figure 74. Required Rolling Performance

The OV-10A is presently incapable of meeting class IV specifications. As stated in Reference 21, from flight test evaluation, the OV-10A has "poor roll performance." It did not meet MIL-F-8785 class IV requirements but "class I or II requirements look about right." Class I and II requirements are not as stringent as those of class IV.

From the curves of Reference 19, the roll performance available from the OV-10A aileron-spoiler combination was estimated at pb/2V = 0.10. As shown in Figure 74, this performance is below that specified for class IV aircraft. The rolling capability of a VDT primary flight control system will be designed to meet class IV requirements and, therefore, be an improvement over conventional control.

To examine the performance of a VDT roll control system, the rolling moment available from VDT blowing can be approximated using the experimental results at AR = 5.17. As shown earlier in this report, full-span blowing is the most effective blowing configuration for producing a rolling moment as well as lift. Therefore, a full-span VDT device on the OV-10A aircraft wings is the first case considered.

As previously shown (eqn 10), if one-half of the OV-10A VDT wing is blowing, the rolling moment can be approximated by

$$C_{M_r} = C_L^{(3-D)} \left(\frac{4}{3\pi} \right)$$

90

When both halves of the OV-10A wing use VDT to produce rolling moment, one blowing at +1 radian and the other at -1 radian, known parameters for the OV-10A aircraft can be substituted into the above expression. This gives a control rolling moment coefficient of

$$C_{M_{r(control_{FS})}} \simeq 0.943 \sqrt{\frac{T_{FS}}{\sigma V^2_{(fps)}}} \qquad \text{(eqn 15)}$$

where subscript FS refers to full-span blowing and PS will refer to part-span blowing.

Assuming a single-degree-of-freedom roll and a rigid wing, the rolling performance of the OV-10A can be approximated from

$$\frac{p_b}{2V} = \frac{C_{M_{r(control)}}}{C_{M_p}} \qquad \text{(eqn 16)}$$

The wing damping term, C_{M_p} is estimated as -0.46 from Reference 19.

The VDT thrust required for any specified rolling maneuver, pb/2V, was found by solving the above equations for T_{FS}:

$$T_{FS} = 0.24 \, \sigma \left[(\tfrac{pb}{2V}) \, V \right]^2 \qquad \text{(eqn 17)}$$

The thrust required to provide the rolling capabilities specified in MIL-F-008785A (Reference 20) are given in Table 2 for various flight phases. These phases cover the range of the categories of Reference 20 and are within typical altitude and speed ranges of counterinsurgency aircraft.

The last column of Table 2 shows the VDT thrust required when blowing from the span which the present OV-10A ailerons occupy. Experimental data was used to calculate the rolling moment coefficient at this position. Following the procedure used for the full-wing-span VDT case, the part-span VDT thrust required for roll can be approximated from

$$T_{PS} = 0.52 \, \sigma \left[(\tfrac{pb}{2V}) \, V \right]^2 \qquad \text{(eqn 18)}$$

91

Table 2. VDT Thrust Required for Typical Maximum OV-10A
Roll Maneuvers

Velocity (ft/sec)	Altitude (1000 ft)	Category and Flight Phase	Max P Specified by MIL-008785A	Full-Span VDT Thrust (lbs)	Part-Span VDT Thrust (lbs)
130	0	C (takeoff, landing)	0.524 rad/sec	26.4	57.1
150	1	C (approach)	0.524 rad/sec	25.9	56.5
150	1	B (climb)	0.924 rad/sec	82.0	169.0
160	1	A (ground attack)	1.21 rad/sec	137.0	290.0
200	5	A (weapon delivery)	1.21 rad/sec	121.0	263.0
240	10	B (cruise)	0.924 rad/sec	60.5	131.0
240	5	A (air-to-air combat)	1.21 rad/sec	121.0	263.0
300	10	B (descent)	0.924 rad/sec	60.5	131.0
300	10	A (air-to-air combat)	1.21 rad/sec	103.7	225.0
360	15	A (air-to-air combat)	1.21 rad/sec	88.4	192.0

It is noted that the expressions for the VDT thrust can be further reduced by multiplying out the velocity and substituting b = 40 ft. The thrust calculated is then a function of the altitude and rolling velocity only. Figure 75 shows the VDT thrust required to execute the roll maneuvers specified in Table 1.
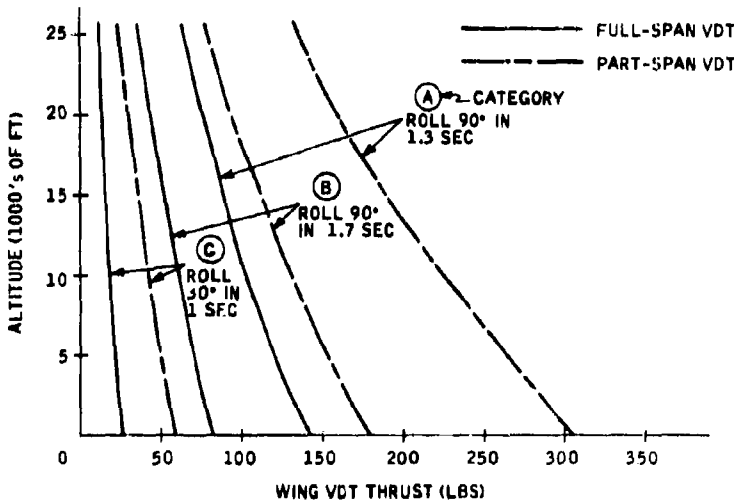
Figure 75. VDT Thrust Required for Roll Control

Yaw Control

Yaw control for the OV-10A aircraft is currently accomplished using nearly full-span rudders on both vertical tail surfaces (Figure 83). The following analysis will consider a VDT configuration which replaces the rudder surfaces with full-span VDT blowing at the vertical tails.

Since the OV-10A aircraft has two engines, the design condition established is that the full rudder control can hold zero sideslip, with one engine out, down to speeds approximately 1.2 times the aircraft stall speed. To balance the moment created by one engines thrust, the VDT vertical tail control must create an equal moment with opposite sign.

At a jet angle of 1 radian the yawing moment coefficient due to vertical tail VDT blowing was estimated from

$$C_{n_{VDT}} = 0.815 \; \frac{T_{VDT}}{\sigma V_{(fps)}^2}$$ (eqn 19)

The OV-10A aircraft employs AiResearch T 76-G-10/12 engines which have a sea level military rating of 715 SHP (Reference 22). Assuming a propeller efficiency of 0.9, the moment due to the antisymmetric thrust of one-engine-out operation at sea level is

$$C_{n_T} = \frac{1.90 \times 10^5}{V_{(fps)}^3}$$ (eqn 20)

By letting $C_{n_{VDT}} = C_{n_T}$, the above equations (19) and (20) were solved for the VDT thrust required to balance the moment created by one engine's thrust:

$$T_{VDT} = \frac{5.41 \times 10^{10}}{V_{(fps)}^4}$$ (eqn 21)

This relation is shown in Figure 76. At a speed approximately 1.2 times the aircraft stall speed, the vertical tail VDTs require about 150 lbs thrust to hold zero sideslip. Above sea level the change is expected to be negligible.
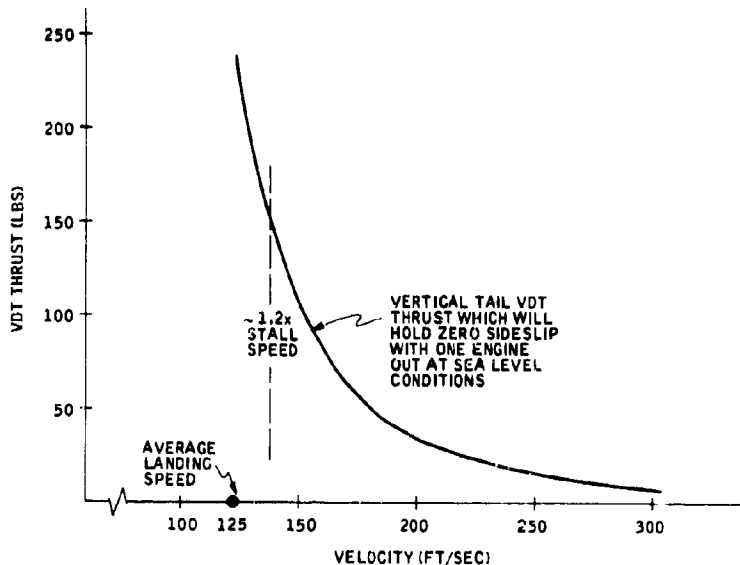
Figure 76. VDT Thrust Required for Yaw Control

Pitch Control

The amount of horizontal tail control required to trim and maneuver is influenced by the wing angle of attack, cg position, tail position, incidence of the tail surface, etc. When jet-flap devices are used for wing direct lift control, as they may be even if intended primarily for flight control, the wing pitching moment and downwash at the tail will be affected. The experimental results proved that the wing moment becomes increasingly negative with wing blowing and will require large nose-up moments from the tail control. With the blown wing, the effective angle of attack at the tail is decreased due to increased downwash, thus providing some nose-up moment.

Rather than designing or redesigning the OV-10A aircraft tail control, the longitudinal characteristics of the conventionally equipped OV-10A were used to estimate the VDT thrust required. This precludes any estimation of the short-period undamped natural frequency or the aircraft damping ratios. It is assumed that the longitudinal characteristics meet the standards set in Reference 20.

The aircraft pull-up maneuver was analyzed to obtain an estimate of the VDT thrust required to replace the OV-10A elevator control surface. The initial response of the aircraft to elevator deflection is a change in angle of attack where the short-period characteristics vanish quickly. The long-period oscillations when the airplane seeks a stabilized airspeed introduce very little angle-of-attack changes and can be ignored.

During the first seconds after an abrupt horizontal tail control input, when the change in angle of attack is large, the change in velocity is small. The airplane will then produce a load factor other than 1 g and start a pull-up maneuver. The magnitude of the load factor will depend on the tail force available to pitch the aircraft to a new angle of attack. As the angle of attack increases at constant speed, the horizontal tail lift creates a restoring pitching moment greater than the pitching moment tending to increase the angle of attack. The horizontal tail control must decrease the tail lift to achieve high angles of attack. High load factors requiring high α would need a powerful tail control and hence a maximum VDT thrust.

The simplified equilibrium equation for an OV-10A with VDT pitch control at the horizontal tail is

$$C_{M_{cg}} = C_{M_{c/4}} + C_L(X_{cg} - 0.25) + C_D(Z/c_w)$$

$$- C_{L_H} \frac{X_H}{c_w} \frac{S_H}{S_w} - C_{L_{VDT}} \frac{X_H}{c_w} \frac{S_H}{S_w}$$

(eqn 22)

95

The previous equation ignores wing VDT blowing and power effects on the dynamic pressure at the tail. The omission of the power effect will keep the VDT lift estimate conservative since the tail dynamic pressure increases in the slipstream flow.

The operational flight envelope of the OV-10A is shown in Figure 77. At the extremes of the envelope, the highest load factors are attained, and the horizontal tail VDT thrust for these conditions is given in Table 3 for an aircraft weight of 9700 lbs.

Table 3. Horizontal Tail VDT Thrust for Pull-up Maneuver at Sea Level

Velocity (ft/sec)	Load Factor n	VDT Thrust (lbs)			
		X_{cg} 0.20	X_{cg} 0.25	X_{cg} 0.30	X_{cg} 0.35
150	1.2	158	108	68	37
200	2.0	230	154	92	47
250	3.0	361	241	145	73
300	4.2	521	348	209	106
350	5.8	712	476	287	145
400	7.8	934	624	377	192

The load factors given in Table 3 are attained using the lift available at the wing stall angle. Above a speed of approximately 250 ft/sec, the drag due to this lift becomes greater than the thrust available from the OV-10A aircraft turboprops. Load factors above a value of 3.0 cannot be sustained for any period of time since the aircraft decelerates to a velocity where the drag equals the propulsive thrust. Thus, the VDT thrust required for a pull-up at high speed need not be maintained. A small pressure accumulator can supply high instantaneous power such that the required VDT thrusts for high-g pull-up maneuvers need not be used to size the continuous compressor power required. Pressure accumulator capabilities will be discussed later in this report.

Table 3 indicates that the most rearward-placed cg position possible would minimize the VDT thrust required for the pull-up maneuvers considered. This would also reduce the required control forces during landing, as the landing configuration uses $C_{L_{max}}$ in the presence of the ground. The ground

96

SEA LEVEL   W = 9700 LBS

AVERAGE LANDING SPEED   125 FT/SEC
2-g TURN (FLAPS UP)   200 FT/SEC
AVERAGE CRUISE SPEED   280 FT/SEC
V_{MAX} (MRT) HORIZONTAL SPEED 400 FT/SEC
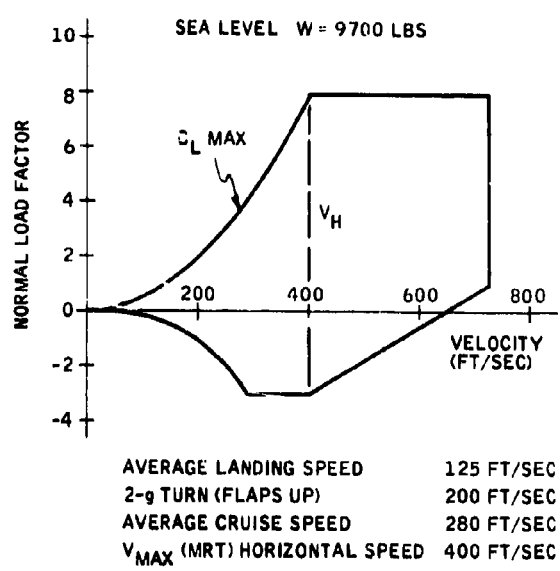
Figure 77.   OV-10A Flight Envelope

effect reduces the downwash at the tail, thereby increasing the tail angle of attack positively which increases tail lift and creates a nose-down moment. The control force must negate this increased tail lift to maintain equilibrium. However, even during extremely difficult landing conditions the VDT thrust required does not exceed approximately 190 lbs. The increment in the tail lift coefficient due to 190 lbs VDT at the landing speed is close to the maximum available from conventional elevator control, -0.8.

As aircraft spend the majority of their flight time in level flight (n = 1), the tail control for this condition must be considered. Using the equilibrium equation (eqn 22), the tail VDT thrust required to maintain n = 1 was calculated, and the results are shown in Figure 78. At or slightly above the cruise speed of the OV-10A aircraft, the tail control force needed decreases as the cg position shifts forward. Although these required VDT thrusts are small compared to the requirements of Table 3, the aft cg locations may increase the energy consumed over an entire mission. Energy requirements for a typical mission profile should be used to determine the center-of-gravity location best suited to VDT pitch control. The tail positioning, incidence, etc., could be varied to minimize the energy requirements. The remainder of this report will use a cg position of 0.30 c to estimate the thrust, mass flow and horsepower requirements for a VDT primary flight control system.

HORSEPOWER REQUIREMENTS

In the preceding analysis, the thrust required for a VDT primary flight control system was calculated for various selected maneuvers. It is recalled that the calculations were done assuming a jet angle of 1 radian. This is considered to be conservative as it is possible to achieve greater jet angles. However, for the purposes of the present study, a jet angle of 1 radian is a practical maximum to examine the feasibility of NEMS primary flight control.

The maneuvers chosen to size the thrust requirements for VDT primary flight control were assumed to present the most severe demands on the primary flight control surfaces. A VDT system which has these thrusts available could provide handling qualities which meet or exceed those specified for class IV "highly maneuverable" aircraft (Ref. 20).

A VDT primary flight control system requires a supply of compressed air for the VDT control devices. This can be accomplished by oversizing the aircraft's main power plants, normally used for propulsion, and bleeding the required air from the engine, or by adding an auxiliary power plant to supply the VDT. A number of variations and combinations of these methods is possible. Any method selected will necessitate some additional aircraft energy to be used to compress air needed for VDT operation.

The power to adiabatically compress the freestream air to the VDT supply pressure is given by:
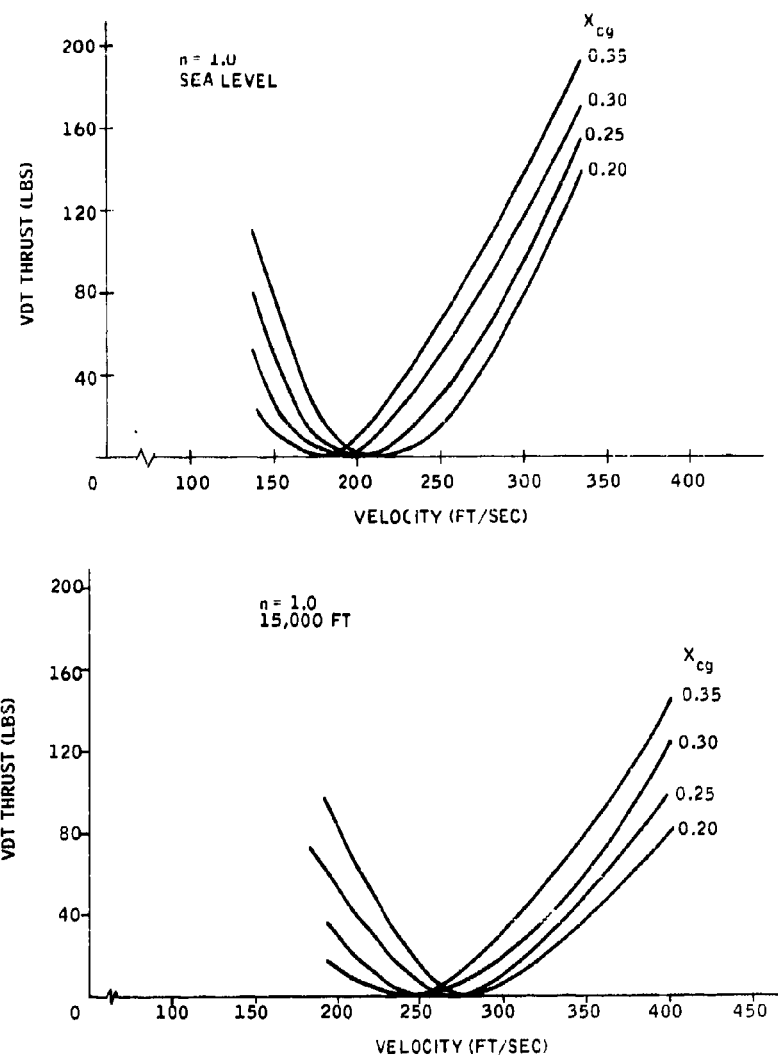
Figure 78. Steady-Flight Tail VDT Thrust Required to Maintain
Equilibrium at Sea Level and at 15,000 ft

99

$$\text{Power} = \frac{\dot{m} P_1}{\eta \, \rho_1} \frac{\gamma}{\gamma - 1} \left[\left(\frac{P_{VDT}}{P_1} \right)^{(\gamma-1)/\gamma} - 1 \right] \qquad \text{(eqn 23)}$$

where η is the compressor efficiency. Assuming that negligible pressure losses occur in ducting the air to the VDT, the power can be written in terms of the VDT jet velocity and mass flow.

$$\text{Power} = \frac{\dot{m}}{2\eta} \left(V_j^2 - V^2 \right) \qquad \text{(eqn 24)}$$

The thrust required can be converted to a compressor power in the following way. For a given thrust required the mass flow $\dot{m}$ and jet velocity V_j can be calculated by assuming an isentropic expansion from the VDT supply pressure to the ambient pressure. It has been shown (Ref. 1) that the isentropic relations can overestimate the available jet thrust by 25%. Thus, the power required could be 25% greater than the values predicted by the isentropic flow equations.

Figure 79 shows the relation between the VDT thrust and compressor horsepower for several compressor pressure ratios, $P_{VDT}/P_1 = P_R$. The results assume that $V_j^2 \gg V^2$, which is true for the speed range of the OV-10A aircraft and the pressure ratios considered.

The compressor power required to provide a VDT thrust can be estimated from Figure 79. The weight flow corresponding to this power can also be estimated from the figure. It is seen that the compressor power, at a given VDT thrust, decreases as the pressure ratio decreases, and a simultaneous increase in weight flow is evident. As an example, at a VDT thrust of 140 lbs, the following horsepower and weight flow are required:

P_R	Compressor Horsepower	Weight Flow (lb/sec)
2.0	200	5.18
4.0	298	3.40
8.0	385	2.64

The next step necessary to evaluate the feasibility of a VDT primary flight control system is an estimate of the compressor horsepower which must be available at any time.

The maximum required VDT thrust was previously calculated for roll, pitch and yaw control acting separately, but for some flight conditions more than one axis is controlled at one time. This is especially true for a single-engine

100
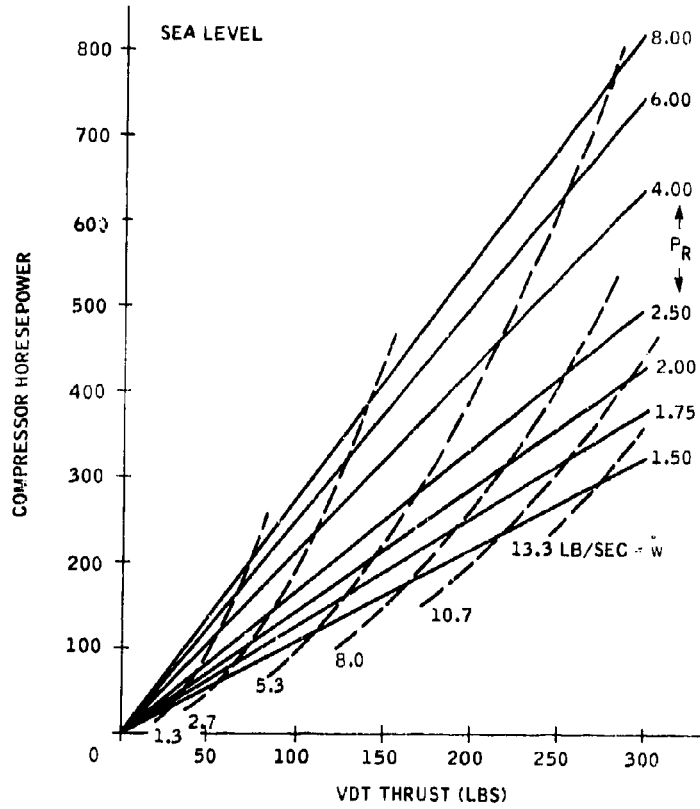
Figure 79. Compressor Horsepower for VDT Control System

landing. Under the worst possible landing conditions, the vertical tails would require 150 lbs thrust and the horizontal tail approximately 190 lbs thrust. Some minimal roll control would be required, but relaxed specifications under the given circumstances would require less than 10 lbs thrust for full-span VDT blowing. Summing the requirements, it was estimated that a one-engine-out landing requires 340 lbs of VDT thrust. This is nominally the same thrust required at the horizontal tail for a 7.8-g pull-up. Using 340 lbs VDT thrust for a maximum, the maximum compressor horsepower at a compressor pressure ratio of 2.0 is about 486 HP. At a pressure ratio of 8.0 the compressor horsepower required would be 930.

Duct Losses

The compressor horsepower requirements shown in Figure 79 were computed independently of any power losses which may occur in ducting the air to the VDT device. If losses did occur, the compressor horsepower would have to be increased to supply the required VDT thrust. A brief analysis of duct losses was conducted to determine the duct area required to ensure that duct power losses remain negligible.

In Reference 23 the differential equation of the flow in a one-dimensional duct was derived in detail. To keep the present analysis brief, without obtaining an overly optimistic estimate of duct losses, a constant-area duct, with constant total temperature, constant mass flow and adiabatic flow were assumed. That is, no mass subtraction takes place along a duct with assumed constant area. To remain conservative, the length of the duct was equated to the total length from the compressor unit to the point of VDT blowing furthest from the compressor. The compressor was assumed to be at the position occupied by the turboprop engines. The equation for the change in Mach number along the duct is given by

$$\frac{dM}{d(r/D)} = \frac{2\gamma f M^3 \left(1 + \frac{\gamma-1}{2} M^2\right)}{D(1 - M^2)} \qquad \text{(eqn 25)}$$

where f is the friction factor for smooth pipes and is a function of the Reynolds number, and D is the hydraulic diameter of the pipe.

To determine the duct pressure losses, the mass flow and pressure at the VDT are taken as known quantities and the ratio of compressor pressure to VDT pressure can be calculated using the results of Reference 23:

$$\frac{P_{comp}}{P_{VDT}} = \frac{M_{VDT}}{M_{comp}} \left[\frac{1 + \left(\frac{\gamma-1}{2}\right) M_{VDT}^2}{1 + \left(\frac{\gamma-1}{2}\right) M_{comp}^2}\right] \qquad \text{(eqn 26)}$$

The power loss was calculated from the results for the pressure losses.

102

The above equations were solved for a number of VDT thrusts with air supplied through several duct areas. The various duct areas were chosen such that they could easily be added to the aircraft structure where ducting was required. Figure 80 shows a scale drawing of the wing, vertical tail and tail boom cross sections and the duct cross-sectional areas considered. Each of the stations, designated in tenths of the total chord length, were used as one end of the duct area and the most rearward station the other end. The calculated power losses for several wing duct areas are shown in Figure 81 for the roll control maximum wing VDT thrust with part span blowing.

The power losses decrease rapidly as the compressor pressure ratio or duct area increases. However, the increase in compressor horsepower associated with increasing pressure ratio should be avoided if possible. For $X_{initial}$ = 0.7 c_w, the duct area is reasonably small and less than 1 horsepower is lost for pressure ratios of 1.5 and 2.0. This represents a loss of less than 1% of the total compressor horsepower.

A similar result was obtained for the power supplied to the tail controls through the wing boom. At $X_{initial}$ = 0.5 c_v (see Figure 80), the duct area was estimated to be 0.40 ft^2, approximately the same as that for the wing at $X_{initial}$ = 0.70 c_w. A duct of this area can easily run through the tail boom at its minimum cross section. As can be seen in Figure 80, the vertical tail duct area from 0.5 c_v to 0.8 c_v is smaller than the tail boom's minimum duct area. It was found that at a pressure ratio (P_R) of 2.0 a compressor horsepower of 500 can be delivered to the tail controls with a loss of 1.4 HP in ducts with an area of 0.40 ft^2. Thus, the air for VDT use can be most economically compressed and delivered using a low compressor pressure ratio.

Another aspect of the duct design is the ratio of duct flow dynamic head to the total duct pressure. Aircraft space requirements will require sharp right angle bends in the supply ducts. Each such bend can be assumed to cause a total loss of dynamic head. For the design duct area the ratio of dynamic head to total pressure is $0(10^{-2})$ so that the losses in right angle bends can be neglected.

Fuel Consumption/Maneuver

To estimate the fuel which would be consumed in running the compressor, it was necessary to select some typical COIN maneuvers where the VDT primary flight control would be operating. Reference 24 describes three maneuvers required on COIN aircraft missions. They are:

- First-pass maneuver
- Second-pass maneuver
- Pull-up

MAIN WING CROSS SECTION

VDT
DUCT
AREAS

C_w

$X_{INITIAL} \; (C_w) = 0.4$ 0.5   0.6   0.7   0.8   0.9

VERTICAL TAIL CROSS SECTION

VDT
DUCT
AREAS

C_v

$X_{INITIAL} \; (C_v) = 0.1 \; 0.2$ 0.3   0.4   0.5   0.6   0.7   0.8

MINIMUM
TAIL BOOM CROSS SECTION

CROSSHATCHED REGION INDICATES
DESIGN DUCT AREAS
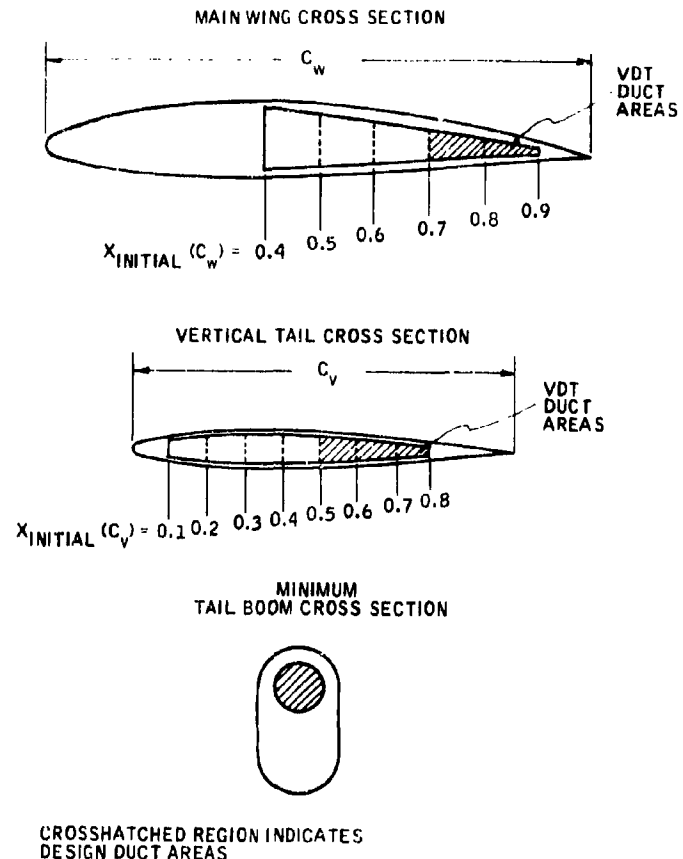
Figure 80. VDT Duct Area in OV-10A Structures

104
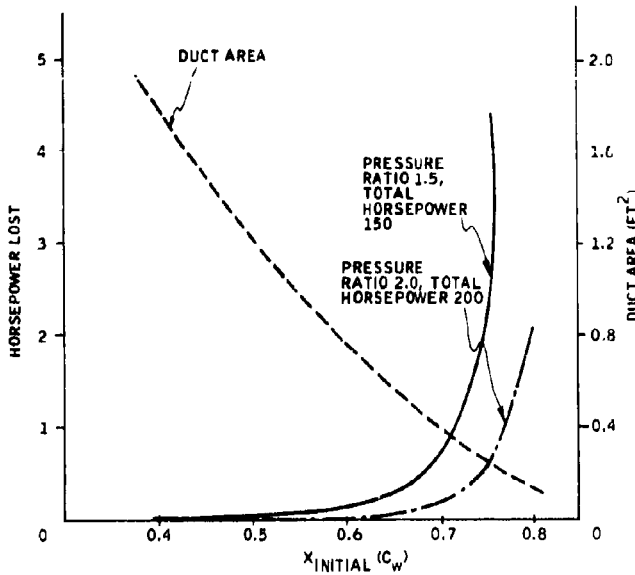
Figure 81. Duct Losses for Wing VDT Supply Area
Delivering 140 lbs Thrust

The following analysis describes these maneuvers and estimates the fuel
required for VDT primary control in each case. A compressor pressure
ratio of 2.0 and a fuel consumption rate appropriate for turbo-shaft engines
was used throughout the analysis. The fuel consumed for other compressor
pressure ratios would increase as rapidly as the compressor horsepower in-
creased.

First-Pass Maneuver (FP) -- One of the functions of COIN aircraft is to
perform reconnaissance-strike (R/S) missions. This is the most difficult
mission assigned in COIN operations, and if an aircraft can perform R/S
satisfactorily, it can adequately accomplish other required missions (Ref. 24).
In R/S missions, the pilot must search the target area and have sufficient
control power to attack the target effectively.

The first-pass maneuver begins after the pilot has identified his target. It
was assumed that identification is possible at a radius of 1200 ft. This was
called the visual radius R_v. The first-pass maneuver consists of the pilot
banking to a high-g turn and then rolling out to attack the target. The area
which can be attacked is determined from the maximum roll rate, the highest
load factor available and the velocity at which the aircraft maneuvers. Fig-
ure 82 defines the maneuver; the shaded region is the attack area. It is noted
that the aircraft is at some bank angle on the turning radius (R_t) and not in an
attack position. Only after the aircraft has rolled out and crossed the attack
radius (R_a) can the run begin.

105
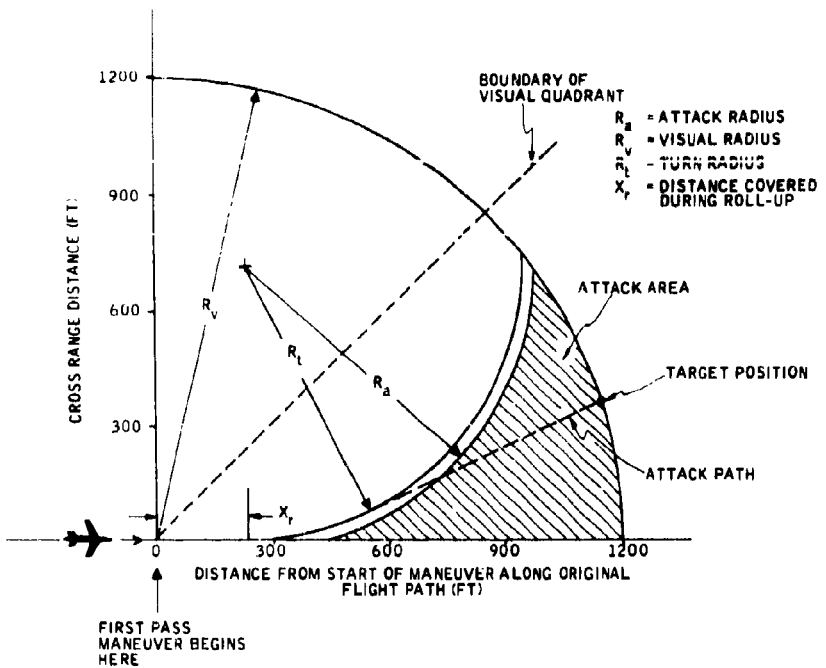
Figure 82. First-Pass Maneuver

The fuel to execute this first-pass maneuver is the fuel to turn plus twice the fuel to roll (roll in and out of the turn). The method of calculation can be found in Appendix B.

The load factor, n, determines the bank angle, ϕ ($\phi = \cos^{-1} 1/n$), and the angle of turn is θ. To calculate the maximum fuel required for this maneuver, we assume that the aircraft turns on R_t until the visual radius is crossed and then rolls out. In practice a first-pass turn to attack would be less severe than this; however, this case provides a conservative estimate of the fuel required. For this maneuver at n = 2 and V = 200 ft/sec, the fuel required is 0.239 lbs/maneuver. Some variability (± 0.040 lbs/maneuver) occurs at other combinations of n and V, however, the case used represents a typical high-g COIN maneuver.

Thus, the first-pass maneuvers require very little fuel to produce the VDT control forces. Even at a compressor pressure ratio of 8.0 the fuel requirement is only about twice that required for $P_R = 2.0$.

Second-Pass Maneuver (SP) -- Many targets spotted by the pilot cannot be attacked on the first-pass maneuver because of late identification. A second pass may then be required to attack the target. In a manner analogous to Reference 24, we have chosen the following model for the second-pass maneuver. An aircraft flies over the target and begins the second-pass maneuver.

106

The aircraft continues in a straight line until the pilot rolls to some bank angle and executes an n-'g' turn starting from R_V at constant V. When the aircraft is aligned toward the original target location the pilot rolls out and attacks using the first-pass maneuver. Figure 83 shows the second-pass maneuver.
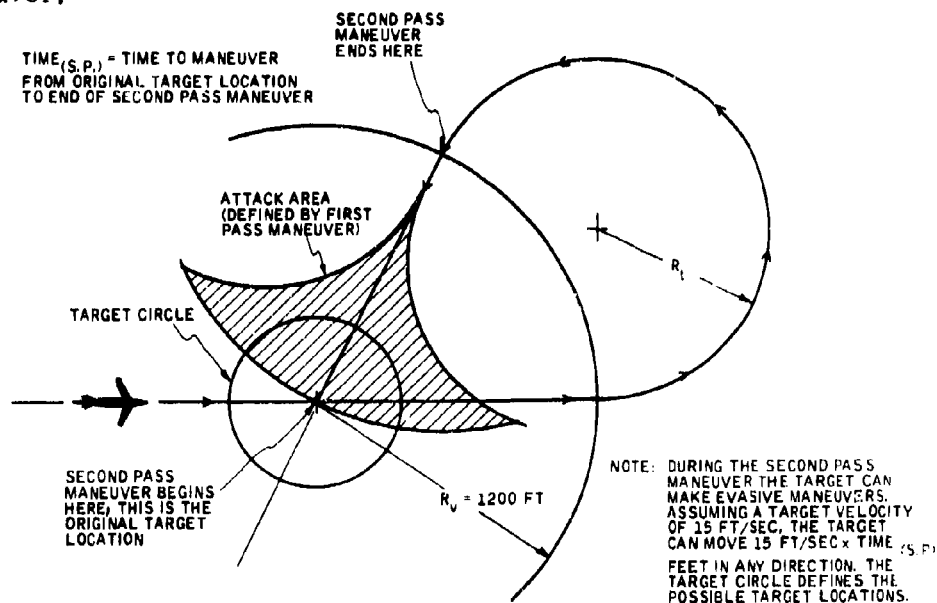
Figure 83. Second-Pass Maneuver

The fuel for the second-pass maneuver is calculated using the same equation as for the first-pass maneuver. The required fuel is the fuel to turn plus twice the fuel to roll (i. e., roll in and out of the turn).

The detailed calculation is found in Appendix B. The only changes in the terms occur because of the larger turn around executed in the second-pass maneuvers. At a load factor n = 2 and V = 200 ft/sec, the fuel required for the second-pass maneuver is 0.418 lbs/maneuver.

Other choices of n and V will yield a variation in fuel of approximately 0.080 lb/maneuver. The given choice of n and V is representative of typical high-g COIN manevuers.

Pull-up -- The final maneuver described in Reference 24 is the pull-up over a 50-ft obstacle. The model used was: the aircraft is approaching a potential target at ground level and constant velocity; and at the visual radius (R_V) the target is identified and attack begins. The target is at the base of a 50-ft obstacle so that the aircraft must pull-up some distance from the target. Figure 84 shows the pull-up maneuver.

107
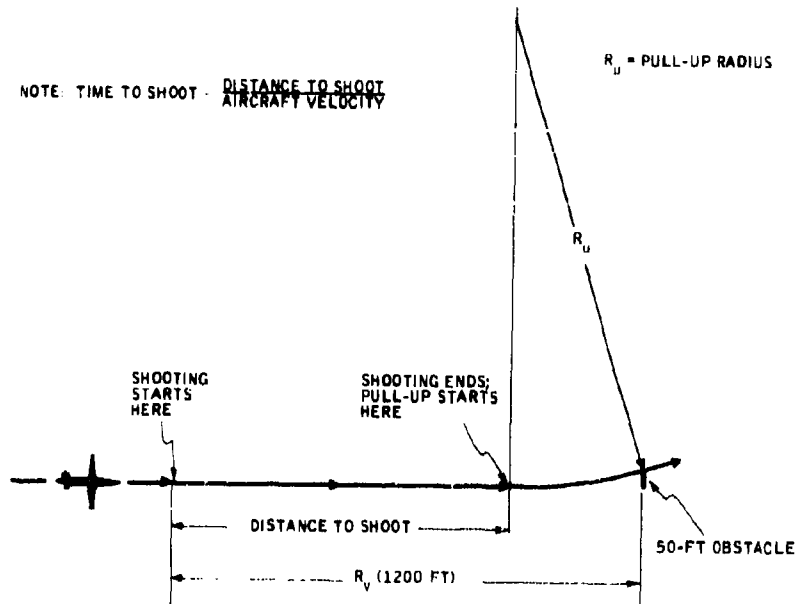
Figure 84. Pull-up Maneuver

The fuel to pull-up was calculated for the pull-up from level flight to the top of the 50-ft obstacle. The method of calculation is presented in Appendix B. Two load factors were chosen to estimate the pull-up fuel. It was found that the required fuel is 0.030 lbs/maneuver at $n = 2$ and 0.057 lbs/maneuver at $n = 3$. Thus, the pull-up is the least fuel consuming maneuver considered.

WEIGHT AND FUEL ESTIMATE

The purpose of this subsection is to estimate the total extra weight that must be added to the OV-10A aircraft to incorporate a NEMS blown control system. To do this we must assume a design configuration. A detailed design is beyond the scope of the present work; however, since this is basically a feasibility study, we need only make a conservative estimate of the weight requirement. If this upperbound of the system weight is within reasonable limits, feasibility will have been shown. A generalized method of powering the VDT device was configured as follows:

- The first design choice is blower pressure ratio. The power required is a function of blown thrust required and blower pressure ratio. If bleed air is drawn from the compressor of a turboshaft engine the pressure ratio will be between 8-13 atmospheres.

108

If bypass air is bled from a turbine specially designed for providing blowing air the supply pressure ratio will be nominally 2 atmospheres. For any given thrust approximately twice as much horsepower is required at a pressure ratio of 8 than is required at pressure ratio of 2. For this reason, we will consider an operating pressure ratio of 2 atmospheres for our design model.

● For most of a typical COIN mission, little or no blowing is required for control. To run the blowing engine at full power throughout the entire mission would require a prohibitive amount of fuel and is not necessary for primary control. Early jet-flap investigators envisioned aircraft for which the entire propulsive thrust and lift control was obtained from jet-flap blowing. While this is theoretically possible at the cruise speed of the OV-10A, it is more power effective to obtain propulsive thrust from the propellers than from the jet flap. To demonstrate this we compare the propulsive efficiency of the turbo-prop engines and the jet flap at the cruise speed of the OV-10A. The propulsive efficiency (η) is defined as the net propulsive thrust (T) multiplied by the forward velocity (V) divided by the power required (SHP) to produce the thrust; i.e.,

$$\eta = \frac{TV}{SHP}$$

For the turbo-prop, η = 0.90, while for the jet flap at pressure ratio of 2.0, η = 0.38. As mentioned earlier, at a pressure ratio of 8.0 the power required to produce a given thrust is about twice as much as it would be at pressure ratio of 2.0. Thus, at a pressure ratio of 8.0 the propulsive efficiency of jet-flaps is 0.19. It would be possible to operate the jet flap at full thrust (340 lbs in this case) and reduce the propeller thrust by the same amount. However, the propellers would require less than half the fuel (0.38/0.90 less fuel) than would be required to provide the same thrust using jet flaps. As the velocity (V) increases the thrust (T) and power (SHP) for the jet flap remain essentially constant. This means that as the speed increases the thrust efficiency for the jet flap will also increase. There may be a speed range and pressure ratio combination for which full-time jet-flap operation is economical. For the OV-10A, however, intermittent VDT thrusting is necessary.

● To provide intermittent thrusting, the system must have a throttleable engine-compressor. In a final design the engine lag time ("rev up time") must be minimized to obtain continuous VDT thrust as quickly as possible. For the present

109

system, the engine was assumed to operate at 5% rated horsepower throughout the mission and be capable of acceleration to full power in 1 sec.

- During the time required to bring the engine to full power (1 sec lag), an energy accumulator can provide blowing air instantaneously upon pilot demand. The accumulator is a pressure tank filled with compressed air. The air in the tank must be at a pressure higher than the nominal system operating pressure (pressure ratio 2.0) so that the tank air can be supplied through a dropping regulator at pressure ratio 2.0 whenever needed. The pressure ratio in the accumulator should be of the order of 8 to 13 in order to keep the accumulator volume to reasonable proportions. There are many possible combinations of tank volume and pressure ratio to eliminate the engine lag problem. The optimal combination of parameters were not determined for this study. However, a reasonable set of parameters were chosen and the design weights and fuel requirements were determined from them.

  For this study it was assumed that the primary blowing air-flow is bled at pressure ratio 2.0 from the bypass section of a high-bypass turbo-shaft engine, and the accumulator was designed to use air bled from the high-pressure section of the engine compressor at a pressure ratio of 8.0.

- An automatic demand control system must be developed which throttles the engine and alternately drains and fills the accumulator. This control must sense the state of the bleed control system and operate the jet flap at the thrust values required to maneuver the aircraft according to pilot commands.

Before the exact configuration of the VDT powering system is determined, the engine and bleed control will have to be studied in terms of the expected mission profile and engine lag characteristics. However, a schematic diagram of the VDT control system chosen for the weight estimate is shown in Figure 85.

The total extra weight which must be added to modify the OV-10A aircraft to employ a VDT primary flight control system is:

W_t = engine weight + compressor weight + accumulator weight + fuel weight for 30 maneuvers + fuel weight to run the engine at 5% of full power over the entire mission + extra fuel for turboprops to carry W_t over the mission.

110
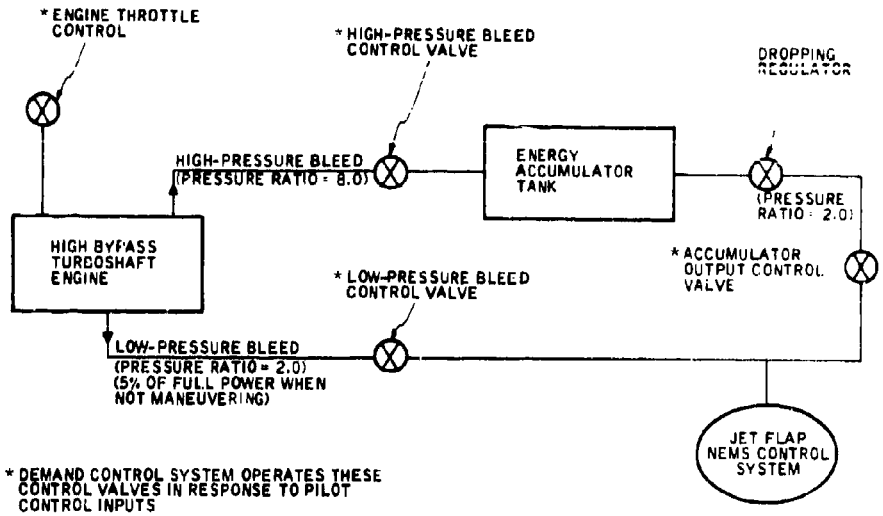
Figure 85. Conceptual Engine-Bleed Control System

The weight of the air supply ducting was neglected in this estimate as it was assumed it would be close to the net weight of the conventional control system linkages which the NEMS devices replace. Each of these weights can be estimated for the preliminary control system design shown in Figure 85.

The total horsepower was sized from the condition of maximum continuous thrust required. This condition is the engine out landing where maximum thrust at the vertical and horizontal tail is required. The horsepower for this maneuver is 486. Horsepower-versus-weight trends were established from Reference 22 for turbo-shaft engines within a power range from 200 to 600 HP. Within this range the engines produce approximately 2 SHP for each pound of engine weight so that the required engine weight will be 243 lbs.

The added weight due to bypass turbine cascade and associated control hardware was taken to be 25% of the engine total weight. The total compressor weight is then estimated to be 62 lbs. The extra engine and compressor weight could be in the form of a third engine acting as an auxiliary power supply for the jet-flap system. Alternatively, the existing engines could be modified to provide the bypass air and high-pressure bleed. In either case, the weight and fuel requirements are determined in the same manner. The weight and fuel required are based on the trends of weight per horsepower-hour for this class of engine.

111

For a design pressure ratio of 8.0, the accumulator volume needed to supply the equivalent of full-power operation for the 1-sec lag time is 8.37 cu. ft. An 8-in. diameter cylinder 13.5 ft long would contain the required volume and fit into one of the tail booms of the OV-10A. If the cylinder were made of aluminum and designed for a safety factor 2.0 it would weigh 24 lbs.

The fuel required to operate the engine at 5% maximum power during a typical COIN mission of 250-nautical-mile cruise with 1.5-hr loiter over the target area is 74 lbs. A fuel consumption rate of 0.70 lbs/horsepower-hr was estimated from turbo-shaft engine trends in Reference 22. During this mission 14 lbs of fuel for performing the maneuvers discussed in the section on maneuvering fuel requirements would be enough for 30 typical high-g attack maneuvers.

The only term which has not yet been calculated is the fuel to carry the extra weight. This extra fuel comes from the need for extra turbo-prop thrust to overcome the induced drag caused by the added weight, W_t. An L/D of 10 and a total mission time of 4.5 hrs at an average velocity of 280 ft/sec were assumed. Using an average VDT system weight, it was estimated that 63 extra pounds of fuel are required. The total extra weight from all the additions considered for this NEMS feasibility study are:

Item	Weight (lbs)
Engine and Compressor	305
Fuel for 30 maneuvers	14
Fuel for 5% engine idle	74
Extra fuel for total weight	63
Accumulator	24
Total	480

This total weight constitutes nearly 4% of the nominal gross weight of the OV-10A.

The 4% increase in the total weight of the OV-10A aircraft can be added without decreasing the payload. If the payload remains constant, the VDT primary flight control system's weight would increase the OV-10A's gross weight. This would require longer landing distances for the one-engine-out landing when all available VDT thrust is needed for primary flight control. However, for normal takeoff and landing conditions, there will be an excess of VDT thrust available which can be used for increasing $C_{L_{max}}$. Therefore, STOL performance will not be degraded but can be improved with the addition of VDT primary flight control. Under normal takeoff conditions, it was estimated that the takeoff distance of the OV-10A could be shortened by 50 ft to 150 ft depending on the payload carried.

112

COIN AIRCRAFT ATTACK EFFECTIVENESS

In studying the feasibility of using VDT blowing for primary flight control, VDT system capabilities can be evaluated in terms of aircraft maneuverability. Reference 24 has shown that the aircraft's "attack effectiveness" during reconnaissance-strike (R/S) missions is a practical criteria for judging COIN aircraft maneuverability. "Attack effectiveness" can be defined as the aircraft's ability to attack targets sighted by the pilot. Quantitative estimates of the OV-10A aircraft "attack effectiveness" are included in this report to compare the OV-10A with NEMS primary flight control to the conventional OV-10A aircraft.

Following the analysis of Reference 24, the "attack effectiveness" was calculated for three types of R/S maneuvers. The selected maneuvers are labeled as: (1) first-pass maneuver, (2) second-pass maneuver, and (3) pull-up maneuver and are defined as before when estimating the fuel consumption per maneuver. A set of definitions for the attack effectiveness of the OV-10A with and without the VDT control system was developed.

The aircraft first-pass effectiveness (AFPE) is defined as the ratio of the area in a visual quadrant which the aircraft can maneuver to attack to the area of the visual quadrant (see Figure 82). The area which can be attacked is determined by the aircraft roll and turn performance. The AFPE increases as the time to roll decreases and the available load factor increases.

In many situations the target cannot be attacked on the first pass and a second pass is required. The aircraft second-pass effectiveness (ASPE) was defined in Reference 24 as the ratio of the attack area to the area of the target circle (see Figure 83).

Since this definition makes the ASPE heavily dependent upon the AFPE, it was decided that the second pass could be more simply evaluated by the time to maneuver the aircraft to a position where the first pass can be executed. That is, the second-pass attack effectiveness was investigated by calculating the time required to maneuver from the original target location to the pilot's visual radius and complete an n-'g' turn until the aircraft is aligned toward the original target location. At this time the pilot may attack with the first-pass maneuver.

The aircraft pull-up maneuver can be used to assess the potential attack of a target at the base of a 50-ft obstacle. In COIN operations, the time to fire at such a target is relatively short since positive identification is usually required. A high volume of precise weapon delivery must be directed at the target to be effective. The time to shoot is the time the aircraft takes in traveling from the visual radius to a point where a pull-up must be executed to avoid striking the obstacle. Since the time to shoot determines the number of rounds which can be fired, it was used to measure the attack effectiveness for the pull-up maneuver.

113

At low velocities, the load factor is limited by the maximum lift, and at higher velocities the available power restricts n. This is shown in Figure 86 for three lift configurations. The three lift limits shown are: (1) $C_{L_{max}}$ without high-lift flaps, (2) $C_{L_{max}}$ with high-lift flaps, and (3) $C_{L_{max}}$ with full-span jet-flap blowing. The thrust required for longitudinal flight control was estimated from Table 2 at a cg location 0.30 c from the wing leading edge. The remainder of the available jet thrust was allocated to the full-span jet-flap blowing.

The power limits shown in Figure 86 represent the load factors which can be maintained at constant velocity. Above these limit lines the aircraft drag becomes greater than the thrust available from the turbo-prop engines. The unblown power limit is shown for the turbo-props at their current power rating.
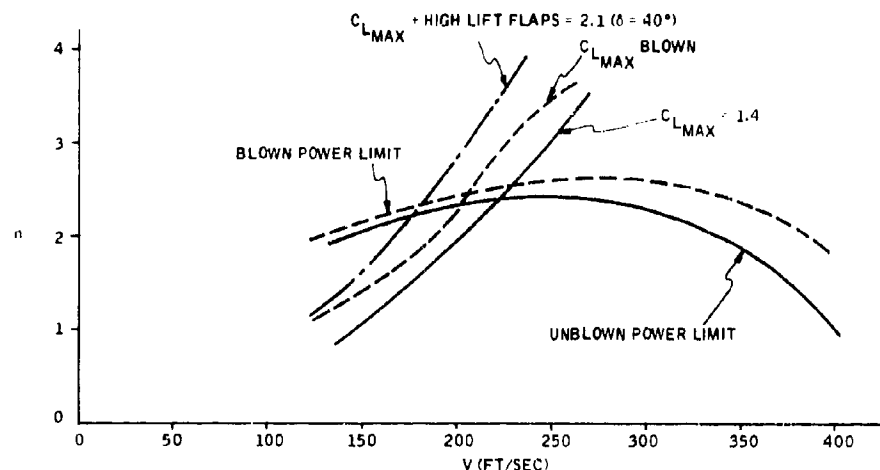
Figure 86. Power and Lift Limits for Steady Maneuvers

The attack effectiveness can be calculated using the limit lines shown in Figure 86. The maximum attack effectiveness is constrained by the maximum load factor available at any speed. Figures 87 through 89 show the AFPE, the second-pass turn-around time, and the time to shoot.

Figure 87 shows that the aircraft first-pass effectiveness is improved for the VDT-assisted wing. At speeds below 200 ft/sec, the high-lift flaps provide nominally the same AFPE as the VDT device. However, there is a
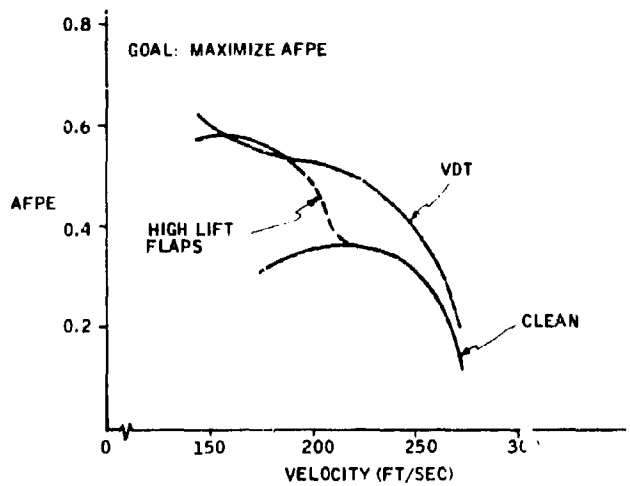
Figure 87. Aircraft First-Pass Effectiveness
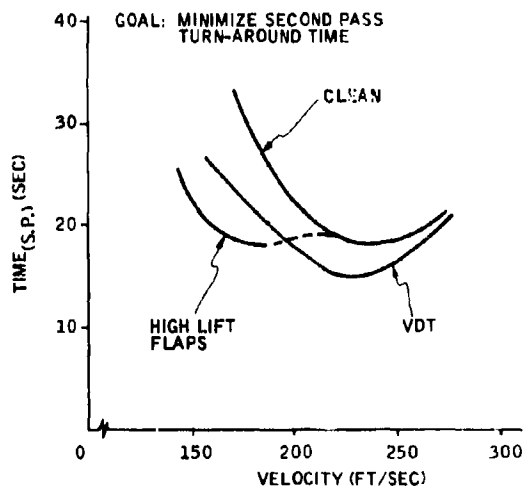
Figure 88. Second-Pass Turn-Around Time

115

possibility that the high-lift flaps can become overstressed at aircraft speeds exceeding those normally encountered in landing and takeoff. This particular danger is avoided in the NEMS system. The VDT control can also respond rapidly to pilot commands. Changes in the maneuvering path can be executed quickly and accurately with high-lift VDT blowing.
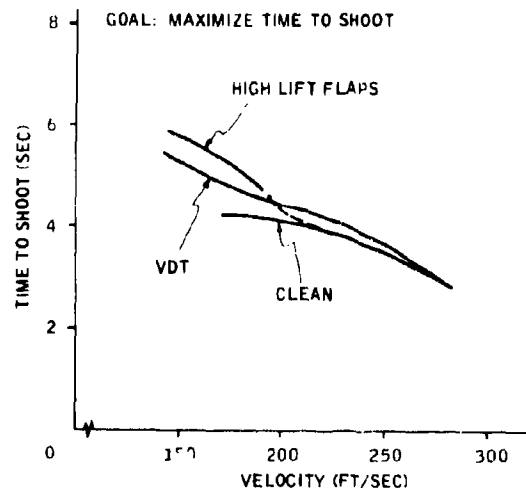
Figure 89. Time to Shoot at Base of 50-ft Obstacle

The second-pass turn-around time (Figure 88) is shown to be minimized for the VDT-augmented wing. At low velocities the high-lift flaps can provide a shorter turn-around time, but the above mentioned disadvantage still exists. At a velocity corresponding approximately to the point where the load factor becomes power-limited (Figure 86), the attack effectiveness is maximized, and there is no advantage to increasing speed.

The time to shoot at the base of a 50-ft obstacle is shown in Figure 89. It seems that little time is gained over the unassisted wing for either the VDT- or high-lift-flap-assisted case. At an aircraft velocity of 175 ft/sec, for example, the VDT case increases the shooting time by approximately 0.6 sec, and the high-lift flaps increase the time by 1.0 sec. With a cyclic rate of fire of 1200 rounds/min for two guns, the OV-10A with VDT can fire 24 more rounds and the high-lift-flap-assisted wing can fire 40 rounds more than the unassisted or "clean" aircraft. Physically, it is seen that more firing time is obtained by flying slower, even though it is necessary to terminate fire at a greater distance from the target.

116

The results presented in Figures 87 through 89 indicate that the AFPE and the time to shoot are maximized at low velocity. The advantages of the high-lift devices are also apparent. Figure 88 shows that the turnaround time is shortest at a higher airspeed. Therefore, the second-pass maneuver is most effectively accomplished by increasing the speed to execute the second-pass maneuver and decreasing the speed immediately after rolling out of the turn to prepare to perform the first-pass maneuver.

BLANK PAGE

SECTION VI
CONCLUSIONS

The analytical and experimental investigations of this research program yield the following conclusions:

- **Experimental**

    1. Full-span jet-flap blowing can provide high lift at finite aspect ratio and low external airspeeds. The lift distribution due to full-span jet blowing was similar to the distribution due to wing angle of attack without blowing; that is, a nearly elliptic loading was indicated.

    2. Part-span jet-flaps show decreasing lifting capability as the ratio of the blown span to the total wing span decreases. The "lift effectiveness" $[\Delta C_L / C_{\mu_T} \sin (\tau + \alpha)]$ and "efficiency" (L/D_e) both decrease as the percentage of blown-wing area decreases.

    3. At a constant part-span blown wing area, the lift produced by jet blowing is influenced by the spanwise position of the blown area. Moving the blown area toward the wing root furnishes higher lift than outboard stations.

    4. Satisfactory predictions of lift are possible with the theory of Reference 8 for full-span blowing. The tentative method of analysis presented in Reference 11 can be used to estimate the lift available with part-span jet-flaps. However, there is clearly a need for further theoretical jet-flap work, particularly in connection with the flow field arising from part-span blowing.

    5. Blown sections strongly influence the lift distribution on neighboring unblown sections.

    6. Control rolling moments from jet-flap blowing can be produced most efficiently (with the least thrust and compressor power) with full-span blowing, and the rolling moment available is reduced as the blown-wing area is reduced.

    7. The quarter-chord moment coefficient becomes more negative (diving moment) and the center of lift moves appreciably aft on the airfoil chord as jet blowing is increased.

PRECEDING PAGE BLANK

● Aircraft Application Study

1. Calculation of the military requirements for roll-, pitch-, and yaw-axis control of an OV-10A aircraft showed that a VDT primary flight control system can meet the requirements and improve on the conventional control system capabilities.

2. To implement a VDT primary flight control system, auxiliary power must be added to the OV-10A aircraft. The added power can be used for direct lift control as well as primary flight control.

3. At a compressor pressure ratio of 2.0, it was estimated that 486 horsepower would be needed to supply high-pressure air to the VDT during a single-engine landing which was assumed to demand the greatest VDT control forces.

4. Duct losses can be ignored with a careful choice of duct area.

5. The auxiliary engine, blower, ducting, accumulator and surplus fuel required for an OV-10A aircraft VDT primary flight control system would add approximately 480 lbs to the aircraft weight. This weight represents a 4% increase in aircraft weight.

6. First-pass, second-pass and pull-up maneuvers executed with blowing thrust used for direct lift control were shown to be more effective in attacking targets than the "clean" wing configuration. High-lift flaps also improve the aircraft "attack effectiveness", but incur disadvantages avoided with blown-control high-lift devices.

7. For aircraft which fly at speeds where high-bypass engines can be operated efficiently, the jet-flap device can utilize bypass air with little loss of propulsive efficiency.

SECTION VII

RECOMMENDATIONS

The following recommendations are made for continued efforts in developing
the NEMS concept:

- Wind tunnel tests of a finite-aspect-ratio wing model with a
  chord length sufficiently large to enable extrapolation of aero-
  dynamic characteristics to full scale are needed. Such a model
  could also be heavily instrumented with pressure taps to allow
  an investigation of the pressures needed to sense the spanwise
  lift distribution.

- Before designing aircraft for NEMS system control, full aircraft
  component wind tunnel tests are needed to determine propeller
  slipstream effects and the downwash pattern at tail control sur-
  faces.

- The water analogy techniques should be applied to VDT jet-flap
  development. This technique offers great promise for exploring
  new VDT configurations and optimizing existing ones. It should
  be a valuable tool for improving the transonic and supersonic
  performance characteristics of VDT configurations. It should
  also prove valuable for studying the unsteady flow characteristics
  of NEMS jet-flap configurations.

- The effects of NEMS systems on aircraft survivability, relia-
  bility, response, range, etc., should be studied in greater
  detail.

- Further investigations of the power supply configurations for
  VDT-blown control should be conducted with the goal of mini-
  mizing power, weight and fuel consumption.

- A more detailed report of the maneuvering rate (mission profile)
  of COIN or TRIM aircraft is needed to optimize a jet-flap pri-
  mary control system.

- Greater effort should be directed toward the development of the
  ducting and control system connections necessary to enable pilot
  commands to be transferred to jet-flap control actuation.

- Additional studies of the optimum jet angle for jet-flap devices
  should be conducted; the study should not be restricted to jet
  angles attainable with a VDT device, but may indicate other
  jet-flap devices suitable to the NEMS concept.

- Further theoretical work is needed in the study of jet-flaps; in particular, a method of analysis is needed which can include part-span blowing configurations and a variety of planforms.

122

REFERENCES

1. A. P. Kizilos, "Fluid Flight Control Feasibility Study Using the Variable Deflection Thruster (U)," Honeywell Inc. Doc. No. 12016-FR1, December 1966, Confidential. Prepared under Contract NOw 65-0556-d for Naval Air Systems Command, Department of the Navy.

2. A. P. Kizilos and R. E. Rose, "Experimental Investigations of Flight Control Surfaces Using Modified Air Jets," Honeywell Inc. Doc. No. 12055-FR1, October 1968. Prepared under Contract N00019-67-C-026 for Naval Air Systems Command, Department of the Navy.

3. A. P. Kizilos, B. M. Kizilos, and G. A. Smith, "Study of Blowing Transverse Jets from Airfoils for Flight Control Applications in the Mach Number Range 0.2 to 3.0," Honeywell Inc. Doc. No. 12146-FR, November 1970. Prepared under Contract N00019-69-C-0286 for Naval Air Systems Command, Department of the Navy.

4. G. K. Korbacher and K. Sridhar, "A Review of the Jet Flap," UTIA Review No. 14, May 1960.

5. D. A. Spence, "The Lift Coefficient of a Thin, Jet-Flapped Wing," Proc. Roy. Soc., Series A, Vol. 238 No. 121, December 1956.

6. R. E. Rose, J. M. Hammer, and A. P. Kizilos, "Feasibility Study of a Bidirectional Jet-Flap Device for Application to Helicopter Rotor Blades," Honeywell Inc. Doc. No. 12081-FR1, November 1970.

7. N. A. Dimmock, "Some Early Jet-Flap Experiments," The Aero. Quarterly, Vol. VIII, Part 4, November 1957.

8. E. C. Maskell and D. A. Spence, "A Theory of the Jet Flap in Three Dimensions," R.A.E. Rep. Aero. 2612, Sept. 1958. Proc. Roy. Aero. Soc. Vol. 251, June 1959.

9. J. Williams and A. J. Alexander, "Three-Dimensional Wind-Tunnel Tests of a 30° Jet-Flap Model," ARC-17990, Perf. 1399, FM 2326 S and C 3049, November 1956.

10. A. Pope, Basic Wing and Airfoil Theory, First Edition. McGraw-Hill Book Co., Inc., 1951.

11. J. Williams, S. F. J. Butler, and M . N. Wood, "The Aerodynamics of Jet Flaps," R.A.E. Report No. Aero. 2646-A.R.C. 22823, January 1961.

12. E. C. Maskell, "The Interference on a Three-Dimensional Jet-Flap Wing in a Closed Wind Tunnel," R.A.E. Tech. Note No. Aero. 2650-A.R.C. 21598, August 1959.

13. R. C. Pankhurst and D. W. Holder, Wind-Tunnel Technique, Sir Isaac Pitman and Sons, LTD., 1952.

14. C. C. Critzos, H. H. Heyson, R. W. Boswinkle, Jr., "Aerodynamic Characteristics of NACA 0012 Airfoil Section at Angles of Attack from $0°$ to $180°$," NACA Tech. Note 3361, January 1955.

15. D. Kuchemann, "A Method for Calculating the Pressure Distribution of Jet-Flapped Wings," R.A.E. Rep. Aero - 2573, May 1956 or A.R.C. 18474, R. and M. No. 3036, 1957.

16. A. Pope, Wind-Tunnel Testing, John Wiley and Sons, Inc., 1947.

17. I. H. Abbott and A. E. Von Doenhoff, Theory of Wing Sections, Dover Publications, Inc., 1959,

18. A. J. Alexander and J. Williams, "Wind-Tunnel Experiments on a Rectangular-Wing Jet-Flap Model of Aspect-Ratio 6," A.R.C. Reports and Memoranda, No. 3329, June 1961.

19. "Estimated Aerodynamic Characteristics of the 40-Foot Span OV-10A Airplane," Columbus Division, North American Rockwell Corporation, Report No. NA 67H-596, Feb. 20, 1968.

20. "Flying Qualities of Piloted Airplanes," Military Specification MIL-F-008785A (USAF) Dept. of Air Force, Air Force Flight Dynamics Lab., Wright-Patterson Air Force Base.

21. Background Information and User Guide for MIL-F-8785B(ASG), "Military Specification - Flying Qualities of Piloted Airplanes," Chalk, Neal, Harris and Pritchard, Cornell Aero. Lab. for the Air Force Flight Dynamics Lab., Wright-Patterson Air Force Base.

22. Jane's All the Worlds Aircraft, McGraw-Hill, 1969.

23. J. R. Henry, "One-Dimensional, Compressible, Viscous Flow Relations Application to Flow in a Ducted Helicopter Blade," NACA T.N. 3089, December 1953.

24. H. C. Larson, "Considerations in the Design of COIN Aircraft," Air Force Institute of Technology, Wright-Patterson Air Force Base, Ohio, J. Aircraft Vol. No. 3, June 1968.

25. William T. Thomson, Vibration Theory and Applications, Prentice Hall, Englewood Cliffs, N. J., 1965 (pp 36-55).

APPENDIX A

BALANCE TABLE DESIGN AND USE

FORCE TABLE DESCRIPTION

A force table balance was made which measures force components in the x and y direction as well as the moment in the x, y plane. Figure A1 shows the basic configuration of the table balance and the location of the x and y axes on the table top. All forces and moments are measured in the plane of the table top.

The location of the F_x and F_y flexure reeds is clearly shown in Figure A2. Figure A2 shows the moment reeds attached to the baseplate with the rest of the balance system removed.

The shape and position of each flexure reed was chosen to provide the highest possible bending stiffness to oppose the loadings not being measured by the reed. The bending stiffness in the direction of the force measured was low enough to allow sufficient bending strain for measurement with strain gage instrumentation. The F_x reeds, for example, are 1000 times stiffer in the y-direction than they are in the x-direction, and similarly the F_y reeds are much stiffer in the x-direction than they are in the y-direction. In this way y-loadings and moments are transmitted "edgewise" through the F_x reeds, and the x-signal is not affected by the other forces. The analogous argument holds for the F_y reeds. (See Figure A3 also, to further clarify this point.)

The moment reeds (See Figure A2) are positioned so that any x- or y-load is taken edgewise by one or the other set of moment reeds. The four moment reeds are relatively flexible to rotation about the x, y origin, however, and this permits them to respond to the torsional loads.

The wiring diagram for the three channels is shown in Figures A4 and A5.

FORCE TABLE STATIC RESPONSE

If the arguments presented above are true, the various output channels should respond only to the appropriate loadings, and the position of the load on the table should not effect the output.

To test this out, forces were applied at the points shown in Figure A6, and the output of each channel was recorded. The strain gage output was amplified by the BAM-1 amplifier-meter, and the voltage was measured with an oscilloscope. Figures A7, A8 and A9 are plots of the loading-versus-voltage output for the F_x, F_y, and moment output channels, respectively. The BAM-1 was set to regular range amplification with the potentiometer set at 500.

125
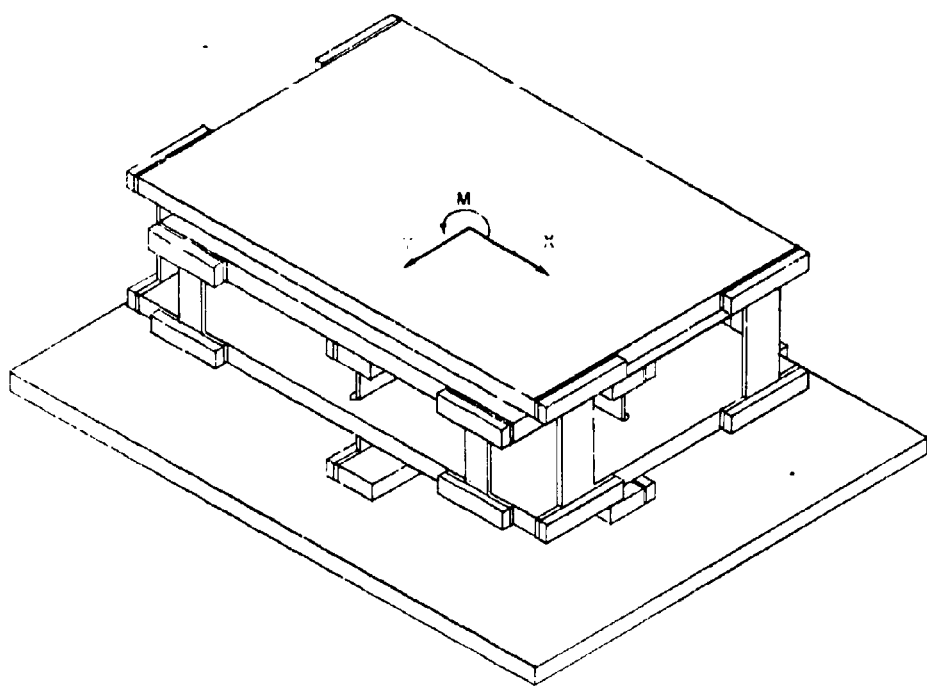
Figure A1. Force Balance Table Configuration
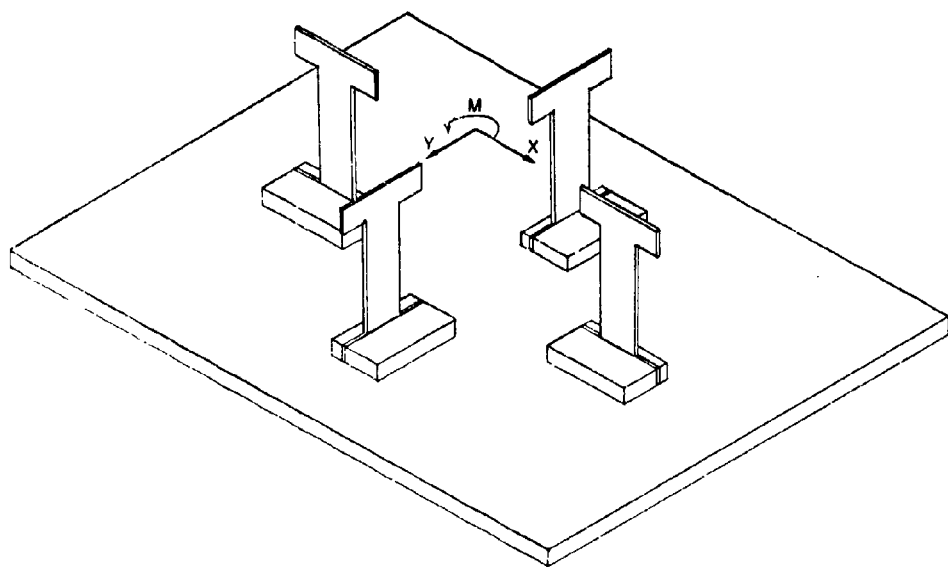
Figure A2. Force Balance Table Flexure Reeds

126
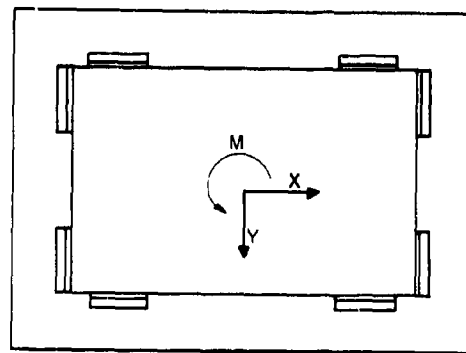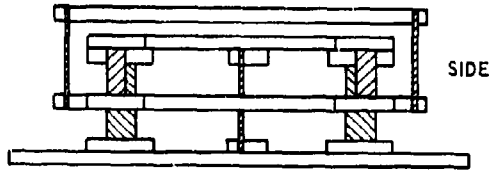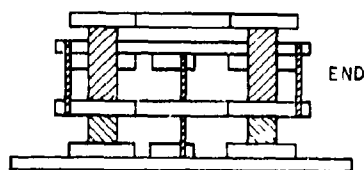
Figure A3.   Three Views of Force Balance Table

127
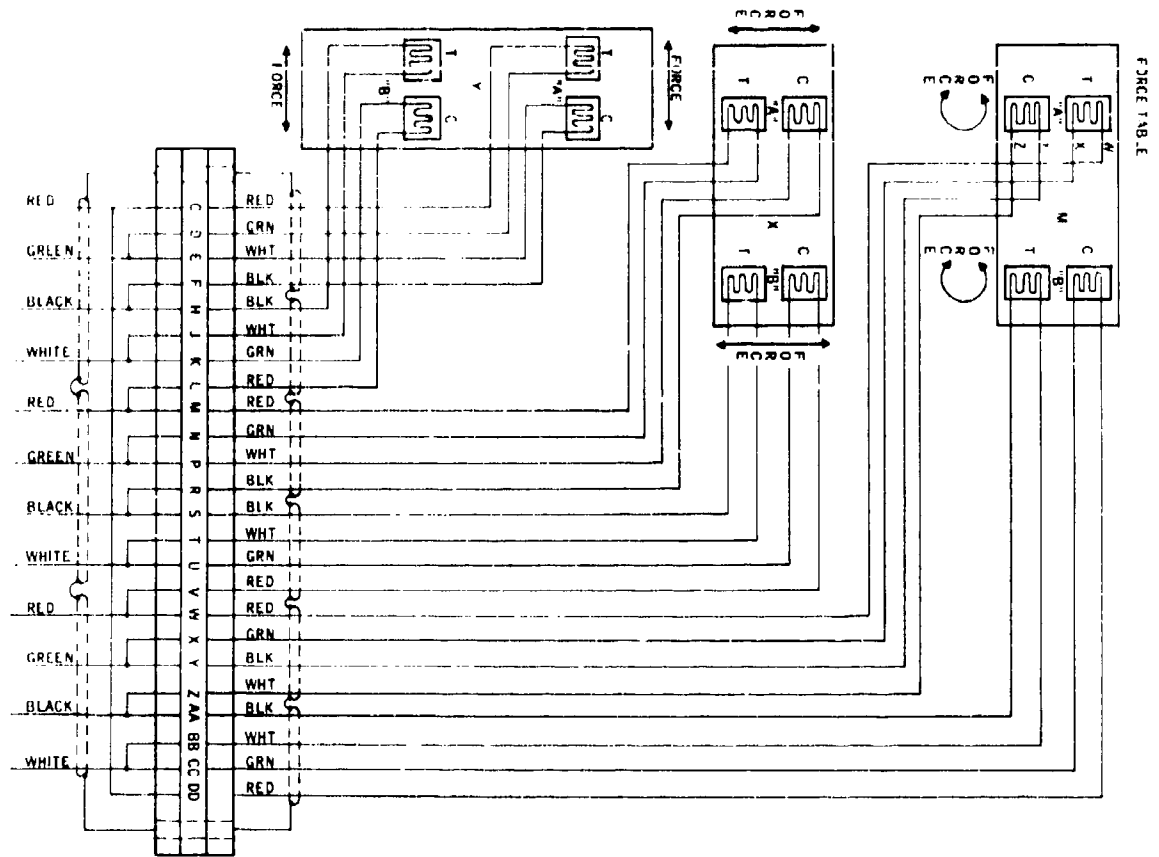
Figure A4. Strain Gage Wiring Diagram for Force
Table Flexure Reeds
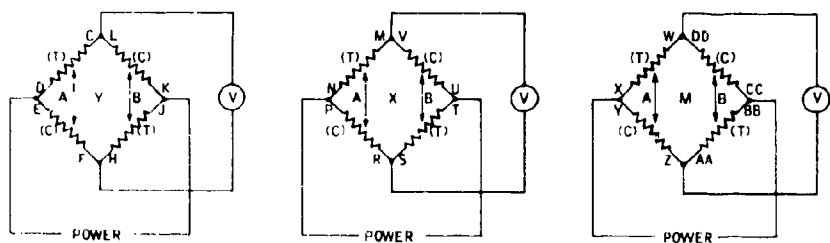
Figure A5. Bridge Circuits for Strain Gage Measurement
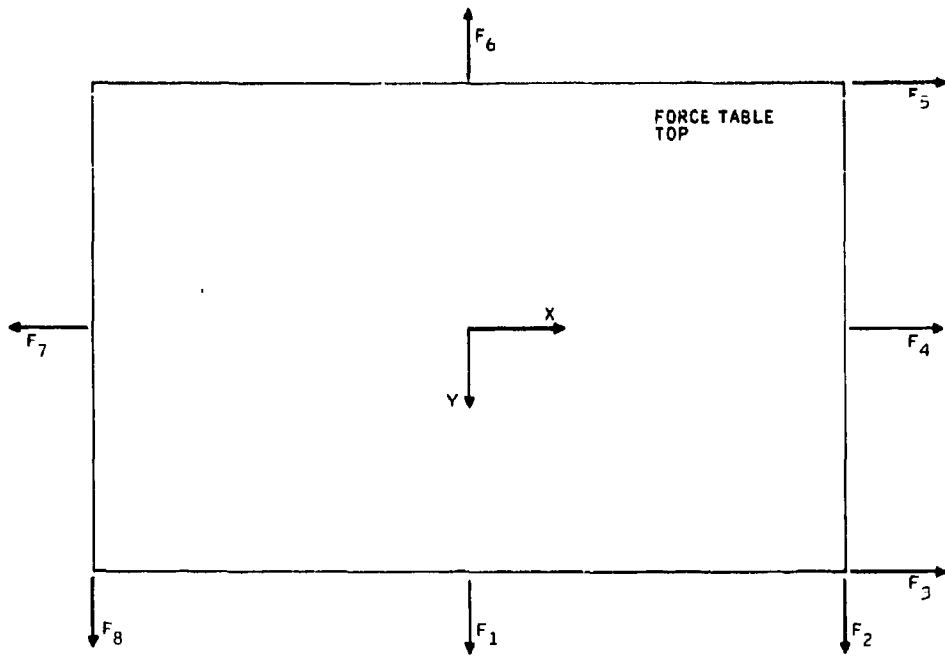
Figure A6. Position of Applied Forces for Balance
Table Calibration
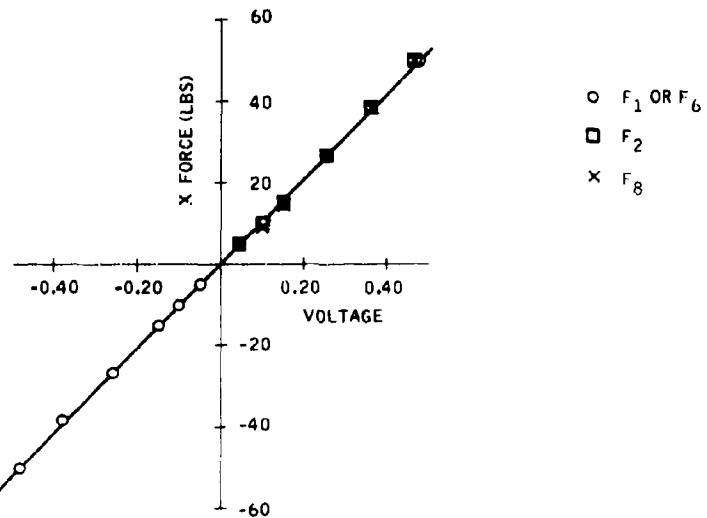

Figure A7. Calibration of Forces in X-Direction
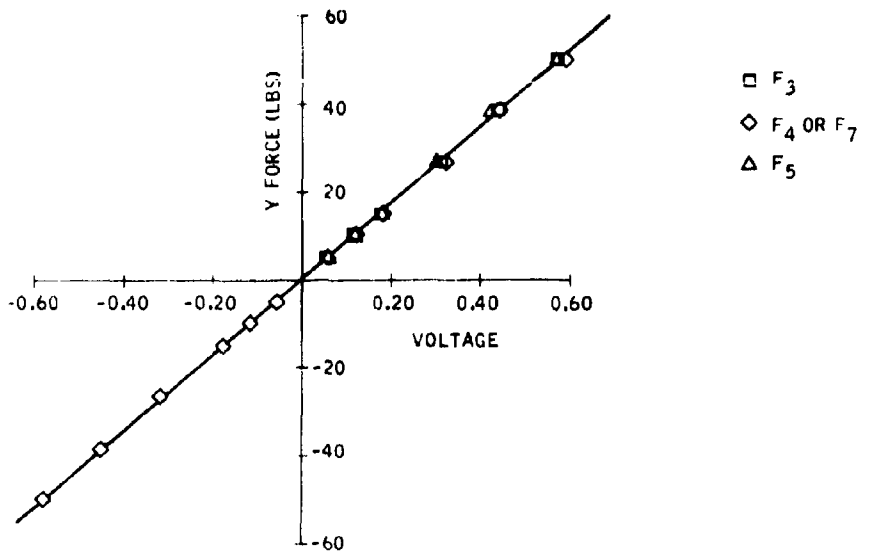
Figure A8. Calibration of Forces in Y-Direction
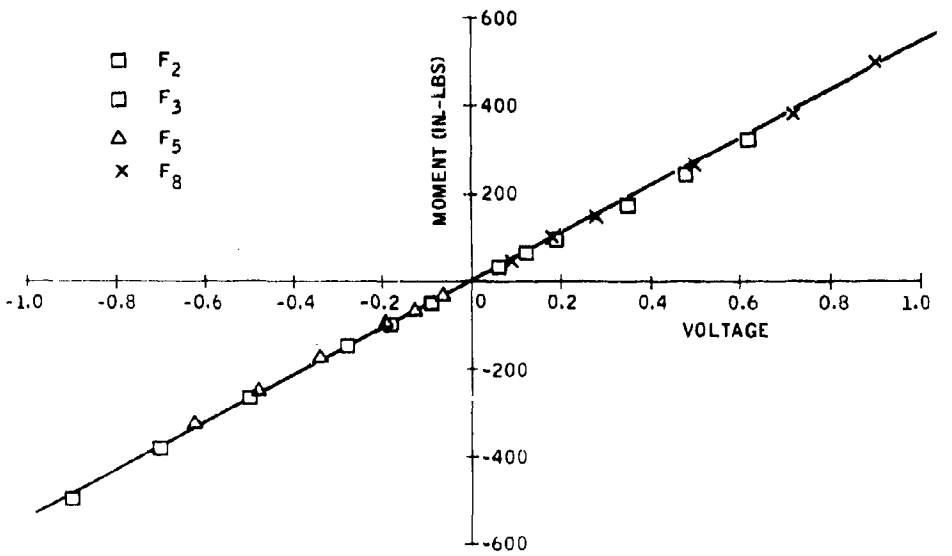
Figure A9. Calibration of Applied Moments

130

It is clear, from inspection of these plots, that the location of the force does not affect the output. The F_y channel indicated zero force for all the x-loadings tried, as did the F_x channel for the y-loading. The application of the forces F_1, F_4, F_6, and F_7 produced no moment about the x, y origin, and the moment channel produced no measurable signal under these loads.

DYNAMIC RESPONSE

The balance was designed to give maximum sensitivity for steady low-level (less than 150 lbs) force measurement. The result is the natural frequency of oscillation of the various table levels is low.

The strain gage output was monitored with a "memory" oscilloscope, and the free vibration behavior was recorded. The period of oscillation τ (sec) was recorded for each channel along with the relative amplitude of first and N^{th} oscillations. With this data the natural frequency ω_n and damping ratio ζ was calculated using the following equations as obtained from Reference 25:

$$f_d = \frac{1}{\tau_D} \quad (Hz) \tag{eqn A1}$$

$$\omega_D = 2\pi f_D \quad \left(\frac{Rad}{Sec}\right) \tag{eqn A2}$$

$$\omega_n = \frac{\omega_D}{\sqrt{1 - \zeta^2}} \quad \left(\frac{Rad}{Sec}\right) \tag{eqn A3}$$

$$\delta = \frac{1}{N} \ln \frac{x_o}{x_N} \tag{eqn A4}$$

$$\delta = \frac{2\pi \zeta}{\sqrt{1 - \zeta^2}}$$

or

$$\zeta = \frac{\delta}{\sqrt{4\pi^2 + \delta^2}} \tag{eqn A5}$$

where

f_D is damped natural frequency

131

τ_D is damped period

ω_n is natural frequency

δ is logarithmic decrement

x_0 is the amplitude of the first cycle

x_N is the amplitude of the Nth cycle

ζ is the damping ratio $\dfrac{c}{c_c}$

The time required for an oscillation to damp to 5% of its original amplitude is t^*, where

$$0.05 = e^{-\zeta \omega_n t^*}$$

$$\text{Log}_e (0.05) = - \zeta \omega_n t^*$$

$$t^* = \frac{\log_e (0.05)}{-\zeta \omega_n} = \frac{-2.995}{-\zeta \omega_n} \qquad \text{(eqn A6)}$$

A table of these parameters is shown below.

Channel	f_n (hz)	ζ	t^* (sec)
F_x	26.7	0.0027	6.8
F_y	19.6	0.0042	5.9
M	13.9	0.0053	6.4

These results indicate that, where dynamic measurement is necessary, the flexure reeds must be stiffened, at the cost of sensitivity, to eliminate resonance problems.

The balance was designed to facilitate this procedure. The reed holder (see Figures A1 through A3) is removed, and a new reed with the desired thickness is "sandwiched" in the holder with the original reed. The stiffening is done to a pair of reeds in the same plane. For example the pair of F_x and F_y reeds

clearly visible in Figure A2 could be stiffened and the other pair left unchanged. The best pair of moment reeds to stiffen is the pair shown parallel to the x-axis in Figure A2.

A formula for selection of the "sandwich" reed thickness is given below (note this relation holds only if two of the four reeds are stiffened):

$$\frac{T_h{}'}{T_h} = \left[2\left(\frac{\omega_n{}'}{\omega_n}\right) - 1\right]^{1/3} \qquad \text{(see Figure A10)} \qquad \text{(eqn A7)}$$

where

$T_h{}'$ = thickness of original reed plus sandwich reed

T_h = thickness of original reed

$\omega_n{}'$ = desired natural frequency

ω_n = original natural frequency

The sensitivity change is given by

$$\frac{S'}{S} = \left(\frac{\omega_n{}'}{\omega_n}\right)^{-2} \qquad \text{(see Figure A10)} \qquad \text{(eqn A8)}$$

where

S' is the sensitivity of the altered balance.

S is the original sensitivity

If the system is subjected to a sinusoidal forcing function of the form

$$F = F_o \sin(\omega t)$$

its response F_m will be

$$F_m = \frac{F_o}{\sqrt{1 - (\omega/\omega_n)^2 + 2\xi(\omega/\omega_n)^2}} \sin\left(\sqrt{1 - \xi^2}\ \omega_n t + \phi\right) \qquad \text{(eqn A9)}$$

133
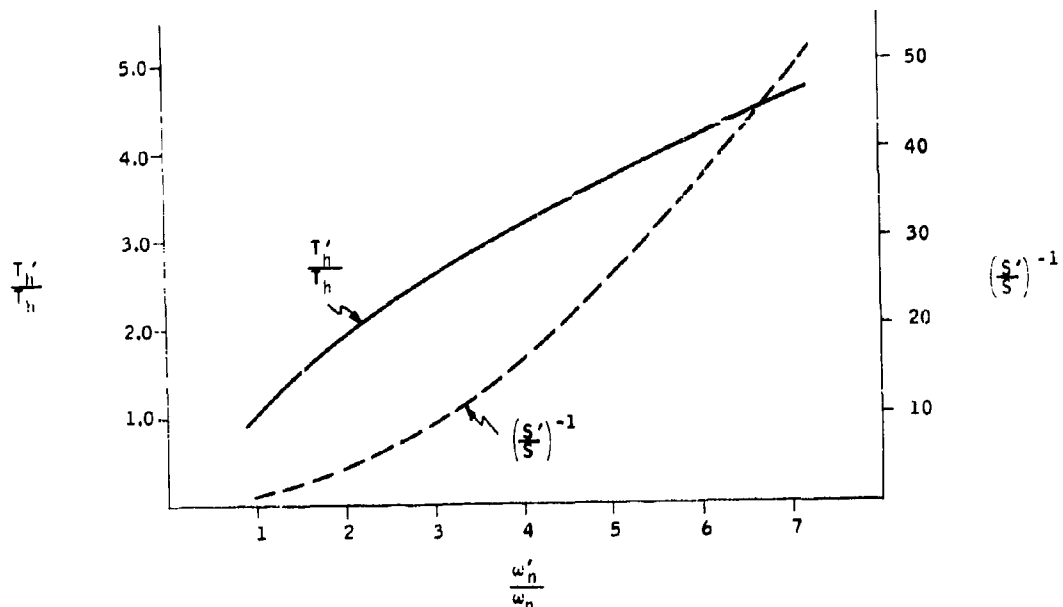
Figure A10. Effect of Flexure Reed Thickness on Force
Table Natural Frequency and Sensitivity

where

$$\tan \phi = \frac{2\xi(\omega/\omega_n)}{1 - (\omega/\omega_n)^2}$$

BALANCE SYSTEM USE AND LIMITATIONS

The balance system has been shown to have no measurable interaction be-
tween the force components. With appropriate choice of stiffness, the system
can measure a wide range of static and dynamic loads. The dynamic behavior
of the various channels is uncoupled and will remain so if care is taken to
keep the center of mass of any test equipment placed on the balance at the x,
y origin.

APPENDIX B

OV-10A AIRCRAFT, VDT CONTROL SYSTEM

This appendix briefly gives the aircraft steady-state equations used in the analysis of these common reconnaissance/strike maneuvers and shows the method used to estimate VDT control system fuel consumption for each maneuver.

FIRST-PASS MANEUVER

First-pass maneuver geometry is shown in Figure B1.
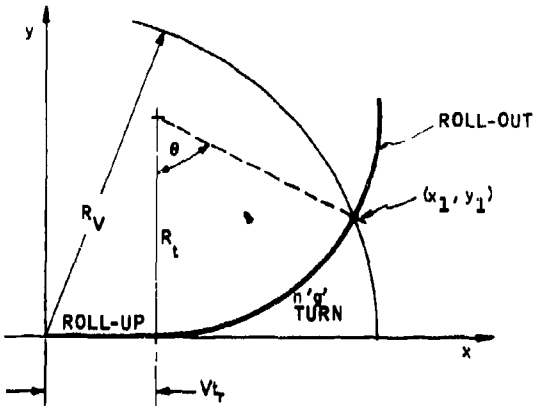
Figure B1. First-Pass Maneuver Geometry

Symbols used in the figure and in the following discussion are:

ϕ = bank angle (rad)

p = roll rate (rad/sec)

n = load factor

V = aircraft velocity (ft/sec)

R_t = radius of turn (ft)

t_r = time to roll (sec)

t_t = time to turn (sec)

135

R_v = visual radius (ft)

θ = angle of turn (rad)

$\dot{f}$ = fuel consumption rate (0.70 $\dfrac{\text{lbs fuel}}{\text{hp-hr}}$, for turbine engines surveyed in Ref. 22)

F_r = fuel to roll (lbs)

F_t = fuel to turn (lbs)

Equations for the roll maneuver are

$$\phi = \cos^{-1}\left(\frac{1}{n}\right) \qquad \text{(eqn B1)}$$

$$t_r = \frac{\phi}{p} = \frac{\cos^{-1}\left(\frac{1}{n}\right)}{p} \qquad \text{(eqn B2)}$$

where n was selected as n=2 at V=200 $\frac{\text{ft}}{\text{sec}}$ and n=3 at 250 $\frac{\text{ft}}{\text{sec}}$. The roll rate, p, was assumed to be the maximum available, p = 0.121 rad/sec.

$$t_r = 0.87 \text{ sec } (n=2)$$

$$t_r = 1.00 \text{ sec } (n=3)$$

The fuel to roll is calculated from

$$F_r = \text{Roll hp} \cdot \dot{f} \cdot tr/3600 \qquad \text{(eqn B3)}$$

At a roll hp of 400 (near maximum for part-span VDT roll control) the fuel to roll is

$$F_r = 0.0665 \text{ lbs } (n=2)$$

$$F_r = 0.0763 \text{ lbs } (n=3)$$

The equation for the turn maneuver is

$$R_t = \frac{V^2}{g\,(n^2-1)^{1/2}} \qquad \text{(eqn B4)}$$

and, using the x-y coordinate system shown

136

$$y_1 = R_t (1 - \cos\theta)$$

$$x_1 = Vt_r + R_t \sin\theta$$

$$x_1^2 + y_1^2 = R_v^2$$

such that

$$\cos\theta = \left(\frac{R_v^2}{2R_t^2} - \frac{1}{2} - \frac{V^2 t_r^2}{2R_t^2}\right) - \left(\frac{Vt_r}{R_t}\right)\sin\theta \qquad \text{(eqn B5)}$$

The above equation was solved for θ by squaring both sides and solving a quadratic for $\sin\theta$:

let $\qquad A = \left(\dfrac{R_v^2}{2R_t^2} - \dfrac{1}{2} - \dfrac{V^2 t_r^2}{2R_t^2}\right) \qquad$ and $\quad B = \dfrac{Vt_r}{R_t}$

then

$$\theta = \sin^{-1}\left[\frac{AB \pm \sqrt{B^2 - A^2 + 1}}{B^2 + 1}\right]$$

This expression was solved and the correct root selected for θ. The time to turn is

$$t_t = \frac{\theta}{V/R_t} \qquad \text{(eqn B6)}$$

and at n=2 and n=3, we find

$$t_t = 6.2 \text{ sec. } (n=2)$$

$$t_t = 4.4 \text{ sec } (n=3)$$

The fuel to turn was calculated using the horsepower values found in Table 3 at the appropriate load factor and speed.

137

$$F_t = \text{Turn HP} \times \dot{f} \times \frac{t_t}{3600} \qquad \text{(eqn B7)}$$

such that:

$$F_t = 0.106 \text{ lbs } (n=2)$$

$$F_t = 0.122 \text{ lbs } (n=3)$$

The total fuel required for a first-pass maneuver where the pilot turns all the way out to his visual radius is

$$F_{(FP)} = 2 F_r + F_t \qquad \text{(eqn B8)}$$

Substituting in, we obtain

$$F_{(FP)} = 0.239 \text{ lbs } (n=2)$$

$$F_{(FP)} = 0.274 \text{ lbs } (n=3)$$

SECOND-PASS MANEUVER

Second-pass maneuver geometry is shown in Figure B2.
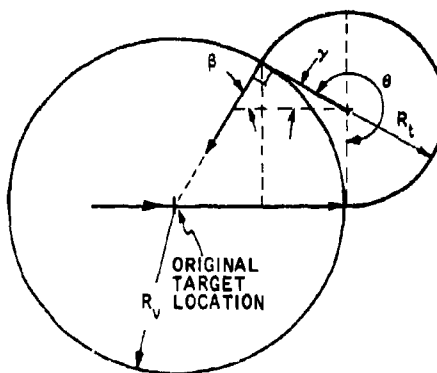
Figure B2. Second-Pass Maneuver Geometry

138

The symbols used are the same as for the first-pass maneuver, and ϕ, t_r, F_r, R_t, t_t and F_t expressions do not change. However, the expression for the turn angle is solved from

$$\theta = 270 - \gamma \qquad \text{(eqn B9)}$$

where

$$\cos \gamma = \frac{R_t}{R_v} (1 + \sin\gamma) \qquad \text{(eqn B10)}$$

Squaring both sides, a quadratic can be solved for $\sin \gamma$ to obtain

$$\gamma = \sin^{-1} \left[\frac{-\left(\frac{R_T}{R_v}\right)^2 \pm 1}{\left(\frac{R_T}{R_v}\right)^2 \pm 1} \right]$$

Then θ was readily calculated, and the results are

$$t_t = 16.7 \text{ sec} \qquad (n=2)$$

$$t_t = 12.4 \text{ sec} \qquad (n=3)$$

and

$$F_t = 0.285 \text{ lbs} \qquad (n=2)$$

$$F_t = 0.343 \text{ lbs} \qquad (n=3)$$

Since the load factors considered are the same as those used in the first-pass maneuver, the roll quantities calculated remain unchanged. The total fuel required in the second-pass maneuver is then

$$F_{sp} = 0.418 \text{ lbs} \qquad (n=2)$$

$$F_{sp} = 0.495 \text{ lbs} \qquad (n=3)$$

139

PULL-UP MANEUVER

Pull-up maneuver geometry is shown in Figure B3.
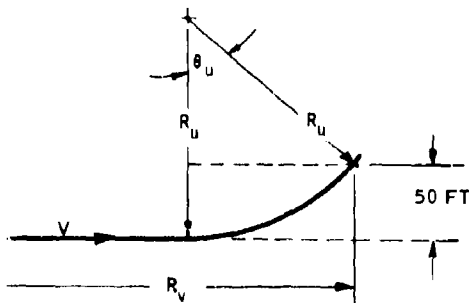
Figure B3. Pull-up Maneuver Geometry

The new symbols introduced are

θ_u = pull-up angle (rad)

R_u = pull-up radius (ft)

t_u = time to pull-up

The equations for the pull-up are

$$R_u = \frac{V^2}{g(n-1)} \qquad \text{(eqn B12)}$$

$$\theta_u = \cos^{-1}\left(\frac{R_u - 50}{R_u}\right) \qquad \text{(eqn B13)}$$

$$\dot{\theta}_u = \frac{V}{R_u} \qquad \text{(eqn B14)}$$

and the pull-up time is given by

$$t_u = \frac{\theta_u}{\dot{\theta}_u} \qquad \frac{V \cos^{-1}\left[1 - \frac{50g\,(n-1)}{V^2}\right]}{g\,(n-1)} \qquad \text{(eqn B15)}$$

At n=2 and n=3 at 200 and 250 ft/sec. respectively, the time to pull up is

$t_u = 1.75$ sec (n=2)

$t_u = 1.20$ sec (n=3)

The horsepower to pull-up was taken from Table 3 such that the fuel to pull-up was found to be

$F_u = 0.030$ lbs (n=2)

$F_u = 0.057$ lbs (n=3)